İMALAT TEKNOLOJİLERİ VE UYGULAMALARI

CİLT: 3 SAYI: 3 YIL: 2022 e-ISSN: 2717-7475

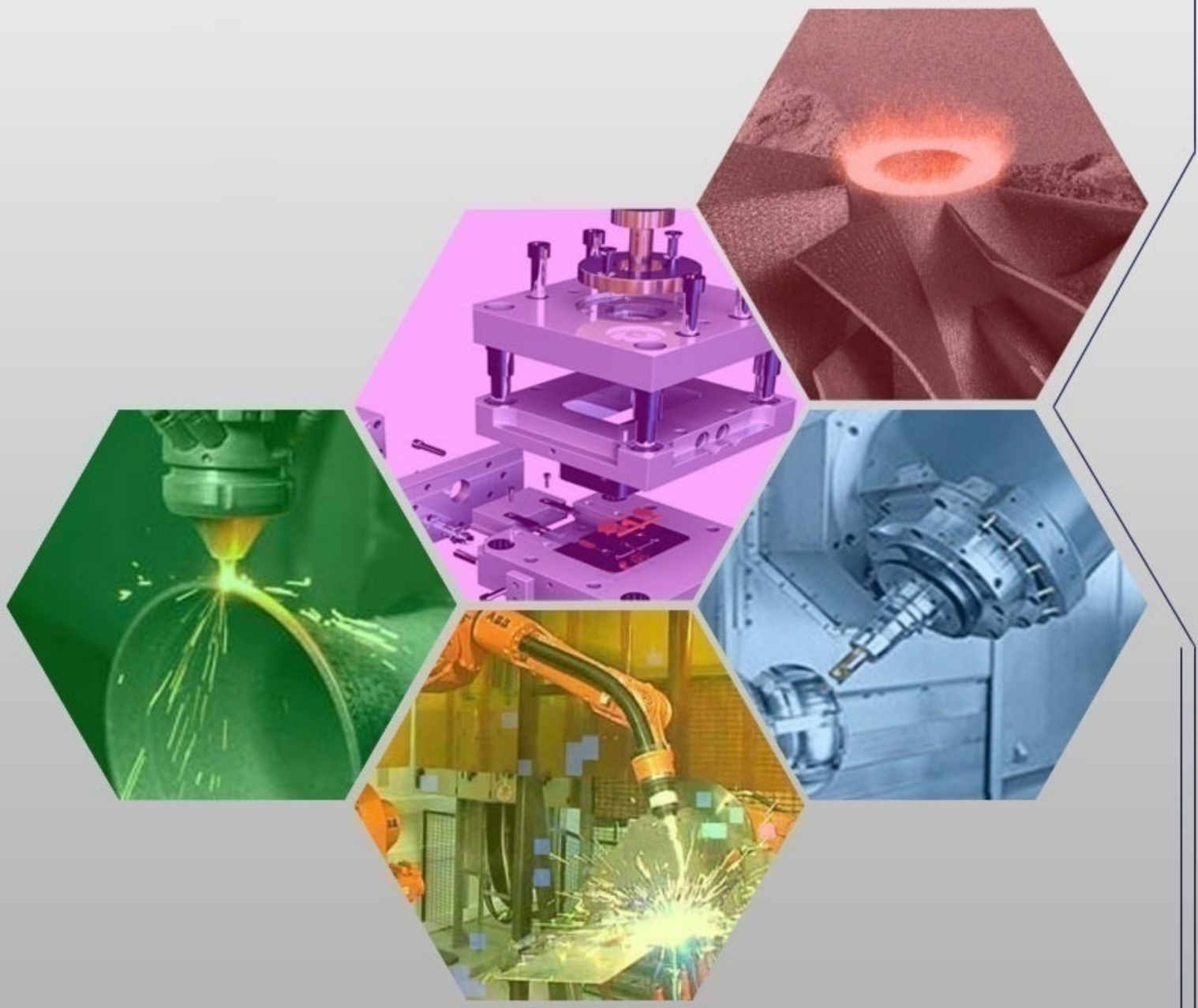

MANUFACTURING TECHNOLOGIES AND APPLICATIONS

VOLUME: 3 ISSUE: 3 YEAR: 2022

Cilt (Volume) : 3
Sayı (Issue) : 3
Yıl (Year) : 2022
e-ISSN: 2717-7475

İmalat Teknolojileri ve Uygulamaları
Manufacturing Technologies and Applications
(MATECA)

https://dergipark.org.tr/tr/pub/mateca

Cilt (Volume) : 3
Sayı (Issue) : 3
Yıl (Year) : 2022
e-ISSN: 2717-7475

Yayıncı *(Publisher)*
Mustafa GÜNAY

Web Sayfası *(Web Page)*
http://dergipark.gov.tr/pub/mateca

Yayın Tarihi *(Publication Date)*
Aralık 2022 (*December 2022)*

Yayın Dili *(Publication Language)*
Türkçe / İngilizce (Turkish/English)

Yayın Aralığı *(Publication Frequency)*
Yılda üç kez yayınlanır *(Tri-annual)*

Yayın Türü *(Publication Type)*
Süreli yayın *(Periodical)*

Kapak Tasarımı *(Cover Design)*
Ozan YETKİN

İletişim

Prof. Dr. Mustafa Günay (Editör)
Telefon: +90 370 4187400
E-posta: matecajournal@gmail.com, mgunay@karabuk.edu.tr

https://dergipark.org.tr/tr/pub/mateca adresinden dergiye ilişkin bilgilere ve makalelerin tam metnine ulaşılabilir.

Contact

Prof. Dr. Mustafa Günay (Editor)
Phone: +90 370 4187400

E-mail: matecajournal@gmail.com, mgunay@karabuk.edu.tr

Instructions for authors and all articles in this journal can be reached at *https://dergipark.org.tr/en/pub/mateca*

Cilt (Volume) : 3
Sayı (Issue) : 3
Yıl (Year) : 2022
e-ISSN: 2717-7475

İÇİNDEKİLER (CONTENTS)

Araştırma Makalesi (Research Article) **Sayfa (Page)**

The Investigation of Performance Properties of the Epoxy/Glass Flake Composite Coating on Steel Pile Pipes
(Çelik Kazık Borular Üzerindeki Cam Pulcuk Takviyeli Epoksi Kompozit Kaplamanın Performans Özelliklerinin Araştırılması)
Gökhan ÇİL, Mahmut GEL 1-7

Analyzing the Effects of Cutting Parameters on Machinability Criteria in Milling of 17-4PH Stainless Steel Under Dry Environment *(17-4PH Paslanmaz Çeliğin Kuru Ortamda Frezelenmesinde Kesme Parametrelerinin İşlenebilirlik Kriterlerine Etkilerinin Araştırılması)*
Hakan YURTKURAN, Mustafa GÜNAY 8-19

Optimization of Welding Parameters in MAG Lap Welding of DD13 Sheet Metal with Taguchi Method and FEM Analysis
(Taguchi Metodu ve FEM Analizi ile DD13 Sacların MAG Bindirme Kaynağında Kaynak Parametrelerinin Optimizasyonu)
Serkan APAY 20-30

Design and Manufacturing of Pneumatic Driven Extension Spring Fatigue Machine
(Pnömatik Tahrikli Çekme Yayı Yorulma Makinesi Tasarım Ve İmalatı)
Fatih ÖZEN, Muhammet Kaan ÇOBANOĞLU, Ahmet İLHAN, Hakkı Taner SEZAN, Salim ASLANLAR 44-54

Investigation of the Impacts of Cutting Parameters on Power Usage in Cryogenic-Assisted Turning of AISI 52100 Bearing Steel by FEM
(AISI 52100 Rulman Çeliğinin Kriyojenik Destekli Tornalama İşleminde Kesme Parametrelerinin Güç Tüketimi Üzerine Etkilerinin FEM ile İncelenmesi)
Levent UĞUR, Hakan KAZAN, Barış ÖZLÜ 55-61

Derleme Makale (Review Article)

Paslanmaz Çeliklerin Farklı Akımlarda MİG Kaynak Yöntemiyle Birleştirilmesinin İncelenmesi
(Investigation of Joining Stainless Steels with MIG Welding at Different Current)
Ebrar KARAKAYA, A. Fulin KÖSEOĞLU 31-43

İmalat Teknolojileri ve Uygulamaları
Cilt: 3, No: 3, 2022 (1-7)
Araştırma Makalesi
e-ISSN: 2717-7475

Manufacturing Technologies and Applications
Vol: 3, Issue: 3, 2022 (1-7)
Research Article
e-ISSN: 2717-7475

The Investigation of Performance Properties of the Epoxy/Glass Flake Composite Coating on Steel Pile Pipes

Gökhan ÇİL[1,*], Mahmut GEL[1]

[1]*Erciyas Steel Pipe Co., Design Center, Düzce, Turkey*

ARTICLE INFORMATION

Received: *24.10.2022*
Accepted: *01.11.2022*

Keywords:
Steel pile pipe
Corrosion
Splash zone
Glass flake epoxy

ABSTRACT

Steel pile pipes used for offshore applications and port construction are subject to high levels of corrosion. To protect the top end of the steel pile pipe against aggressive corrosion conditions, the splash zone of the steel pile pipe is coated with epoxy. For a high strength offshore system applications, the requirement of the long term durability of coating was specified as C5(H)Im2 according to ISO 12944. The coated specimens with glass flake reinforced epoxy were exposed to neutral salt spray (NSS) for 1440 hours according to EN ISO 9227 and examined adhesion strength of the coatings. The corrosion and adhesion results of the samples which are coated in single and 2 layers with a dry film thickness of 600 microns, were found to be suitable and the painting operation was applied on the pipe to specify application condition. When the application results were examined, it was seen that the sample with a dry film thickness of 600 microns, coated in 2 layers, met the desired requirements.

Çelik Kazık Borular Üzerindeki Cam Pulcuk Takviyeli Epoksi Kompozit Kaplamanın Performans Özelliklerinin Araştırılması

MAKALE BİLGİSİ

Alınma: *24.10.2022*
Kabul: *01.11.2022*

Anahtar Kelimeler:
Çelik kazık boru
Korozyon
Sıçrantı bölgesi
Cam pulcuk takviyeli epoksi

ÖZET

Açık deniz uygulamaları ve liman inşaasında kullanılan çelik kazık boruları yüksek düzeyde korozyona maruz kalır. Çelik kazık borunun üst ucunu saldırgan korozyon koşullarına karşı korumak için çelik kazık borusunun sıçrama bölgesi epoksi ile kaplanmıştır. Yüksek mukavemetli açık deniz sistem uygulamaları için, kaplamanın uzun süreli dayanıklılık şartı ISO 12944'e göre C5(H)Im2 olarak belirtilmiştir. Cam pulcuk takviyeli epoksi ile kaplanmış numuneler 1440 saat boyunca EN ISO 9227'ye göre nötr tuz spreyine (NSS) maruz bırakılmış ve kaplamaların yapışma mukavemeti incelenmiştir. Korozyon ve yapışma test sonuçları uygun bulunan tek kat ve iki katlı 600 mikron kuru film kalınlığına sahip boyama sistemi ile uygulama koşullarının belirlenmesi için boru üzerine boyama uygulaması yapılmıştır. Uygulama sonuçları incelendiğinde 600 mikron kuru film kalınlığına sahip ve 2 katta kaplanmış numunenin istenilen şartları sağladığı görülmüştür.

1. INTRODUCTION (GİRİŞ)

Steel pile pipes are widely used in the construction of onshore and offshore foundations. The low transportation damages, high material strength and high vibration absorption during driving are among the most important advantages of steel pile pipes [1-4]. The corrosion zones of port structures generally consist of atmospheric, splash, tidal, seawater and mud & backfill parts. Fig. 1 schematizes an example of corrosion environments for a steel pile pipe. The corrosion rate in the splash zone is approximately 0.3 mm/year, while the rate of the atmospheric zone is less than 0.1 mm/year. The steel surface exhibits wet and dry cycles in the splash zone. Thus, the conditions at the splash zone are generally more aggressive than at the full immersion zone since compared to the latter, the steel surface is exposed to a thin layer of water which can easily carry dissolved oxygen. For that reason, a coating is applied to the splash zone to avoid the corrosion of the steel pipe [5, 6].

**Sorumlu yazar, e-posta: gcil@erciyas.com*
To cite this article: G. Çil, M. Gel, The Investigation of Performance Properties of the Epoxy/Glass Flake Composite Coating on Steel Pile Pipes, 3(3), 1-7, 2022. https://doi.org/10.52795/mateca.1193296,

Organic coatings are a coating commonly used to protect metallic surfaces from corrosion. Compared to other organic coatings, glass flake filled epoxy coatings are preferred in the marine atmosphere due to their abrasion resistance, low water vapor permeability, chemical stability and excellent cathodic disbondment properties. In recent years, paints containing glass flakes have been investigated for metal protection in extremely corrosive environments, with the expectation that composite coatings will significantly inhibit water penetration in the polymeric matrix [7-9]. The improved barrier properties of glass flakes in the coating have attracted the interest of researchers to study composite coatings containing glass flakes for corrosion resistance. In addition to corrosion resistance, the use of glass flakes to improve some properties such as thermal and viscoelastic properties is among some studies [10].

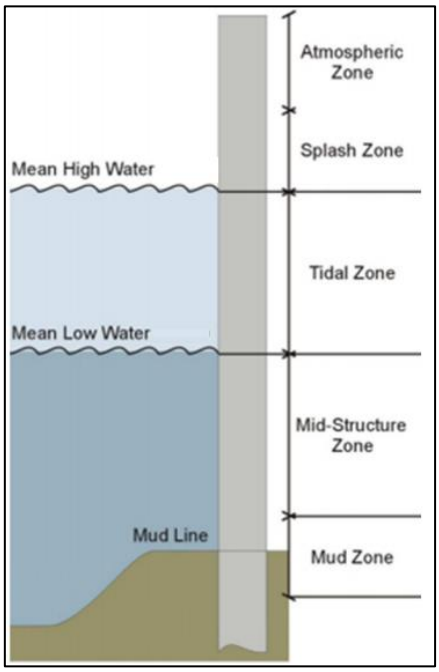

Figure 1. Corrosion zones of steel pile pipe (Çelik kazık boruların korozyon bölgeleri)

Salt spray testing is among the common methods for accelerated corrosion testing. Salt spray test results have been associated with results obtained from atmospheric interaction in subtropical environments, increasing its validity [11]. In addition, the accelerated non-electrochemical test is the salt spray test, which is widely used for coating evaluation [12].

In this study, the corrosion properties of the steel coated with glass flake reinforced epoxy under different conditions and the adhesion strength properties of the coatings were investigated.

2. MATERIAL AND METHOD (MATERYAL VE YÖNTEM)

In this study, three samples were prepared for each condition to be used in the experiments. Two of them were used for the salt spray test and the remaining sample was used for the adhesion strength test. For surface preparation of steel plates having dimensions of 150x50x3 mm, blasted by using grit/shot steel mix. The grit/shot ratio was 1/1. The surface roughness values of all steel plates were measured between 60 μm and 90 μm. The surface roughness was analysed by the Mitutoyo surface roughness tester. In addition, the surface quality level was found to be at Sa 2.5 according to the ISO 8501-1 standard and the surface was cleaned from visible oil and dirt.

After blasting, the paint mixing denoted as components A and B was prepared according to the product technical data sheet. The paint application was performed on blasted steel plates by the airless spraying technique. The theoretical dry film thickness (DFT) of coating types is given in Table 1. The DFT measurements of coatings were performed by Elcometer 456 coating thickness gauge. After the painting application, the curing temperature was selected as room temperature (23±2º C) for all specimens. For the two-layer coating types, the painting of the second layer was applied after the first layer had dried.

Table 1. Coating condition (Kaplama şartları)

Coating Type	Number of coating layer	DFT of first layer	DFT of second layer	Total nominal DFT on plates
1	Single layer	300 µm	-	300 µm
2	Two-layer	300 µm	300 µm	600 µm
3	Single layer	600 µm	-	600 µm

The test samples were prepared for neutral salt spray (NSS) test. This test was performed according to ISO 9227 [13]. Atmospheric corrosivity and immersion categories were specified as C5(H)Im2 according to ISO 12944-6 [14].

During the test process, the samples are placed into the chamber and a solution of 50 ± 5 g of sodium chloride (NaCl) per litre of deionized water is evaporated at a test temperature of 35 °C. The conductivity of the used deionized water was measured as 4.64 µS/ cm. The PH level of the salt-rich solution was specified as 7.0. The salt-rich NaCl vapor performs a corrosive attack on the samples. In order to determine the long-term durability for C5(H)Im2 requirement, the samples were kept in a salt spray cabinet (5% NaCl) up to 1440 hours and the tests were carried out under the same aggressive conditions for all samples. After neutral salt spray test (NSS), the examination of the coated specimens was performed according to ISO 4628-1 [15] standard requirements. Pull-off tests of the coatings were performed according to ISO 4624 standard. The adhesion strengths of coatings were measured by Positest AT-M digital pull-off adhesion tester.

3. EXPERIMENT AND OPTIMIZATION RESULTS (DENEY VE OPTİMİZASYON SONUÇLARI)

The dry film thickness (DFT) of the coated specimens were measured. Fifteen gage readings were made on each plate and their average DFT values were calculated. For coating type 1, the average DFT of coating was measured as 311 µm. For the two-layer type 2, the average DFT of the first layer was 309 and the average of the top layer was 612 µm.

Table 2. The scale for designating the size and quantity of defects (Kusurların boyutunu ve miktarını belirlemek için ölçek)

Rating	**Quantity of defects**	**Size of defects**
0	none, i.e. no detectable defects	not visible under ×10 magnification
1	very few, i.e. small, barely significant number of defects	visible under magnification up to ×10
2	few, i.e. small but significant number of defects	just visible with normal corrected vision (< 0.2 mm)
3	moderate number of defects	clearly visible with normal corrected vision (between 0,2 mm and 0.5 mm)
4	considerable number of defects	between 0.5 mm and 5 mm
5	dense pattern of defects	> 5 mm

For single-layer type 3, the average thickness was measured as 610 µm. The accelerated neutral salt spray (NSS) test provides valuable information regarding the protective performance of coatings for the assessment of coating defects. This evaluation was carried out by following a numerical scale (0-5) in accordance with ISO 4628-1 [15] standard, where "0" means no degradation and "5" points out the maximum degradation. The details of these information are given in Table 2. The type of defect, the quantity and its size, is expressed as indicated in the following examples: blistering; degree of blistering 2(S2), i.e. quantity 2/size 2.

Table 3. Data of the coating performance after NSS test (NSS testi sonrası kaplama performansı verileri)

Evaluation Criteria	**Acceptance Criteria**	**Coating Type**		
		1	**2**	**3**
Blistering (Acc. to ISO 4628-2)	Max. 0 (S0)	0 (S0)	0 (S0)	0 (S0)
Rusting (Acc. to ISO 4628-3)	Max. Ri0	Ri 1	Ri 0	Ri 0
Cracking (Acc. to ISO 4628-4)	Max. 0 (S0)	0 (S0)	0 (S0)	0 (S0)
Flaking (Acc. to ISO 4628-5)	Max. 0 (S0)	0 (S0)	0 (S0)	0 (S0)
Corrosion around a scribe (Acc. to ISO 4628-8)	Max. Grade 1 (Max 1.5 mm as average of the nine values)	Grade 3	Grade 1	Grade 1

The results of the NSS tests are given in Table 3. When the test results were examined, it was seen that the NSS results of coating type 2 and type 3 were within acceptable limits. Sample images after 1440 NSS tests are given in Figure 3. The sample images support the results in Table 3. The increase in coating thickness positively affected the corrosion resistance. The type-1 sample with a dry film thickness of 300 microns showed unsatisfactory results compared to coating type 2 and type 3.

In figure 2, the adhesion test results of coating types are given. It is seen that the adhesion results of all coating types are close to each other. In a study of coating application on steel, Altuncu et al. [16] stated that the surface roughness value between 60µm-90µm is the most appropriate range for corrosion resistance. In another study [17], examining the effect of surface roughness on the adhesion between steel and coating, it was reported that the increased surface area caused by surface roughening positively affected the adhesion. The increase in surface roughness of the samples used in this study was limited in order to keep the paint consumption at an optimum level and to prevent corrosion problems. The adhesion test results of coatings 2 and 3 are above the minimum requirement of 5 MPa [14].

For type 2 and type 3 coatings that are suitable for NSS and adhesion tests, the application was made on the pipe. After applying the type 3 coating system, sagging occurred on the paint. On the other hand, no visual defect was observed on the type 2 coating.

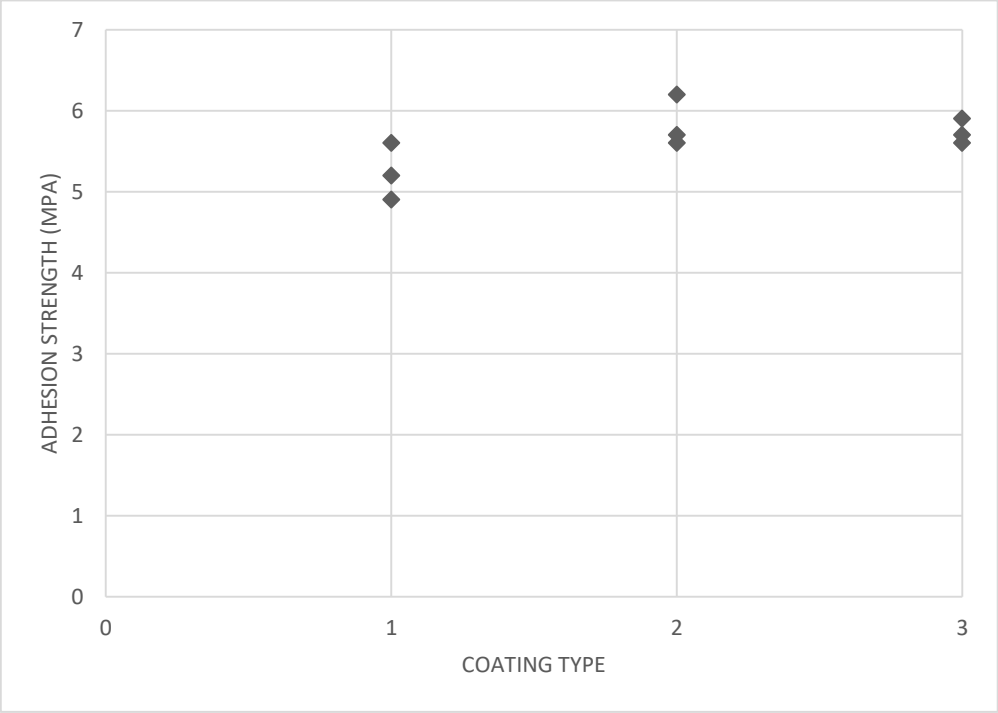

Figure 2. The adhesion test results of the coating types (Kaplama tiplerinin yapışma test sonuçları)

Condition	Before NSS test	After NSS test for 1440 hours
Type 1	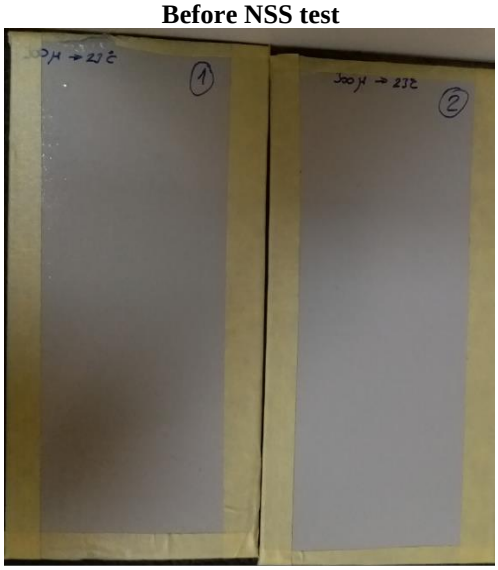	
	(a)	(b)
Type 2	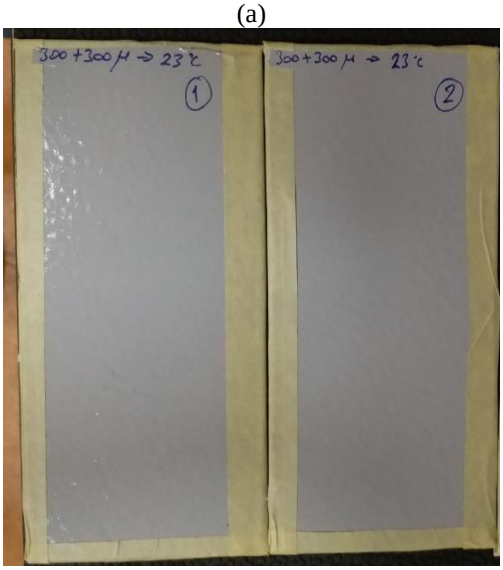	
	(c)	(d)
Type 3	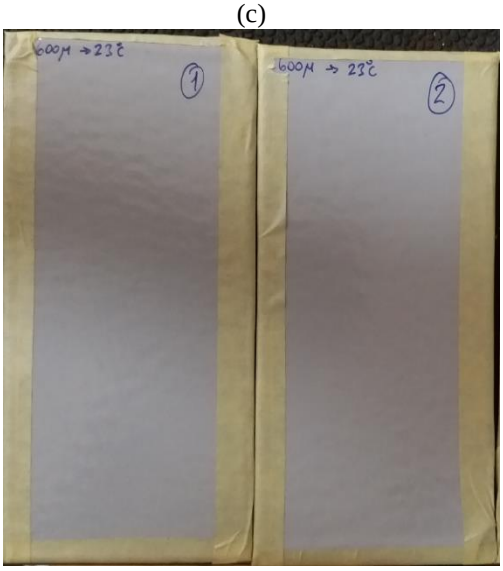	
	(e)	(f)

Figure 3. (a), (b) Type 1, (c), (d) Type 2, (e), (f) Type 3, Neutral salt spray test for coating conditions ((a), (b) Tip 1, (c), (d) Tip 2, (e), (f) Tip 3, Kaplama koşulları için nötral tuz püskürtme testi)

Figure 4. Coated pipe with coating type 2 on splash zone (Tip 2 kaplama ile kaplanan borunun sıçrantı bölgesi)

4. CONCLUSIONS (SONUÇLAR)

The results obtained from the experiments are listed below;

1. Corrosion resistance of the coating decreased depending on the decrease in the coating thickness. The type 1 coating system could not meet the desired corrosion conditions.
2. The surface roughness value between 60µm-90µm is sufficient to provide C5(H)Im2 requirement.
3. The type 2 and type 3 system coatings with glass flake reinforced epoxy meet the C5(H)Im2 requirement in accordance with ISO 12944.
4. The type-2 coating system is more applicable and has a high visual quality during the pipe coating application.

ACKNOWLEDGMENTS (TEŞEKKÜR)

This study is supported by Erciyas Steel Pipe Co., Design Center.

REFERENCES (KAYNAKLAR)

1. V. Uotinen, J. Rantala, Applications and development of modern steel pile technology, Procedia Engineering, 57: 1173-1182, 2013.
2. F. Yu, J. Yang, M. Asce, Base capacity of open-ended steel pipe piles in sand, Journal of Geotechnical and Geoenvironmental Engineering, 138(9): 1116-1129, 2012.
3. H. G. Kempfert, B. Gebreselassie, Chapter 6 - Pile foundation, Excavations and Foundations in Soft Soils, 1st Ed., Springer-Verlag, Berlin, Germany, 2006.
4. F. Özen, V. Onar, G. Çil, M. Gel, Wear resistance and microstructural evaluation of a hardfacing welded S355J2 steel pipe piles, Materials Testing, 64(6): 800-808, 2022.
5. K. Zen, Corrosion and life cycle management of port structures, Corrosion Science, 47(10): 2353–2360, 2005.
6. A. Ul-Hamid, H. Saricimen, A. Quddus, A.I. Mohammed, L.M. Al-Hems, Corrosion study of SS304 and SS316 alloys in atmospheric, underground and seawater splash zone in the arabian gulf, Corrosion Engineering, Science and Technology, 52(2): 134–140, 2017.
7. M. Echeverria, C.M. Abreu, K. Lau, C.A. Echeverria, Viability of epoxy – siloxane hybrid coatings for preventing steel corrosion, Progress in Organic Coatings, 92: 29-43, 2016.
8. S. Sathiyanarayanan, S. S. Azim, G. Venkatachari, Corrosion protection coating containing polyaniline glass flake composite for steel, Electrochimica Acta, 53(5): 2087–2094, 2008.
9. J. González-Guzmán, J.J. Santana, S. González, R.M. Souto, Resistance of metallic substrates protected by an organic coating containing glass flakes, Progress in Organic Coatings, 68(3): 240–243, 2010.
10. H. Alhumade, R.P. Nogueira, A. Yu, A. Elkamel, L. Simon, A. Abdala, Role of surface functionalization on corrosion resistance and thermal stability of epoxy/glass flake composite coating on cold rolled steel, Progress in Organic Coatings, 122: 180–188, 2018.

11. E.D. Kiosidou, A. Karantonis, G.N. Sakalis, D.I. Pantelis, Electrochemical impedance spectroscopy of scribed coated steel after salt spray testing, Corrosion Science, 137: 127-150, 2018.
12. S. L. Esfahani, Z. Ranjbar and S. Rastegar, Comparison of corrosion protection of normal and galvanised steel coated by cathodic electrocoatings using EIS and salt spray tests, Corrosion Engineering, Science and Technology, 51(2): 82-89, 2016.
13. ISO 9227, Corrosion tests in artificial atmospheres – Salt spray tests, 4. Edition, 2017.
14. ISO 12944-6, Paints and varnishes – Corrosion protection of steel structures by protective paint systems – Part 6. Laboratory performance test methods, 2. Edition, 2018.
15. ISO 4628-1, Paints and varnishes - Evaluation of degradation of coatings - Designation of quantity and size of defects, and of intensity of uniform changes in appearance - Part 1: General introduction and designation system, 2. Edition, 2016.
16. E. Altuncu, G. ÇİL, M. GEL, Testing and characterization of FBE coatings against corrosion of spiral welded steel pipes, El-Cezeri Journal of Science and Engineering, 7(2): 679-689, 2020.
17. J. P. B. V. Dam, S.T. Abrahami, A.Yilmaz, Y. Gonzalez-Garcia, H. Terryn, J.M.C. Mol, Effect of surface roughness and chemistry on the adhesion and durability of a steel-epoxy adhesive interface, International Journal of Adhesion & Adhesives, 96(2): 679-689, 2020.

İmalat Teknolojileri ve Uygulamaları
Cilt: 3, No: 3, 2022 (8-19)
Araştırma Makalesi
e-ISSN: 2717-7475

Manufacturing Technologies and Applications
Vol: 3, Issue: 3, 2020 (8-19)
Research Article
e-ISSN: 2717-7475

Analyzing the Effects of Cutting Parameters on Machinability Criteria in Milling of 17-4PH Stainless Steel under Dry Environment

Hakan YURTKURAN[1,*], Mustafa GÜNAY[2]

[1]*Yozgat Bozok University, Akdağmadeni Vocational School, Yozgat, Turkey*

[2]*Karabük University, Faculty of Engineering, Karabük, Turkey*

ARTICLE INFORMATION

Received: *28.09.2022*
Accepted: *10.11.2022*

Keywords:
17-4 PH
Milling
Cutting force
Energy consumption
Surface roughness

ABSTRACT

17-4PH steel is a martensitic precipitation hardening stainless steel with an excellent convenience of good corrosion resistance and high mechanical properties. At the same time, it has been determined from the literature that very little research has been done on the milling of this steel, which is one of the materials that are difficult to process. Therefore, an experimental research was focused on the milling of the steel with coated carbide inserts in a dry cutting environment, which is an eco-friendly cutting regime. In the experiments performed with the up milling technique, the changes in the resultant cutting force (*Fr*), surface roughness (Ra) and total cutting power or energy consumption (Pc_T) during machining were investigated. Experiments were performed according to the L_9 experimental design by choosing three different cutting speeds (*V*), feed rate (*f*) and cutting depth (*ap*). *Fr* values were calculated with the help of cutting force components measured with Kistler brand dynamometer and equipment. The magnitude of *Fr* mostly depends on the cutting depth (64.92%) and then the feed rate (30.26%), and it was determined that the forces relatively decreased with the increase in cutting speed. While Ra was mainly affected by the feed rate (65.52%), it was observed that the cutting speed had a substantial positive effect (33.78%). According to the Pc_T results, although the energy consumption owing to the spindle speed increased at high cutting speed without changing the chip cross-section, the decrease in material strength as a result of the increased cutting temperature led to a decrease in the total energy consumption. However, the lowest value was obtained at the smallest levels of the machining parameters.

17-4PH Paslanmaz Çeliğin Kuru Ortamda Frezelenmesinde Kesme Parametrelerinin İşlenebilirlik Kriterlerine Etkilerinin İncelenmesi

MAKALE BİLGİSİ

Alınma: *28.09.2022*
Kabul: *10.11.2022*

Anahtar Kelimeler:
PH 17-4
Frezeleme
Kesme kuvveti
Enerji tüketimi
Yüzey pürüzlülüğü

ÖZET

17-4PH çelik, iyi korozyon direnci ve yüksek mekanik özelliklerin olağanüstü bir uyumuna sahip olup martensitik çökeltme ile sertleşen bir paslanmaz çeliktir. Aynı zamanda, işlenebilirliği zor olan malzemelerden olan bu çeliğin özellikle frezelenmesi üzerine yok denecek kadar az araştırma yapıldığı literatürden belirlenmiştir. Bu nedenle, söz konusu çeliğin kaplamalı karbür uçlar ile çevreye duyarlı bir kesme rejimi olan kuru kesme ortamında frezelenmesi üzerine deneysel bir araştırmaya odaklanılmıştır. Zıt yönlü frezeleme tekniği ile yapılan deneylerde, işleme sırasında ortaya çıkan bileşke kesme kuvveti (*Fr*), yüzey pürüzlülüğü (Ra) ve toplam kesme gücü veya enerji tüketiminin (Pc_T) kesme parametrelerine göre değişimleri araştırılmıştır. Üç farklı kesme hızı (*V*), ilerleme oranı (*f*) ve kesme derinliği (*ap*) seçilerek L_9 deneysel tasarıma göre deneyler yapılmıştır. Kistler marka dinamometre ve ekipmanları ile ölçülen kesme kuvveti bileşenleri yardımıyla *Fr* değerleri hesaplanmıştır. *Fr*'nin büyüklüğü daha çok kesme derinliği (%64.92) ve ardından ilerleme miktarına (%30.26) bağlı olup, kesme hızının artmasıyla kuvvetlerin nispeten azaldığı belirlenmiştir. Ra ise esasen ilerleme oranı (%65.52) etkilenirken, kesme hızının küçümsenmeyecek düzeyde olumlu bir etkiye (%33.78) sahip olduğu görülmüştür. Pc_T sonuçlarına göre, talaş kesiti değişmeksizin, yüksek kesme hızında

Sorumlu yazar, e-posta: *hakan.yurtkuran@bozok.edu.tr*
To cite this article: *H. Yurtkuran, M. Günay, Analyzing the Effects of Cutting Parameters on Machinability Criteria in Milling of 17-4PH Stainless Steel under Dry Environment, Manufacturing Technologies and Applications, 3(3), 8-19, 2022.*
https://doi.org/10.52795/mateca.1181213,

fener mili devir sayısına bağlı enerji tüketimi artmasına rağmen, artan kesme sıcaklığı yüzünden malzeme dayanımındaki azalma toplam enerji tüketiminin azalmasını sağlamıştır. Bununla birlikte, en düşük Pc_T değeri kesme parametrelerinin en küçük seviyelerinde elde edilmiştir.

1. INTRODUCTION (GİRİŞ)

The developments in the aviation industry have enabled the development of factors such as correct use of time in machinability and appropriate cost by reviewing production technologies, especially material quality. Accurate analysis of the machinability processes of PH (precipitation hardening) stainless steels, which are particularly difficult to process and weld, plays an important role in reducing the machinability costs [1,2]. 17-4PH stainless steel is a martensitic PH type, which has the great strength of martensitic stainless steel along with superb corrosion resistance of austenitic stainless steel. Aircraft engine parts, gears, chemical apparatus, nuclear reactor and ship board components etc. Many important apparatuses in industrial applications such as these are produced by shaping this material [3]. It is becoming a quite new and progressively popular material for medical devices, as well as being frequently used in the defense industry and aerospace industry due to its superior mechanical properties and high corrosion resistance. In particular, many of the surgical and orthopedic instruments can be produced using conventional or unconventional manufacturing methods [4,5].

On the other side, the machinability of 17-4PH material is poor due to bad surface quality as well as chip formation with built up edge creation in carbide tools due to high cutting temperatures during machining [6]. As is known, one of the key factors defining the efficacy of material use is surface topography. Biomedical material has an important effect on the working properties of parts, especially on wear and corrosion characteristics [7]. However, changing cutting parameters during machining operations such as turning, milling, drilling, etc. can seriously alter surface integrity properties for example surface roughness, residual stress, and microstructure. It has been proven that surface properties can significantly affect the facility performance of components such as fatigue life and corrosion resistance [8,9]. Besides, the milling method is often used in the production of various machine parts, especially in the aerospace, automotive, aerospace, molding and cutting tool industries. Depending on the milling kinematics, two types of milling operations are applied as down milling and up milling, and the surface roughness and cutting forces change according to these milling types [10]. At the same time, estimation or measurement of cutting forces is an important factor for reducing power consumption in machining process. By optimizing the cutting parameters such as cutting speed, cutting depth and feed rate, reducing the cutting force can directly regulate the energy consumption in the metal cutting industry, resulting in a greener and more environmentally friendly production process [11]. In general, estimation models developed for calculating cutting forces require a measured cutting force profile [12]. Literature studies show that the direct measurement of cutting force is more convenient than the data obtained from cutting simulations based on material models, and advanced cutting force measurement dynamometers are used for these studies, which can make simultaneous measurements throughout the machining process and can be adapted to any machine tool [11,13]. It provides substantial records about the procedure, such as cutting forces, design of bench tools, machining equilibrium, and even estimation of tool wear and energy consumption. Machine tools have great influence for energy efficiency advances and carbon emission reduction. Because a 1% drop in energy consumption with processing activities can save ~55 kWh/year. In addition, reducing energy consumption in the processing process is a way to minimize the environmental effect of production [14]. In this context, researches on the power consumption of bench tools and the surface quality is very important, and with existing processing equipment in the manufacturing industry, ensuring energy-saving production while advancing surface quality in machining is a critical issue in reducing energy consumption [15]. Some of the recent works on the machining of PH stainless steels are summarized below.

Leksycki et al. analyzed changes in chip forms and surface structure in machining 17-4PH steel in dry, wet and near-dry machining for a certain range of feed and cutting speeds. Under dry, wet, minimum quantity lubrication (MQL) and high pressure MQL environments, small curved chips suitable for the cutting speed of 456 m/min and feed rate of 0.27 mm/rev were obtained. Matched to dry machining, there was a 38-48% reduction in the parameters Sa, Sq, and Sz for the near-dry condition. Depending on the processing conditions, it was determined that different textures were formed on the machined surfaces, especially with anisotropic mixture and periodicity. Surface isotropy was found in the range of ~6-10% under all studied cooling conditions, with Sa= 0.8–15.0 mm [16]. Palanisamy et al. investigated the performance of three types of tools; conventional, horizontal texture and diamond texture on tangential cutting force, surface roughness, and insert wear in semi-solid lubrication (MoS_2) condition when turning 15-5PH stainless steel. It has been detected that the diamond-textured cutting tool performs better in reducing cutting force and tool wear, and also improves surface quality [17]. Sivaiah and Chakradhar investigated the effects of LN_2 coolant and process parameters on temperature (T), tool wear, MRR, surface topography and microhardness during machining 17-4PH material. Test results shown that Mode-I (modified toolholder cooling) reduced T and tool wear by up to 61% and 29%, respectively, compared to Mode-II (classical cryogenic cooling). In addition, it was emphasized that Mode-I approach positively affects surface properties according to Mode-II approach and this will lead to a significant improvement in final product performance [1]. Liu et al. investigated the insert damage process and its effects on machined surface roughness in high speed milling of 17-4PH stainless steel. Although fracture, adhesive and diffusion wears contribute to insert damage, it has been found that the insert is more prone to damage from fatigue fracture at lower cutting speed and from peeling when speed is increased. During the machining, the mean roughness and deflection from the processed surface increased considerably after notch wear. The spindle vibration caused by bit damage and the large clearance between the tool edge and the workpiece cause severe chip wrapping as well as scratches and ridges [18]. Basmacı et al. examined the effects of feed rate, cutting depth and insert radius on surface roughness and cutting force when turning 17-4PH steel in dry cutting condition with wiper and conventional inserts. While test results verify the efficiency of wiper tips in providing excellent surface roughness, the most useful factor for Ra is feed. In terms of cutting force, depth of cut was found to be the main factor for both cutter geometries. On the other hand, tip radius is a secondary factor for surface roughness after feed [19]. Ondin et al. investigated the changes in surface topography and insert wear during turning of PH13-8 Mo steel by PVD TiAlN-$(AlCr)_2O_3$ tool in dry, pure-MQL and nanofluid-MQL cutting regimes. Comparing the dry cutting, about 5% and 12% lower surface roughness was obtained with MQL and nanofluid-MQL, respectively. Similarly, flank wear was 40.2% and 69% lower under MQL and nanofluid-MQL. On the other hand, they emphasized that nanofluids have some disadvantages such as high production cost, machining steadiness, uniform distribution of nanoparticles, increased pumping power and pressure fall [20]. Liu et al. conducted a study on fatigue performance after machining 17-4PH stainless steel using surface integrity changes and three-point bending tests. Fatigue performance generally tended to decrease with increasing cutting speed due to increased plastic deformation and strain hardening. The fatigue performance of the machined samples decreased rapidly at first as the cutting depth increased due to the ever-increasing plastic deformation. Because of the curved propagation tracks, the effects on fatigue life were overshadowed when the surface roughness changes were small [21]. Popovici and Dijmărescu analyzed the effect of cutting parameters (axial and radial cutting depth, cutting and feed speed) on surface quality once machining 17-4PH steel with the same direction milling regime using carbide end mills. Experimental results showed that the biggest effect on the Ra belonged to the radial cutting depth, and Ra increased by the rise of cutting parameter. It was stated that the smallest effect on the surface roughness belonged to the cutting speed [22].

When the literature is evaluated, it has been determined that the researches on surface quality, cutting force, tool wear and energy consumption in the processing of PH group steels are mostly done by using the turning method. However, in rare studies on milling 17-4PH steel, it is

understood that only the effects of cutting parameters on surface roughness were investigated. Therefore, the presented research investigated the changes in cutting force, surface quality and energy consumption during milling of 17-4PH stainless steel in dry cutting regime. Accordingly, it is aimed to contribute to sustainability by optimizing the amount of energy consumed in the milling of a material that is difficult to process.

2. EQUIPMENT AND RESEARCH METHODOLOGY (EKİPMANLAR VE ARAŞTIRMA METODOLOJİSİ)

2.1. Material and Tool (Malzeme ve Takım)

In this study, 17-4PH (630 quality) stainless steel in sizes of 120 × 100 × 20 mm without any heat treatment was used as workpiece. This steel is used for production of parts plays critical roles in many industrial areas, especially in the aerospace and defense industry due to very high mechanical strength and corrosion resistance. The chemical composition and mechanical properties of its in line with the information received from the supplier (Birçelik A.Ş.) are given in Table 1 and Table 2, respectively.

Tablo 1. Chemical composition of 17-4PH steel (wt.%) (17-4PH çeliğin kimyasal bileşimi)

C	Mn	Si	P	S	Cu	Mo	Nb	Cr	Ni
0.07 (max)	1.0	0.7	0.04	0.03 (max)	3-5	0.6 (max)	0.15-0.35	15-17	3-5

Tablo 2. Mechanical specification of 17-4PH steel (17-4PH çeliğin mekanik özellikleri)

Tensile strength (MPa)	Yield strength (MPa)	Percentage elongation (%)	Hardness (HRC)
1094	910	15	36

In the machining experiments, coated carbide inserts with the code APMT11T0308PDSR-MM supplied from KORLOY were used as cutting tools (Figure 1a). As the tool holder, a KORLOY product holder with the code AEM90-AP11-D20-W20-L150-Z03-H was used, which enables the rigid attachment of the cutting tools (Figure 1b).

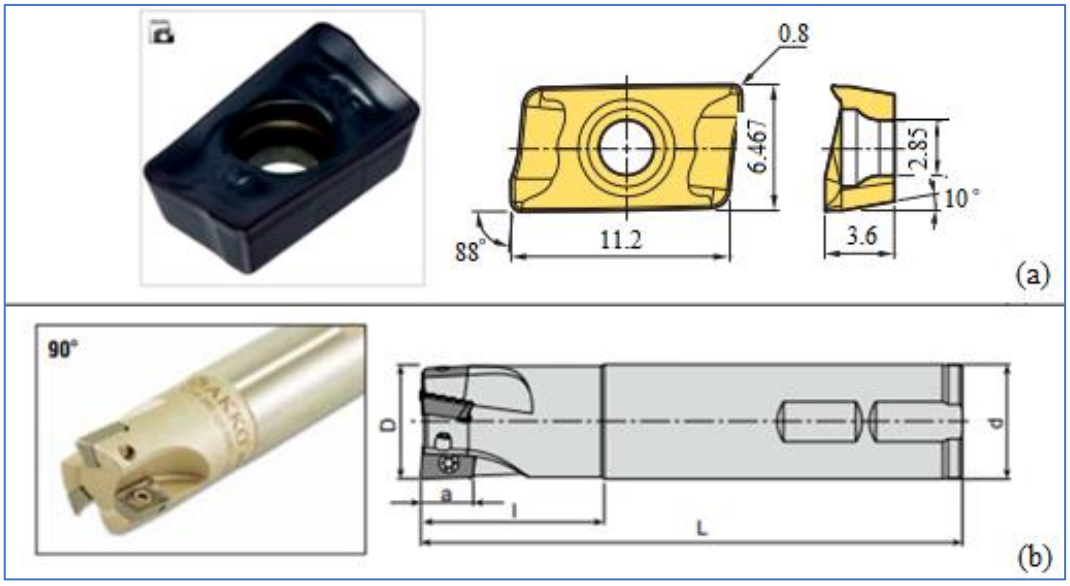

Figure 1. a) Cutting tool and b) Tool holder (a) Kesici takım ve b) Takım tutucu)

2.2. Machinability Criteria Measurement (İşlenebilirlik Kriterleri Ölçümü)

In the milling of 17-4PH stainless steel, cutting force, surface roughness and cutting power are based on machinability criteria. While the resultant force (*Fr*) was taken as the basis for the evaluation of the cutting forces, the average roughness value (Ra) was taken as the basis for the surface roughness. In the analysis of cutting power, the total energy consumption during chip removal was taken into account. The experiments were carried out on the VMC-550 model industrial CNC milling machine. The 5 kW machine can operate at a maximum of 6000 rpm.

Cutting force measurements were performed using a Kistler 9257B piezoelectric dynamometer and a 5070A type amplifier. Then, the cutting force data was converted into graphics using Dynoware software. Experiments were carried out using the up milling method (Figure 2). Though three inserts can be mounted to the holder, a single insert was milled to clearly observe the tool quality performance. Symmetrical face milling operations were applied in a dry cutting rejime and machining length was 100 mm. Here, the *Fx* component (force in the X direction), the *Fy* component (force in the Y direction) and the *Fz* component (force in the Z direction) are the cutting forces occurring in the three axes. The experimental setup used to measure cutting forces is shown in Figure 2.

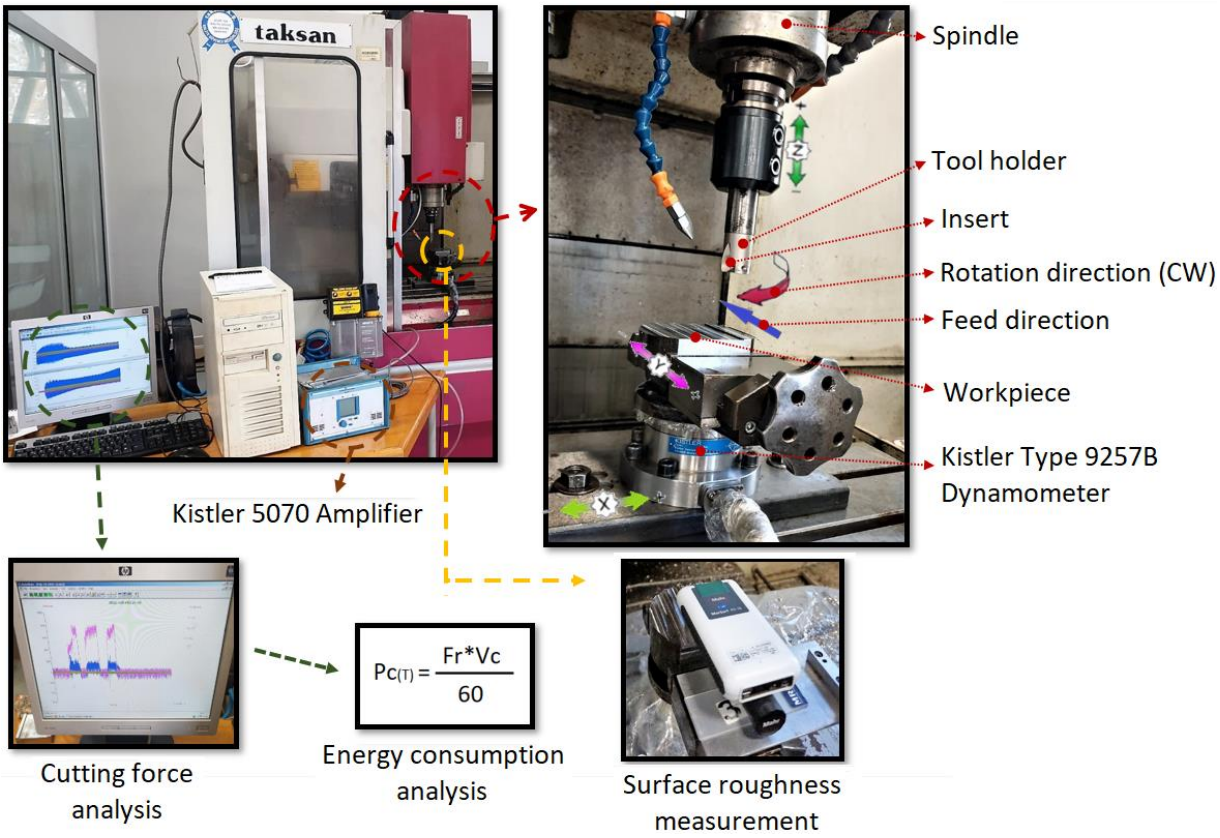

Figure 2. Experiment and analysis processes (Deney ve analiz işlemleri)

In milling, the oblique cutting theory is valid, and naturally there are three force components. Instant cutting forces in *Fx*, *Fy* and *Fz* directions were recorded when the cutting tool reached the maximum chip height using Dynoware software. Also, the force in the Z direction (*Fz*) has a value that cannot be underestimated due to the radius at the insert. Therefore, the resultant cutting force (*Fr*) resulting from the three force components was calculated (Eq.1).

$$Fr = \sqrt{(Fx^2 + Fy^2 + Fz^2)} \tag{1}$$

The surface roughness (Ra) was selected as the secondary machinability criterion, and was measured according to the international norm (ISO 4287). Ra values were recorded by MarSurf M300 device by applying a cutting and sampling length, 0.8 mm and 5 mm, respectively. The

roughness measurements were made from three regions (front, middle and end) along the cutting length and evaluated by averaging them.

Energy or power consumption, which is the third machinability criterion in the presented research, is an important tool that can be measured or calculated to contribute to sustainability in metal cutting processes. On the other hand, the cutting power (*Pc*) in the bench tool mostly depending on the machining parameters. Reducing the cutting force by optimizing the cutting parameters can directly regulate the power consumption in machining applications, thus enabling a greener and more eco-friendly production process. So, the specific cutting energy can be used to estimate the total power consumption of the bench tool in machining. This expression is labeled as the power or energy required to remove 1 mm^3 of material. In brief, specific energy consumption is the ratio of *Pc* to MRR, which is a function of cutting parameters. In this context, Pc is one of the main machinability criterions that affect tool life, dimensional precision of part and machining efficiency. Energy consumption can be measured as well as calculated using cutting force data. Eq.2 is usually applied to calculate the power (in kW) required for removing the material in milling [23].

$$Pc = (ae * ap * Vf * ks)/(60 * 10^6 * n) \quad (2)$$

Here, cutting depth (*ap* in mm), cutting width (*ae* in mm), table feed speed (*Vf* in mm/min), specific cutting force or energy (*ks* in J/mm^3) and machine efficiency (*n*) has been determined. The *ks* value is the specific cutting resistance of the material and varies according to the cutting parameters. In this context, in turning and milling operations, the power consumption can be obtained as an occupation of the cutting force (*Fc*) and cutting speed (*Vc*) (Eq.3). In the presented study, the total cutting power or energy consumption for each test condition was calculated using Eq.4.

$$Pc = (Fc * Vc)/60 \quad (3)$$

$$Pc_T = (Fr * Vc)/60 \quad (4)$$

2.3. Experimental Design and Analysis (Deney Tasarımı ve Analiz)

The cutting parameters and values to be used in the experimental design are given in Table 3. Cutting speed, feed rate and cutting depth were determined by considering the recommendations of the tool manufacturer and the machinability properties of PH group steels in the literature. Accordingly, three different cutting speeds (90-150 m/min), feed (0.05-0.15 mm/rev) and cutting depth (0.5-1.5 mm) were selected. Milling experiments were done using the Taguchi L_9 orthogonal array (Table 3).

Table 3. Experimental design (Deney tasarımı)

Exp.no	*V*, m/min	*f*, mm/rev	*ap*, mm
1	90	0.05	0.5
2	90	0.1	1
3	90	0.15	1.5
4	120	0.05	1
5	120	0.1	1.5
6	120	0.15	0.5
7	150	0.05	1.5
8	150	0.1	0.5
9	150	0.15	1

In addition, variance analysis at 95% significance level was applied to analyze the influence ranks of cutting parameters on the machinability criteria taken into account in the milling of 17-4PH steel. Minitab software was used for experimental design and statistical analysis.

3. RESULTS AND ASSESSMENT (SONUÇLAR VE DEĞERLENDİRME)

In this study, the changes in cutting forces, surface roughness and energy consumption versus the cutting parameters were analyzed in the machining of 17-4PH steel with the counter milling technique. With the help of the data obtained as a result of the experiments, interaction graphs were drawn depending on the cutting parameters for all machinability criteria.

3.1. Resultant Cutting Force (Bileşke Kesme Kuvveti)

Cutting forces offers valuable data on processes such as project of machine tools, machining stability, and even predicting tool wear and energy consumption. In this context, the arithmetical averages were taken for each force component (*Fx*, *Fy* and *Fz*) measured as a result of repeated experiments. Later, the resultant cutting forces were calculated via the force components measured in the milling process with a coated carbide insert. In Figure 3, the variation of cutting parameters and *Fr* values is presented graphically.

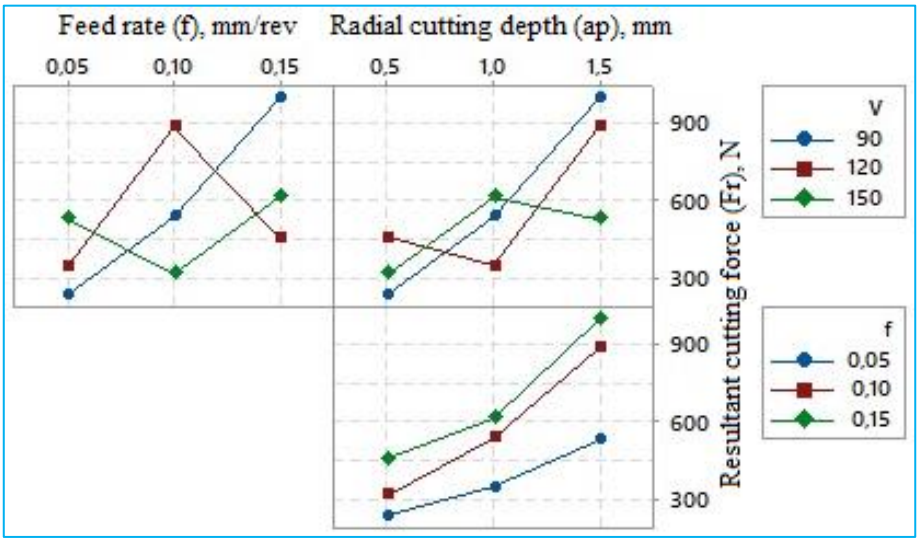

Figure 3. Variation of Fr versus cutting parameters (Kesme parametrelerine karşılık Fr'nin değişimi)

As can be seen from the interaction graphs in Figure 3, when the cutting speed is kept constant, the changes in the resultant force can be clearly seen in the feed rate-cutting depth interaction. The highest *Fr* value (883.07 N) obtained in the experiments was reached at the lowest cutting speed and the highest feed and cutting depth (*f*=0.1 mm/rev, *ap*=1.5 mm). It is expected that the resultant cutting force will increase with the increase of cutting depth and feed rate. This outcome is ascribed to the increase in the chip cross-sectional area (*ap* x *f*) with the increase in the feed rate, similar to the studies in the literature [24, 25]. In other words, the cutting area gradually enlarges with increasing the cutting depth and feed rate, and therefore increasing the overall deformation resistance or raising the power necessary for chip formation [26]. When the graph is examined, it can be said that the changes in *Fr* in the cutting speed-cutting depth and cutting-feed speed interactions have a complex trend except for the cutting speed of 90 m/min. This is mainly dependent on the experimental design and may be partly related to the cutting temperature, which varies by the cutting speed. For example, although the chip cross-section was the same in the 5th and 9th experiments, which can be understood Table 3, *Fr* was measured lower at 150 m/min cutting speed. The reason for this is the drop in material strength owing to high cutting temperature at the higher cutting speed, as mentioned in Ref. [27]. At the same time, especially in the machining of ductile materials, the built-up edge (BUE) creation is reduced once high cutting speed is applied,

and the cutting force is stabilized. In the milling of 17-4PH steel, the smallest *Fr* value was obtained as 235.25 N under the 1st experiment condition.

3.2. Surface Roughness (Yüzey Pürüzlülüğü)

The changes in the mean surface roughness (Ra) according to the cutting parameters during the milling of 17-4PH steel in the dry cutting regime are shown in the graphs in Figure 4.

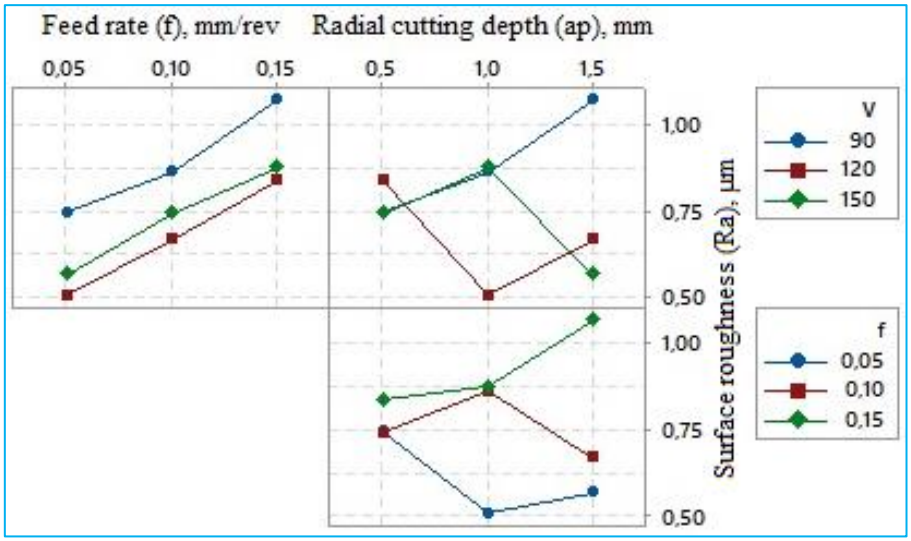

Figure 4. Variation of Ra versus cutting parameters (Kesme parametrelerine karşılık Ra'nın değişimi).

When the surface roughness changes are examined, it is clearly seen that the Ra values increase with the increase in the feed rate, similar to the results obtained in the processing of various materials [28, 29]. This result is similar in all machining methods and is clearly evident in milling, where an interrupted cutting operation takes place. On the other hand, it is seen from the *V-f* interaction that the cutting speed has a positive effect on the surface roughness up to a certain value. At the same time, this positive effect was clearly felt at the middle value of the depth of cut, as can be seen from the *V-ap* interaction. Therefore, the smallest Ra value was measured as 0.427 µm at cutting speed of 120 m/min, the smallest feed rate and cutting depth of 1 mm. This result indicates that the tool holder runout and vibrations are optimum at the mentioned cutting parameters levels. Besides, increasing cutting temperature with increasing cutting speed reduces vibrations, helping to create a more stable cutting, as can be mentioned in literature [26]. From this it can be concluded that a more stable cutting process is experienced up to a certain point at a depth of cut greater than the tool radius. Namely, when the *ap* value is smaller than the tool radius, the cutting process will be rubbing, which will make plastic deformation difficult and increase tool vibrations [23, 30]. As a result, an increase in surface roughness is inevitable. At the same time, the increased cutting forces in both cases contribute to the worsening of the surface quality, especially in up-milling. As a result, an unstable cutting process caused an irregular structure in the surface profile, resulting in an increase in Ra. As can be seen from Figure 4, the highest Ra value was found at the cutting speed of 90 m/min and the highest values of feed rate and cutting depth.

3.3. Energy Consumption (Enerji Tüketimi)

Optimizing energy consumption in production technologies helps both reduce processing costs and create a cleaner environment. So, it is extremely important to calculate the energy consumption spent during the machining of material groups that require experience and time to be processed. In recent years, researchers have focused on the analysis of processing costs of materials that are difficult to process, such as superalloys and PH stainless steels. The fact that there are not enough studies on the milling of PH group steels in the literature reveals that this area needs to be investigated. In Figure 5, the relations between the theoretically calculated total energy

consumption (Pc_T) and machining parameters in milling of the 17-4PH stainless steel are given graphically.

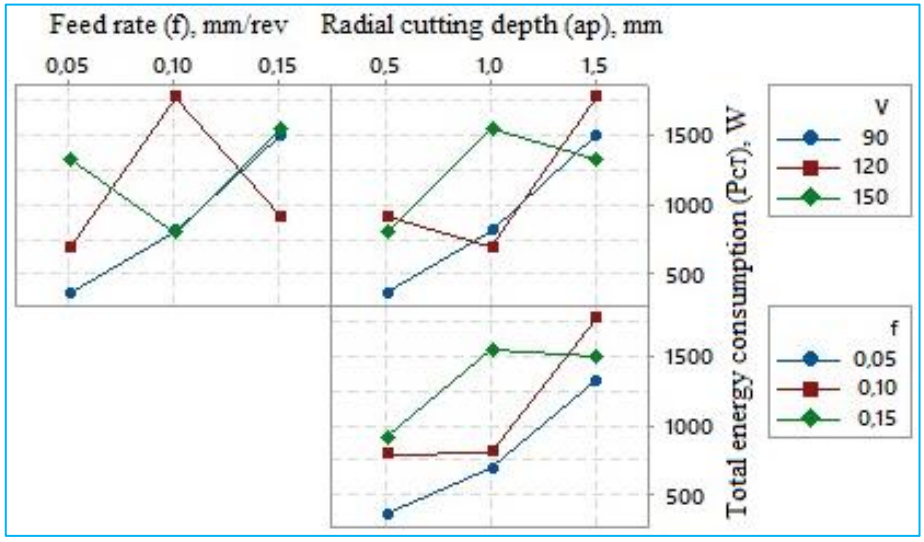

Figure 5. Variation of Pc_T versus cutting parameters (Kesme parametrelerine karşılık Pc_T'nin değişimi).

As can be understood from Figure 8, it is understood that energy consumption exhibits an uneven trend in all interactions of the cutting parameters, except for the experiments performed at a cutting speed of 90 m/min. This is mainly due to the random distribution of the ap value in the last six experiments due to the experimental design (Table 3). However, it is observed that Pc_T is constantly increasing in the feed rate-cutting depth interaction. This result is possible to attribute to the increasing chip cross-section with increasing the feed rate and cutting depth, and therefore the need for more cutting power for chip formation [11]. Therefore, it is inevitable to measure the lowest Pc_T (352.8 W) at the smallest values of the cutting parameters. On the other hand, although the chip cross-section is the same (5th and 9th experiments), the highest total energy consumption is 1766.15 W at 120 m/min. This result can be explained by the energy consumed by the machine spindle and the heat generated during cutting. The increase of cutting speed means the increase in energy consumption due to the increase in the spindle speed of the machine, as can be seen in literature [31]. At the same time, the high cutting temperature caused by the increase in cutting speed causes the material to soften, resulting in a decrease in deformation resistance. From this, it is understood that increasing the cutting speed decreases the cutting force on the one hand and increases the energy consumption on the other hand. Similar results have been obtained in the literature [14], revealing the need for optimum use of cutting speed. As a result, even if the rise in cutting speed increments the energy consumed in the spindle, the decrease in the energy required to form the chip with the decrease of material strength caused Pc_T to be lower at high cutting speed.

3.4. ANOVA for Machinability Criteria (İşlenebilirlik Kriterleri için ANOVA)

In the above sections, the resultant cutting force, surface roughness and energy consumption changes in the interaction of cutting parameters are tried to be explained. However, learning how effective these parameters are on the machinability criteria will be of significant benefit to optimizing the cutting process. At this point, the results of ANOVA applied to determine the effect levels of the parameters in the milling process of 17-4PH steel are given in Table 4.

Table 4. ANOVA for machinability criteria (İşlenebilirlik kriterleri için ANOVA)

Variable	Degree of freedom	Sum of square	Mean of square	F-value	%PCR
Resultant cutting force					
Cutting speed	2	17138	8569	2.18	3.31
Feed speed	2	156909	78454	20	30.26
Cutting depth	2	336633	168316	42.91	64.92
Error	2	7845	3922		1.51
Total	8	518525			100
Surface roughness					
Cutting speed	2	0.08028	0.04014	176.73	33.78
Feed speed	2	0.1557	0.07785	342.78	65.52
Cutting depth	2	0.00121	0.00061	2.66	0.51
Error	2	0.00045	0.00023		0.19
Total	8	0.23764			100
Energy consumption					
Cutting speed	2	173917	86958	1.79	9.78
Feed speed	2	422782	211391	4.34	23.78
Cutting depth	2	1083854	541927	11.13	60.96
Error	2	97389	48694		5.48
Total	8	1777941			100

The ANOVA results indicates that the most effective parameter on Fr and Pc_T is the depth of cut with 64.92% and 60.96% PCR, respectively. The most active parameter for surface roughness is the feed with 65.52% PCR. On the other side, cutting speed was found to be a secondary important cutting parameter for Ra in the machining of 17-4PH steel. The secondary important parameter for Fr and Pc_T was the feed rate, and the effect rates were calculated as 30.26% and 23.78%, respectively. At the same time, it is seen that the cutting speed has an effect of about 10% on the Pc_T. This value has revealed the necessity of optimizing the cutting speed in terms of total energy consumption, especially in the milling of difficult-to-process materials. Because high cutting speed increases the energy consumption depending on the number of revolutions on the one hand, and reduces the energy consumption by providing material softening on the other hand. However, it should be noted that high cutting speed accelerates tool wear, increasing both tool costs and energy consumption, thus negatively affecting sustainable machining.

4. CONCLUSIONS AND SUGGESTIONS (SONUÇLAR VE ÖNERİLER)

The results obtained in dry milling of 17-4PH stainless steel with a coated carbide insert bit are summarized below.

- It has been detected that the resultant cutting force (*Fr*) increases with increasing the feed rate (*f*) and the cutting depth (*ap*), and declines to a certain extent with increasing the cutting speed. This is an expected result; it was found that *Fr* was most affected by cutting depth according to the ANOVA result. The lowest *Fr* value was obtained with cutting parameters namely *V*=90 m/min, *f*=0.05 mm/rev and *ap*=0.5 mm.

- According to the surface roughness (Ra) results, the surface quality is significantly affected by the cutting speed as well as the feed rate. At the same time, more stable chip formation that occurs at a certain cutting speed and *ap*>tool radius minimizes possible tool vibrations and ensures optimum surface roughness. The smallest Ra value (0.427 mm) was obtained at *V*=120 m/min, *f*=0.05 mm/rev and *ap*=1 mm.

- Total energy consumption (Pc_T) naturally increased due to the interaction of the main parameters (*ap* and *f*) forming the chip section. In addition, in the case of the same chip cross-section, although the energy consumed by the machine spindle increases at high cutting speed, the decrease in material strength due to the increase in temperature during machining led to a decrease in total energy consumption. From this, it was concluded that cutting speed is an important parameter to be considered in terms of energy consumption as well as tool wear, especially in milling difficult-to-machine materials.

- The results obtained from the study showed that cutting parameters should be optimized and used in this type of milling operations. In the future, in order to contribute to sustainable processing, it will be useful to conduct research comparing environmentally friendly cutting regimes such as dry cutting and minimum quantity lubrication, vegetable-based cutting oil in terms of processing efficiency in the processing of PH stainless steels.

ACKNOWLEDGMENT (TEŞEKKÜR)

This research was supported by a project carried out within the scope of TÜBİTAK 2209-A.

REFERENCES (KAYNAKLAR)

1. P. Sivaiah, D. Chakradhar, Modeling and optimization of sustainable manufacturing process in machining of 17-4 PH stainless steel, Measurement, 134: 142–152, 2019.
2. N. Khanna, P. Shah, R.W. Maruda, G.M. Krolczyk, H. Hegab, Experimental investigation and sustainability assessment to evaluate environmentally clean machining of 15-5 PH stainless steel, Journal of Manufacturing Processes., 56: 1027–1038, 2020.
3. D. Karthik, S. Kalainathan, S. Swaroop, Surface modification of 17-4 PH stainless steel by laser peening without protective coating process, Surface and Coatings Technology, 278: 138–45, 2015.
4. I. Mutlu, E. Oktay, Characterization of 17-4 PH stainless steel foam for biomedical applications in simulated body fluid and artificial saliva environments, Materials Science and Engineering: C, 33: 1125–1131, 2013.
5. R.I.M. Asri, W.S.W. Harun, M. Samykano, N.A.C. Lah, S.A.C. Ghani, F.Tarlochan, M.R. Raza, Corrosion and surface modification on biocompatible metals: A review, Materials Science & engineering. C, Materials for Biological Applications, 77: 1261–1274, 2017.
6. A. Mohanty, S. Gangopadhyay, A. Thakur, On applicability of multilayer coated tool in dry machining of aerospace grade stainless steel, Materials and Manufacturing Processes, 31(7): 869–879, 2016.
7. X. Ying, Q. Yang, Q.G. Pei, L. Yang, The surface topography in machining of medical metallic materials: A review, Materials Science Forum, 681: 127–132, 2016.
8. M. Sarıkaya, M. K. Gupta, I. Tomaz, D. Y. Pimenov, M. Kuntoğlu, N. Khanna, Ç. V. Yıldırım, A state-of-the-art review on tool wear and surface integrity characteristics in machining of superalloys, CIRP Journal of Manufacturing Science and Technology, 35: 624-658, 2021.
9. D. Novovic, RC. Dewes, DK. Aspinwall, W. Voice, P. Bowen, The effect of machined topography and integrity on fatigue life, International Journal of Machine Tools and Manufacture, 44(2-3): 125–34, 2004.
10. M. Płodzień, Ł. Żyłka, P. Sułkowicz, K. Żak, S. Wojciechowski, High-performance face milling of 42CrMo4 steel: Influence of entering angle on the measured surface roughness, cutting force and vibration amplitude, Materials, 14(9): 2196, 2021.
11. M.E. Korkmaz, M. Günay, Finite element modelling of cutting forces and power consumption in turning of AISI 420 martensitic stainless steel, Arabian Journal for Science and Engineering,43(9): 4863–4870, 2018.
12. P. Sahoo, T. Pratap, K. Patra, A hybrid modelling approach towards prediction of cutting forces in micro end milling of Ti-6Al-4V titanium alloy, International Journal of Mechanical Sciences, 150: 495–509, 2019.
13. K.N. Shi, N. Liu, C. Le Liu, J.X. Ren, S.S. Yang, W.C. Tan, Indirect approach for predicting cutting force coefficients and power consumption in milling process, Advances in Manufacturing, 10: 101–113, 2022.
14. S.S. Pawar, T.C. Bera, K.S. Sangwan, Modelling of energy consumption for milling of circular geometry, Procedia CIRP, 98(2019): 470–475, 2021.
15. G.Y. Zhao, Z.Y. Liu, Y He, H.J. Cao, Y.B. Guo, Energy consumption in machining: Classification prediction, and reduction strategy, Energy, 133:142–157, 2017.

16. K. Leksycki, E. Feldshtein, G. M. Królczyk, S. Legutko, On the chip shaping and surface topography when finish cutting 17-4 PH precipitation-hardening stainless steel under near-dry cutting conditions, Materials, 13(9): 2188, 2020.
17. D. Palanisamy, S. Jayasurya, N. Manikandan, D. ArulKirubakaran, V. Divakar, Performance evaluation of textured inserts with MQL in machining of PH stainless steel, Materials Today: Proceedings, 39(1): 279–284, 2021.
18. L. Guoliang, Z. Bin, H. Chuanzhen, W. Xiangyu, W. Jun, L. Zhanqiang, Tool damage and its effect on the machined surface roughness in high-speed face milling the 17-4PH stainless steel, The International Journal of Advanced Manufacturing Technology, 83(1): 257–264, 2016.
19. G. Basmacı, M. Ay, İ. Kırbaş, Optimisation of machining parameters in turning 17-4 PH stainless steel using the grey-based taguchi method, Erzincan University Journal of Science and Technology, 10(2): 243-254, 2017.
20. O. Öndin, T. Kıvak, M. Sarıkaya, Ç.V. Yıldırım, Investigation of the influence of MWCNTs mixed nanofluid on the machinability characteristics of PH 13-8 Mo stainless steel, Tribology International, 148: 106323, 2020.
21. L. Guoliang, H. Chuanzhen, Z. Bin, W. Xiangyu, L. Zhanqiang, Surface integrity and fatigue performance of 17-4PH stainless steel after cutting operations, Surface & Coatings Technology 307: 182–189, 2016.
22. T. D. Popovici, M. R. Dijmărescu, Influence of cutting data on surface quality when machining 17-4 PH stainless steel, IOP Conf. Series: Materials Science and Engineering, 227: 012101, 2017.
23. M. Günay, Modeling and multiple optimization in face milling of hardfacing welding applied steel: Force, roughness, power, Proceedings of the Institution of Mechanical Engineers, Part C: Journal of Mechanical Engineering Science, 236(12): 2022.
24. A. Kaçal, F. Yıldırım, Application of grey relational analysis in high-speed machining of hardened AISI D6 steel, Proceedings of the Institution of Mechanical Engineers, Part C: Journal of Mechanical Engineering Science, 227: 1566–1576, 2013.
25. M. Padmakumar, N. Shiva Pradeep, Effect of cutting edge form factor (K-factor) on the performance of a face milling tool, CIRP Journal of Manufacturing Science and Technology, 31: 305–313, 2020.
26. X. Chuangwen, D. Jianming, C. Yuzhen, L. Huaiyuan, S. Zhicheng, X. Jing, The relationships between cutting parameters, tool wear, cutting force and vibration, Advances in Mechanical Engineering, 10(1):1–14, 2018.
27. Ş. Şirin, M. Sarıkaya, Ç.V. Yıldırım, T. Kıvak, Machinability performance of nickel alloy X-750 with SiAlON ceramic cutting tool under dry, MQL and hBN mixed nanofluid-MQL, Tribology International, 153, 106673, 2021.
28. İ. Demir, T. Kıvak, Ş. Şirin, Performance evaluation of CuO nanofluids with different surfactants in the milling of AISI 329 duplex stainless steel, Manufacturing Technologies and Applications, 3(2): 9-21, 2022.
29. A. Çakır, S. Yağmur, N. Kavak, G. Küçüktürk, U. Şeker, The effect of minimum quantity lubrication under different parameters in the turning of AA7075 and AA2024 aluminium alloys, Internaitonal Journal of Advanced Manufacturing Technology, 84: 2515–2521, 2016.
30. N.M.N. Pa, A.A.D. Sarhan, M.H.A. Shukor, M.A.H. Mohamed, Investigate the lubrication effects on cutting force and power consumption in up and down end milling, Advanced Materials Research, 748: 264–268, 2013.
31. R. Çakıroğlu, M. Günay, Analysis of surface roughness and energy consumption in turning of C17500 copper alloy under different machining environments and modellings with response surface method, Proceedings of the Institution of Mechanical Engineers, Part E: Journal of Process Mechanical Engineering, 0(0): 2022.

İmalat Teknolojileri ve Uygulamaları
Cilt: 3, No: 3, 2020 (20-30)
Araştırma Makalesi
e-ISSN: 2717-7475

Manufacturing Technologies and Applications
Vol: 3, Issue: 3, 2020 (20-30)
Research Article
e-ISSN: 2717-7475

Optimization of Welding Parameters in MAG Lap Welding of DD13 Sheet Metal with Taguchi Method and FEM Analysis

Serkan APAY[1]

[1] *Düzce Üniversitesi, Mühendislik Fakültesi, Düzce, Türkiye*

ARTICLE INFORMATION

Received: *17.10.2022*
Accepted: *13.11.2022*

Keywords:
Finite element analysis
Hardness
Heat input
MAG welding
Taguchi method

ABSTRACT

In this study, DD13 sheet materials used in automobile swing manufacturing were welded with GMAW (Gas Metal Arc Welding) welding method with different parameters such as welding method, welding amperage, and welding speed. The optimized value of the welding parameters, which will give the lowest hardness value in the weld seam hardness, was calculated by the Taguchi method. In addition, the heat input values that are thought to affect the hardness change were calculated, and the results were used to interpret the hardness change and Taguchi optimization values. After the experimental studies, the optimized value was compared with the actual results, and the verification test was performed. As a result of the optimization process, the lowest hardness value was estimated as 172.98 HV0.1 in MAG welding performed at 420 min/mm welding speed, 290 A, and 33.6 V parameters. The validation test result was found to be consistent with 173.4 HV0.1. Based on these values, finite element analysis (FEM) was performed with Simufact Welding 8.0 software. As a result of the investigation, the weld macrostructure, thermal changes, and the amount of distortion were examined. The results obtained are in agreement with the validation experiments.

Taguchi Metodu ve FEM Analizi ile DD13 Sacların MAG Bindirme Kaynağında Kaynak Parametrelerinin Optimizasyonu

MAKALE BİLGİSİ

Alınma: *17.10.2022*
Kabul: *13.11.2022*

Anahtar Kelimeler:
Sonlu elemanlar analizi
Sertlik
Isı girdisi
MAG kaynağı
Taguchi metodu

ÖZET

Bu çalışmada, otomobil salıncak imalatında kullanılan DD13 sac malzemelerinin GMAW (Gas Metal Arc Welding) kaynak yöntemi ile kaynak yöntemi, kaynak amperi ve kaynak hızı gibi farklı parametreler ile kaynatılmıştır. Kaynak parametrelerinin, kaynak dikişi sertliğinde en düşük sertlik değerini verecek optimize değer Taguchi yöntemiyle hesaplanmıştır. Ayrıca sertlik değişimine etkisi olduğu düşünülen ısı girdisi değerleri hesaplanmış, çıkan sonuçlar sertlik değişimi ve Taguchi optimizasyonu değerlerini yorumlamada kullanılmıştır. Yapılan deneysel çalışmalardan sonra çıkan optimize değer gerçek sonuçlar ile karşılaştırılmış ve doğrulama testi yapılmıştır. Optimize işlemi sonucunda en düşük sertlik değeri tahmini 172.98 HV0.1 olarak 420 min/mm kaynak hızında, 290 A ve 33.6 V parametreleri ile yapılan MAG kaynağında ulaşılmıştır. Doğrulama testi sonucu 173.4 HV0.1 ile tutarlı olduğu görülmüştür. Sonlu elemanlar analizi (FEM) bu değerler temel alınarak Simufact Welding 8.0 yazılımı ile yapılmıştır. Analiz sonucu kaynak makro yapısı, termal değişimler ve çarpılma miktarı incelenmiştir. Elde edilen sonuçlar doğrulama deneyleri ile yakınlık göstermektedir.

1. INTRODUCTION (GİRİŞ)

Although automobiles today contain many technological innovations, some mechanical components are still used unchanged. One of these components is the swings. Swings have an essential role in the automotive industry [1,2]. Wishbones are vital parts of the vehicle's front

Sorumlu yazar, e-posta: *serkanapay@duzce.edu.tr*
To cite this article: *S. Apay, Optimization of Welding Parameters in MAG Lap Welding of DD13 Sheet Metal with Taguchi Method and FEM Analysis, Manufacturing Technologies and Applications, 3(3), 20-30, 2022.*
https://doi.org/10.52795/mateca.1190277,

suspension, from the classic cars of the past to today's modern vehicles [2,3]. It is the element that connects the swing wheel to the vehicle chassis [4]. There is a wheel at one end of the swing and a chassis [5]. In general, wishbones are produced from medium-carbon and low-carbon steels. These parts have been made from aluminum and similar light metals for fuel economy [6]. Figure 1 shows the swing picture.

Figure 1. Vehicle swing arm (Araç salıncak kolu)

Gas shielded welding methods are preferred as the welding method in most productions made from low carbon and medium carbon steel materials [7,8]. The welded connection method must also be made according to the end-use point where the produced part becomes the final product. Metal microstructures that change after welding can cause problems for long-term working details [9]. Since this problem minimizes welded joints made with the lowest possible heat input, low heat input welding methods are preferred in most joints [10]. Laser, plasma, TIG, and CMT welding are just a few of the low heat input welding methods used today [11–16].

In cases where speed is of great importance in the mass production of parts for the automotive sector, laser welding is not widely used due to the initial setup cost. TIG welding and plasma welding are not widely used due to their slowness. Point resistance welding, MIG-MAG welding, and CMT welding methods, which have faster joints, are frequently used [17–19]. Manufacturing with low heat input welding methods increases the working life of the parts in automobile parts where pulsed work is involved, such as swing manufacturing. With the low heat input generated during welding, the weld seam microstructure is finer-grained and has a faster joining process than the other [20,21]. This situation minimizes the problems that may arise from the welding seam in part.

In this study, welding of DD13 sheets used in swing manufacturing was performed with the MAG welding method at three different volts, three different amperes, and three different welding speeds. The changes in weld seam hardness were examined the results obtained were optimized by the Taguchi method.

2. MATERIAL AND METHOD (MATERYAL VE YÖNTEM)

2.1. Experimental Setup (Deney Düzeneği)

In the experiments, 2.5 mm thick DD13 (EN 10111-2008) sheet metal suitable for cold forming and deep drawing was used. The chemical compositions of the test pieces are given in Table 1, and their mechanical properties are provided in Table 2. 1.2 mm thick ER70S-6 welding wire was used in the welded joint process. The chemical properties of the welding wire are shown in Table 3, and the mechanical properties are shown in Table 4.

Table 1. Chemical composition of DD13 sheet (% by weight) (DD13 saclarının kimyasal bileşimi - % ağırlıkça)

C	Mn	P	S	Si	Al	Cu	Cr	Ni	Mo	Fe
0.04	0.255	0.024	0.001	0.0395	0.053	0.027	0.036	0.035	0.004	Bal.

Table 2. Mechanical properties of DD13 sheet (DD13 saclarının mekanik özellikleri.)

Yield Strength (N/mm^2)	Tensile Strength (N/mm^2)	Elongation (%)
229.5	337.3	42

Table 3. Chemical properties of ER70S-6 welding wire (ER70S-6 kaynak telinin kimyasal özellikleri)

C	Si	Mn	Fe
0.07	0.8	1.45	Bal.

Table 4. Mechanical properties of ER70S-6 welding wire (ER70S-6 kaynak telinin mekanik özellikleri)

Yield Strength (N/mm^2)	Tensile Strength (N/mm^2)	Elongation (%)	Notch Impact Resistance (J) -30°C
460	530	29	50

Welding parameters and the results of these parameters are shown in Table 5. 18 pieces of DD13 sheet materials, 3 mm thick and 100x200 mm in size, were numbered and welded to each other in the form of overlap welding, as shown in Figure 2.

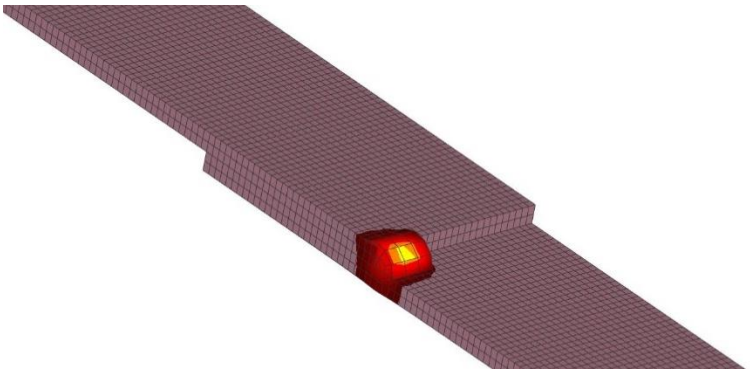

Figure 2. MAG Lap welding schematic (MAG Bindirmeli kaynak şeması)

Table 5. Welding parameters and results for DD13 sheets (DD13 sacları için kaynak parametreleri ve sonuçları.)

Sample No	Welding speed (mm/min)	Amper (A)	Volt (V)	Heat input (KJ/mm)	Hardness result ($HV_{0.1}$)
1	420	250	28	1.0000	177.5
2	420	270	30.2	1.1649	176.2
3	420	290	33.6	1.3920	173.4
4	660	250	30.2	0.6864	183.2
5	660	270	33.6	0.8247	180.6
6	660	290	28	0.7382	181.3
7	900	250	33.6	0.5600	191.7
8	900	270	28	0.5040	194.8
9	900	290	30.2	0.5839	189.7

2.2. Finite Element Modeling

Numerical simulation of the welding process has been one of the crucial topics in welding research for years. Simulation results can explain the physical basis of some unpredictable results in the welding process and optimize welding parameters. However, simulating the welding process is not easy as it involves thermal, mechanical, and metallurgical interactions. Many researchers accept that an essential aspect of the welding process simulation is the correct entry of metallurgical transformations into the model. Correctly entered data has a direct effect on the result.

Finite element analysis of DD13 sheet materials welded in overlapping form with MAG welding method was done with Simufact Welding 8.0 finite element package program. While making the process with a model, it has been ensured that the model is as close to reality as possible by considering the joining method and shape. Modeling and mesh scanning processes were done with

the applications in the same program. The analysis processes examined the microstructure change of the weld zone, the temperature change, and the deformation change. In the analysis process, firstly, the samples were designed as solid models and loaded into the software. The parameters used in the welding process were entered into the software, the materials were loaded into the software, and the analysis process was started.

2.3. Experimental Design and Optimization with Taguchi

Taguchi L9 (3^3) orthogonal array was used for the experimental design; only nine experiments were performed instead of 27 experiments for the full design. It is possible to significantly reduce the number of experiments in the analysis and evaluations made with the Taguchi method. The Taguchi method uses some functions to determine quality characteristics. Since the smallest value is desired in the weld zone hardness measurements, the Taguchi "smallest best" function was used in this study. The selected welding parameters and the levels of these parameters are given in Table 6. The experimental design, experimental results, and signal-to-noise (S/N) ratios calculated according to the experimental results are given in Table 7, considering the L9 orthogonal array.

Table 6. Experiment parameters and levels (Deney parametreleri ve seviyeleri)

Parameters	Level 1	Level 2	Level 3
A Welding Speed (Vw, mm/min)	420	660	900
B Amp (A)	250	270	290
C Volt (V)	28	30.2	33.6

Table 7. Experimental design and experimental results (Deney tasarımı ve deney sonuçları)

Test no	A	B	C	Experimental results and S/N ratios	
	Welding speed (V_W, mm/min)	Amp (A)	Volt (V)	Hardness ($HV_{0.1}$)	S/N_H (dB)
1	420	250	28	177.5	-44.9840
2	420	270	30.2	176.2	-44.9201
3	420	290	33.6	173.4	-44.7810
4	660	250	30.2	183.2	-45.2585
5	660	270	33.6	180.6	-45.1344
6	660	290	28	181.3	-45.1680
7	900	250	33.6	191.7	-45.6524
8	900	270	28	194.8	-45.7918
9	900	290	30.2	189.7	-45.5613

According to the test results, the average value of the hardness results was calculated at 183.156 HV, and the average S/N ratio for the hardness was calculated as -45.25 dB.

2.4. Determining Optimum Levels

In Table 8, the cutting parameters are distinguished by considering the different levels and possible effects of the orthogonal array used in this study. These levels show the average values of the signal-to-noise ratios calculated to analyze the hardness values in the experimental research. These values are used to calculate the estimation values for the determined optimum and random parameters.

Table 8. Averages of S/N ratios (S/N oranlarının ortalamaları)

Welding parameters	Levels			Delta
	Level 1	Level 2	Level 3	
A (Welding speed, V_W)	-44.90	-45.19	-45.67	0.77
B (Amp)	-45.30	-45.28	-45.17	0.13
C (Volt)	-45.31	-45.25	-45.19	0.13

One of the critical steps in the Taguchi method is to determine the optimum levels. Optimum levels are determined by evaluating different levels of experimental parameters, combinations created by the chosen orthogonal array. These levels are used to draw the effect graphs of the levels (Figure 3). When evaluating the main effect graph, the lowest level is considered for these values, as this is the minimum desired stiffness in this study.

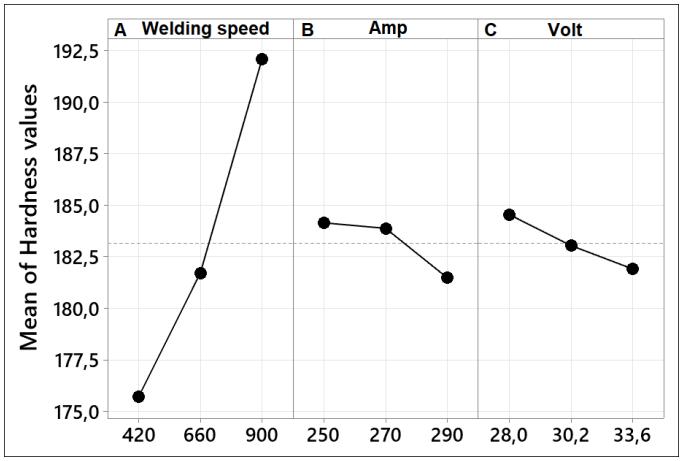

Figure 3. Main effect plot for hardness values (Sertlik değerleri için ana etki grafiği)

According to Figure 3, the optimum combination of test parameters for minimum hardness values was $A_1B_3C_3$ (A_1= 420 mm/min welding speed, B_3 = 290 amp, C_3 = 33.6 Volt).

2.5. Evaluation of Experimental Parameters by Analysis of Variance (ANOVA)

Analysis of variance is used to determine how all control factors used in experimental design affect each other, how this affects performance characteristics, and what changes occur at different levels of the parameters and determine Taguchi confidence intervals [22,23]. The effects of welding speed, amperage, and volt on hardness were evaluated by analysis of variance, and the results of analysis of variance are shown in Table 9.

Table 9. ANOVA results for hardness (Sertlik için ANOVA sonuçları)

Parameters	Degrees of freedom (DoF)	Sum of squares (SS)	Mean squares (MS)	F -Value	P-Value	Percent distribution (%)
A, Welding speed (mm/min)	2	0.915440	0.457720	235.93	0.004	94.16
B, Amp (A)	2	0.029243	0.014621	7.54	0.117	3.008
C, Volt (V)	2	0.023608	0.011804	6.08	0.141	2.42
Error *(e)*	2	0.003880	0.001940			0.412
Total	8	0.972172				100

In Table 9, the analysis results of variance giving the individual effects of the experimental parameters are given. In the table, the most influential parameter affecting the hardness was welding speed with 94.16%. This parameter is followed by Ampere with 3.008%. In addition, according to the analysis of variance, the error value was minimal.

2.6. Confirmation Experiments and Taguchi Prediction Values

The purpose of validation experiments, which is the last step of the Taguchi method, is to analyze the quality characteristics. Validation experiments are also used to test the accuracy of the optimization process. In other words, validation experiments are performed to test the determined optimum combination of test parameters and levels. Considering the individual effects of the test parameters, the estimated temperature value (T_p) of $A_1B_3C_3$ (A_1= 420 mm/min welding speed, B_3 = 290 amp, C_3 = 33.6 Volt) is calculated with the equations given below, according to the optimum combination obtained for hardness [24,25].

$$\eta_{gH} = A_1 + B_3 + C_3 - 2\eta_{\frac{S}{N}-H} \quad (1)$$

$$H_p = 10^{-\eta_{gH}/20} \quad (2)$$

In equations, $A_1B_3C_3$ are the signal-to-noise ratios of the optimum levels of the experimental parameters (Table 8). $\eta_{\frac{S}{N}-H}$ is the average of the S/N ratios of the hardness values. S/N ratio calculated for η_{gH} optimum levels, H_p is the Taguchi estimate value calculated for hardness. The hardness estimation value calculated using Eq. 1 and Eq. 2 was 172.98 $HV_{0.1}$. Confidence interval (CI) compares the result of validation experiments with the predicted value and verifies the quality characteristic. The confidence interval is the maximum and minimum value, and the accuracy of the validation experiments is tested by comparing the calculated value with the predicted values. CI is calculated with the equation given below.

$$CI = \sqrt{F_{\alpha:1,Ve} x V_{ep} x \left(\frac{1}{n_{eff}} + \frac{1}{r}\right)} \quad (3)$$

In Equation 3, $F_{\alpha:1,}\nu_e$, and the significance level are the F ratio of α, α significance level, 1-α confidence interval, and the degree of freedom of the temperature error according to the variance analysis results. When Table 9 is examined, the degree of freedom of the error is 2. In this case, the 1-2 value from the F table of the 95 % confidence level was 18.5128. V_{ep} is again the error variance according to the analysis of variance results, r is the number of validation experiments, and n_{eff} is the number of effective measured results [25].

$$n_{eff} = \frac{N}{1+V_t} \quad (4)$$

In Equation 4, N represents the total number of experiments (9), and Vt represents the experimental parameters' total degrees of freedom (6). The mean is calculated by taking Table 9 into account. In this case, the n_{eff} was calculated as 1.285. In this study, considering the optimum combination determined for hardness, 3 verification tests were performed. Considering Eq. 3 and Eq. 4, the confidence interval (CI)=0.2. The Taguchi estimation value calculated for each parameter is added and subtracted with the confidence interval using the confidence interval. The mean of the validation experiments should be between these two values. The average of 3 verification tests for hardness is 173.07 $HV_{0.1}$. In this case, A range of (172.98-0.2)<173.07<(172.98+0.2)=172.78<173.07<173.18 was obtained, and confirmation experiments for hard results were performed within the confidence interval. In this case, it can be said that the optimization is successful.

Table 10 compares the experimental results with the Taguchi method's predicted values. Eq. 1 and Eq. 2 were used to calculate the estimation values. The estimated values and observed values were close to each other. Error-values should be less than 20 % for reliable statistical analysis [22].

Table 10. Comparison of optimized and random conditions with predicted values (Optimize edilmiş ve rastgele koşulların tahmin edilen değerlerle karşılaştırılması)

Levels	**Taguchi Method**		
	Experimental	**Prediction**	**Error (%)**
$A_1B_3C_3$ (Optimum)	173.07	172.98	0.05
$A_2B_1C_2$ (Random)	183.20	182.81	0.21
$A_1B_3C_3$ (Random)	173.40	172.98	0.24
$A_3B_1C_3$ (Random)	191.70	191.86	0.08
$A_3B_3C_2$ (Random)	189.70	190.33	0.33

In Table 10, experimental results and Taguchi prediction values are compared. It is seen that the error values between the confirmation test results and the results obtained by the Taguchi method

are less than 20 % or even minimal. In this case, the results obtained from the validation experiments show that the optimization has been carried out successfully.

3. EXPERIMENT AND OPTIMIZATION RESULTS (DENEY VE OPTİMİZASYON SONUÇLARI)

3.1.The finite element analysis result

Finite element analysis was performed based on sample no. 3 (420 mm/min welding speed, 290 Amps, and 33.6 Volts), the lowest hardness value was reached due to Taguchi optimization and verification experiments. It is thought that the finite element analysis performed by obtaining the lowest hardness value will be a reference among other results. The change in the macrostructure resulting from the finite elements made is compared with the accurate macro structure results in Figure 4. When Figure 4 is examined, it is seen that the macrostructure image formed after the welding process and the estimated macro structure image formed by the finite element analysis are close to each other. As a result, the estimated finite element method is considered successful.

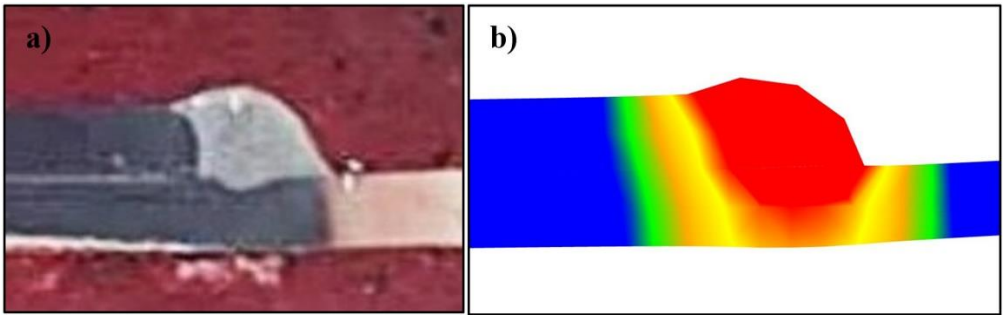

Figure 4. The finite element analysis comparison; a) Welding macrostructure, b) The finite element analysis macrostructure (Sonlu elemanlar analizi karşılaştırması; a) Kaynak makro yapısı, b) Sonlu elemanlar analizi makro yapısı)

The finite element analysis results of heat exchange and distortion rates during welding are given in Figures 5 and 6. When Figure 5 is examined, the values at which the heat generated during welding reaches the highest temperature are shown.

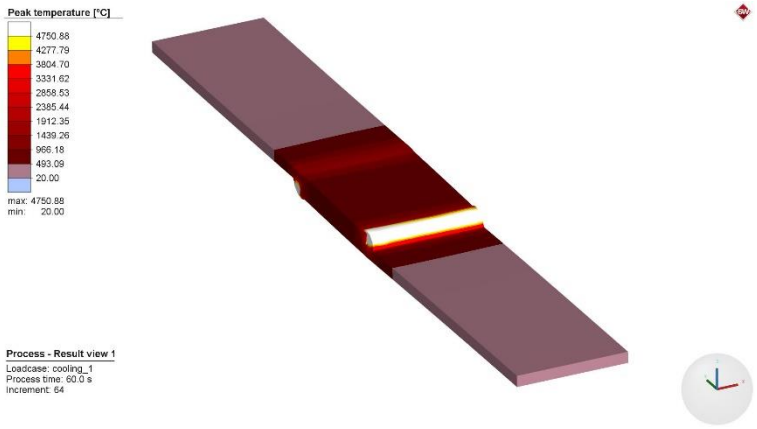

Figure 5. MAG welding temperature peak values (MAG kaynak sıcaklığı tepe değerleri)

In Figure 6, the maximum temperature reached during welding, and the maximum amounts of deformation after welding are given. It is predicted that the maximum amount of deformation after the welding process estimated with finite elements will be 1 mm. As a result of the measurements made after the welding process, the total amount of deformation in the natural welded joint was measured as 1.6 mm. This value is considered close to the weight estimated by the finite element software.

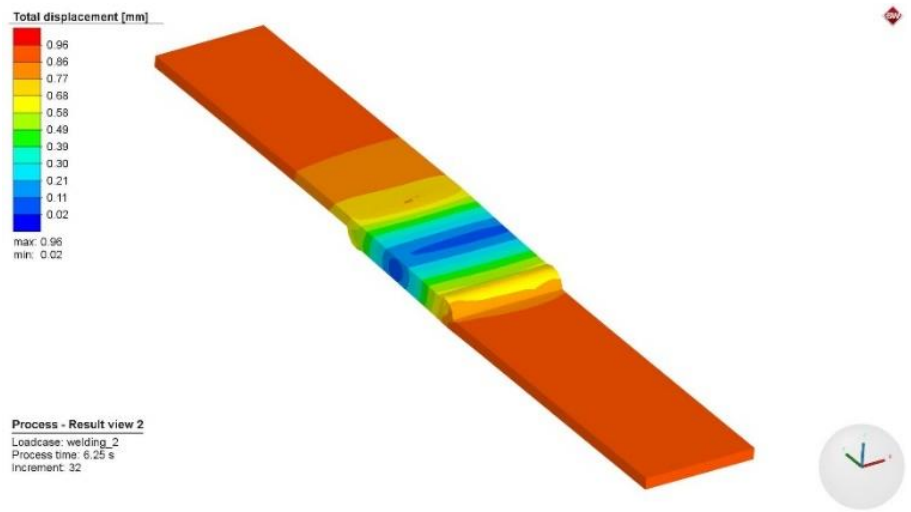

Figure 6. The amount of deformation after welding (Kaynak sonrası deformasyon miktarı)

3.2. A mathematical model with regression method model

This study determined the correlation level between hardness values and experimental parameters using the polynomial regression model. Multiple regression analysis can derive estimation equations of continuous dependent variables obtained through experimental designs with each combination of control factors. The equation (Eq. 5) predicted for the quadratic regression model is shown below:

$$H_r = 73 - 0.0159\ Vw + 1.37\ A - 4.30\ V + 0,.000038\ Vw^2 - 0.00267\ A^2 + 0.0622\ V^2 \quad (5)$$

H_r represents the estimation equation for the hardness values using the test parameters. According to the regression results, the R^2 value of the obtained mathematical model was calculated as 0.995 (99.5%).

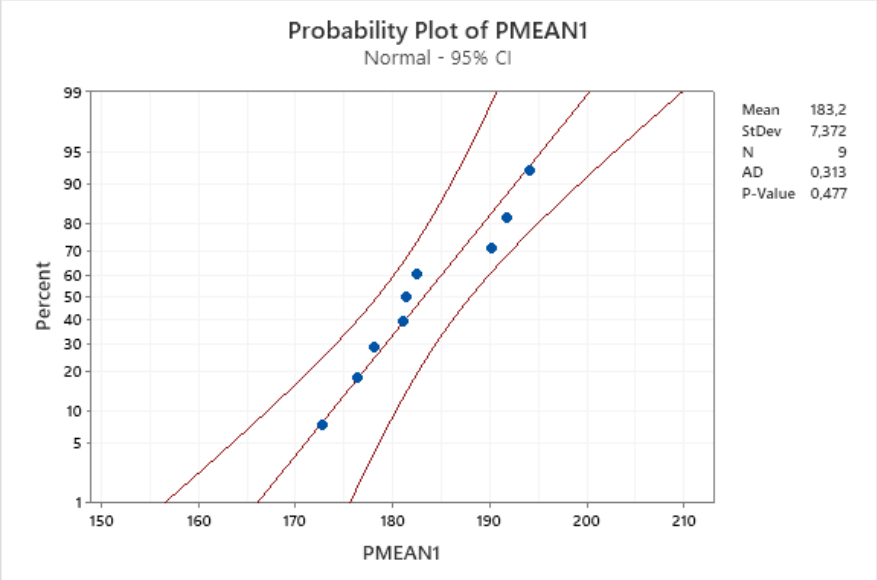

Figure 7. Probability plot (Olasılık grafiği)

The probability plot is given in Figure 7. The figure shows that the prediction values are within the 95 % confidence interval. As a result, it is thought that the estimated values will give results close to the truth.

3.3. Effects of test parameters on hardness

The effects of test parameters on hardness were examined with three-dimensional graphics (Figure 8).

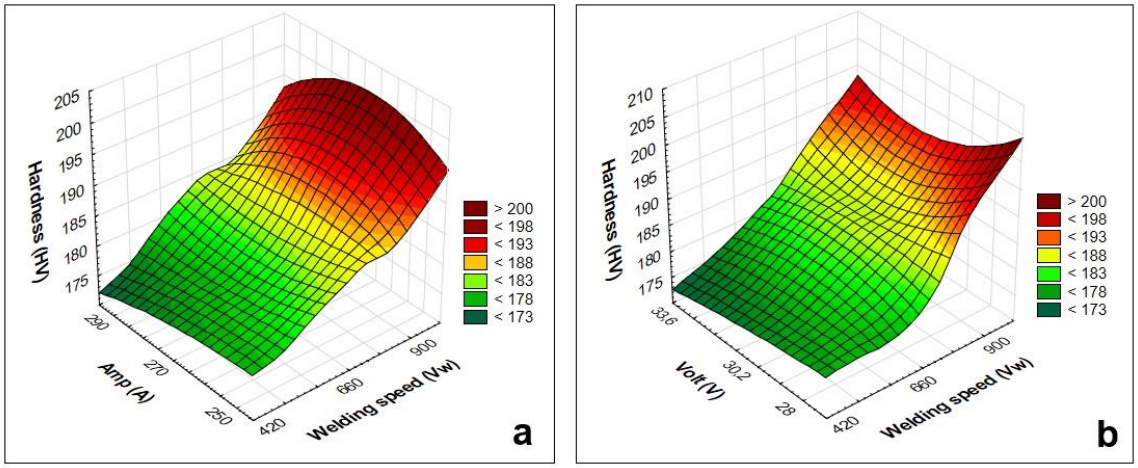

Figure 8. Effect of test parameters on hardness (Test parametrelerinin sertlik üzerindeki etkisi)

In Figure 8a, the effect of amperage and welding speed on hardness is given with a three-dimensional graphic. Here, it is seen that the hardness increases as the welding speed increases. In Figure 8a, it is seen that the best result is 420 mm/min welding speed and 290 A amperes. This result is similar to Taguchi's optimized values. In Figure 8b, a three-dimensional graph showing the effect of volt and welding speed on hardness [26]. Here, it is seen that the hardness increases as the welding speed increases. Figure 8b shows the best results at 33.6 Volts and 420 mm/min welding speed. This situation is similar to Taguchi's optimized values.

4. CONCLUSIONS (SONUÇLAR)

In this study, Taguchi optimization and finite element analysis of the lap welding of DD13 sheets used in the manufacture of automobile swing arms were performed. The data obtained as a result of experimental studies are listed below.

- It has been observed that DD13 sheets are joined together without any problems with the MAG welding method.
- This study successfully applied Taguchi optimization with a 95 % confidence interval. The R^2 value of the mathematical model obtained according to the regression results was calculated as 0.0995.
- As a result of the optimization process, it has been determined that the welding speed is the effective parameter with 94.16 % of the hardness in the weld seam. This parameter is followed by welding amperage with 3.008 % and welding voltage with 2.83 %.
- As a result of Taguchi optimization, the lowest hardness value was estimated as 172.98 $HV_{0.1}$ in MAG welding performed with 420 min/mm welding speed, 290 A, and 33.6 V parameters. The validation test result was found to be consistent with 173.4 $HV_{0.1}$.
- It was observed that the error between the validation experiments and the prediction values obtained by the Taguchi method was less than 20%. In this case, the results obtained with the validation experiments show that the optimization process has been carried out successfully.
- Finite element analysis has been successfully applied in this study. It has been seen that the estimated macro structure image and the natural source macro structure image are close to each other.
- As a result of the analysis, the estimated distortion value obtained after the welding process was seen as approximately 1 mm, while the actual distortion value was measured as 1.6 mm.

ACKNOWLEDGMENTS (TEŞEKKÜR)

Thanks to NETFORM Engineering Machinery Metal Ltd. for their support in the finite element analysis of this study.

REFERENCES (KAYNAKLAR)

1. L. Tang, J. Wu, J. Liu, C. Jiang, W.-B. Shangguan, Topology optimisation and performance calculation for control arms of a suspension, Advances in Mechanical Engineering, 6:1-10, 2014.
2. H.B. Zhang, R.J. Zhang, Y. Chang, Finite element analysis of automobile suspension control arm, Applied Mechanics and Materials, 752–753: 859–863, 2015.
3. H.B. Zhang, Y. Chang, R.J. Zhang, H.Y. Fan, Reverse modeling of vehicle suspension control arm, Applied Mechanics and Materials, 427–429: 1183–1186, 2013.
4. B.K. N, Design and analysis of sheet metal control arm, International Journal of Science and Research, 4 (11): 1241–1248, 2015.
5. James D. Halderman, Automotive Steering, Suspension & Alignment, 5. Edition, Pearson, New Jersey, 2010.
6. M. Bouazara, Improvement in the Design of Automobile Upper Suspension Control Arms Using Aluminum Alloys, Damage Fract. Mech., Springer Netherlands, Dordrecht, 101–112, 2009.
7. M. Shome, M. Tumuluru, Introduction to welding and joining of advanced high-strength steels (AHSS), in: M. Shome, M.B.T.-W. and J. of A.H.S.S. (AHSS) Tumuluru (Eds.), Woodhead Publishing, 1-8, 2015.
8. M.A. Wahab, Manual Metal Arc Welding and Gas Metal Arc Welding, in: S. Hashmi, G.F. Batalha, C.J. Van Tyne, B.B.T.-C.M.P. Yilbas (Eds.), Elsevier, Oxford, 49-76, 2014.
9. Z. Boumerzoug, C. Derfouf, T. Baudin, Effect of welding on microstructure and mechanical properties of an ındustrial low carbon steel, Engineering, 02: 502-506, 2010.
10. P. Kah, R. Suoranta, J. Martikainen, Advanced gas metal arc welding processes, The International Journal of Advanced Manufacturing Technology, 67: 655-674, 2013.
11. J. Frei, B.T. Alexandrov, M. Rethmeier, Low heat input gas metal arc welding for dissimilar metal weld overlays part I: the heat-affected zone, Welding in the World, 60: 459-473, 2016.
12. V. Tandon, M.A. Thombre, A.P. Patil, R. V. Taiwade, H. Vashishtha, Effect of heat ınput on the microstructural, mechanical, and corrosion properties of dissimilar weldment of conventional austenitic stainless steel and low-nickel stainless steel, Metallography, Microstructure, and Analysis, 9: 668-677, 2020.
13. S. Madhavan, M. Kamaraj, B. Arivazhagan, A comparative study on the microstructure and mechanical properties of fusion welded 9 Cr-1 Mo steel, J. Mater. Res. Technol., 9: 2223-2229, 2020.
14. U. Çaligülü, H. Dikbaş, M. Taşkin, Microstructural characteristic of dissimilar welded components (AISI 430 ferritic-AISI 304 austenitic stainless steels) by CO2 laser beam welding (LBW), Gazi University Journal of Science, 25: 35-52, 2012.
15. S. Selvi, A. Vishvaksenan, E. Rajasekar, Cold metal transfer (CMT) technology - An overview, Defence Technology, 14: 28-44, 2018.
16. R. Talalaev, R. Veinthal, A. Laansoo, M. Sarkans, Cold metal transfer (CMT) welding of thin sheet metal products, Est. J. Eng., 18: 243, 2012.
17. M. Grzybicki, J. Jakubowski, Comparative tests of steel car body sheet welds made using CMT and MIG/MAG methods, Welding International, 27: 610-615, 2013.
18. M. Korzeniowski, T. Piwowarczyk, P. Kustroń, A. Czubak, Low-energy welding methods used for semi-automatic thin-walled automotive steels, Advances in Materials Science, 13(3): 2013.
19. Y. Liu, L. Zhang, Y. Chen, Application of Cold Metal Transition Technology in Automobile Manufacture, in: Proc. 2018 7th Int. Conf. Energy, Environ. Sustain. Dev. (ICEESD 2018), Atlantis Press, Paris, France, 1170-1173, 2018.
20. J. Subramanian, S. Ganguly, W. Suder, D. Mukherjee, Investigation of functional and aesthetic quality of weld for different arc modes in CMT, Int. Res. J. Eng. Technol., 07: 4497-4502, 2020.
21. B. Chen, W. Xiao, L. Zhu, F. Zhang, Analysis on the Microstructure and Mechanical Properties of Welding Joint of Low Alloy Structural Steel Plate by Narrow Gap MAG, Proc. Int. Conf. Mechatronics, Electron. Ind. Control Eng., Atlantis Press, Paris, France, 2015.
22. G. Samtaş, S. Korucu, Multiple optimisation of cutting parameters in milling of cryogenically treated Aluminium 6061-T651 alloy with cryogenic and normal cutting inserts, Surface Topography: Metrology and Properties, 9: 2021.
23. H.R. Ghanbari, M. Shariati, E. Sanati, R. Masoudi Nejad, Effects of spot welded parameters on fatigue behavior of ferrite-martensite dual-phase steel and hybrid joints, Eng. Fail. Anal., 134: 106079, 2022.
24. A.K. Pattanaik, S.N. Panda, K. Pal, D. Mishra, A comparative investigation to process parameter optimization for spot welding using Taguchi based grey relational analysis and metaheuristics, Mater. Today Proc., 11408–11414, 2018.

25. G. Samtaş, Optimisation of cutting parameters during the face milling of AA5083-H111 with coated and uncoated inserts using Taguchi method, International Journal of Machining and Machinability of Materials, 17: 211–232, 2015.
26. V. Onar, Robotik MAG kaynak metodunda XAR 500 serisi çeliklerin mikrosertliğine farklı kaynak akımlarının ve hızlarının etkisi, Düzce Üniversitesi Bilim ve Teknoloji Dergisi, 8(1): 1193-1203, 2020.

İmalat Teknolojileri ve Uygulamaları
Cilt: 3, No: 3, 2022 (31-43)
Derleme Makale
e-ISSN: 2717-7475

Manufacturing Technologies and Applications
Vol: 3, Issue: 3, 2022 (31-43)
Review Article
e-ISSN: 2717-7475

Paslanmaz Çeliklerin Farklı Akımlarda MİG Kaynak Yöntemiyle Birleştirilmesinin İncelenmesi

Ebrar Karakaya[1], A. Fulin Köseoğlu[1]

[1]*Düzce Üniversitesi, Mühendislik Fakültesi, Makine Mühendisliği Bölümü, Düzce, Türkiye*

MAKALE BİLGİSİ

Alınma: *21.11.2022*
Kabul: *07.12.2022*

Anahtar Kelimeler:
Double pulse
Pulse
MIG
Gazaltı kaynağı

ÖZET

Bu çalışmada paslanmaz çeliklerin pulse (P-GMAW) ve double pulse (DP-GMAW) kullanılarak gazaltı MIG (Metal Inert Gas) yöntemi ile birleştirilmesi araştırılmıştır. Kaynaklı birleştirilmelerin mekanik özelliklerini belirlemek için sertlik ölçümü, çekme deneyi ve mikroyapıda oluşan değişiklikleri tespit etmek amacıyla mikroyapı çalışmaları incelenmiştir. Bu testler sonucunda MIG kaynak yönteminin diğer kaynak yöntemleri ile karşılaştırıldığında yüksek verimliliğe, daha iyi nüfuziyete ve daha az sıçrama özelliklerine sahip olduğu için endüstride yoğun bir şekilde kullanıldığı saptanmıştır.

Investigation of Joining Stainless Steels with MIG Welding at Different Currents

ARTICLE INFO

Received: *21.11.2022*
Accepted: *07.12.2022*

Keywords:
Double pulse
Pulse
MIG
Arc welding

ABSTRACT

In this study, the joining of stainless steels using pulse (P-GMAW) and double pulse (DP-GMAW) gas metal arc MIG (Metal Inert Gas) method was investigated. In order to determine the mechanical properties of welded joints, hardness measurement, tensile test and microstructure studies were examined to determine the changes in the microstructure. As a result of these tests, it has been determined that MIG welding method is used intensively in the industry as it has high efficiency, better penetration and less spatter compared to other welding methods.

1. GİRİŞ (INTRODUCTION)

Kaynak, dövme, döküm ve perçinli eklemler yerine sıklıkla kullanılmaktadır [1]. Endüstriyel ortamlarda, delici, kesici ve şekil verici olarak kullanılmakta olan metal parçalarının (öğütücü parçalar, kalıplar, pres, matkaplar, haddeler vs.) çalışma alanları sertliğe ve fazla ısı dayanımına sahip olmalıdır. İlaveten teknolojinin gün geçtikçe ilerlemesi ile birlikte iş parçalarının korozyon, yorulma ile aşınma dayanımlarının da arttırılması beklenilmektedir. Bu beklenti beraberinde, geliştirilmekte olan proseslerin ekonomik ve ekolojik dengeye zarara sokmayan teknolojiler olması istenilmektedir[2].

Ülkemizde paslanmaz çeliklere olan ihtiyaç endüstrinin gelişmesiyle günden güne artmaktadır [3]. Paslanmaz çelikler östenitik, ferritik, martenzitik, çift fazlı, çökelme yolu ile sertleşmeli paslanmaz çelikler olmak üzere 5 türe ayrılmaktadır. Paslanmaz çeliklerin bir türü olan östenitik paslanmaz çelik diğer çelik türlerinin içinde %70'lik oranla en fazla yararlanılan çelik türüdür [4]. Östenitik paslanmaz çelikler içerisinde; yüksek mukavemet, korozyona karşı direnç, kaynaklanabilme özelliği ile birlikte iyi biçimlendirilme özelliğine sahiptir. AISI 304 kalite östenitik paslanmaz çelikler bu nedenle yoğun bir şekilde uygulanmaktadır [5]. Şekil 1'de paslanmaz çeliklerde kullanılan Schaeffler ve Delong diyagramları görülmektedir [6]

Sorumlu yazar, e-posta: *ebrarkarakaya52@gmail.com*
To cite this article: *E. Karakaya, A.F. Köseoğlu, Investigation of Joining Stainless Steels with MIG Welding at Different Currents, Manufacturing Technologies and Applications, 3(3), 31-43, 2022.*
https://doi.org/10.52795/mateca.1207819,

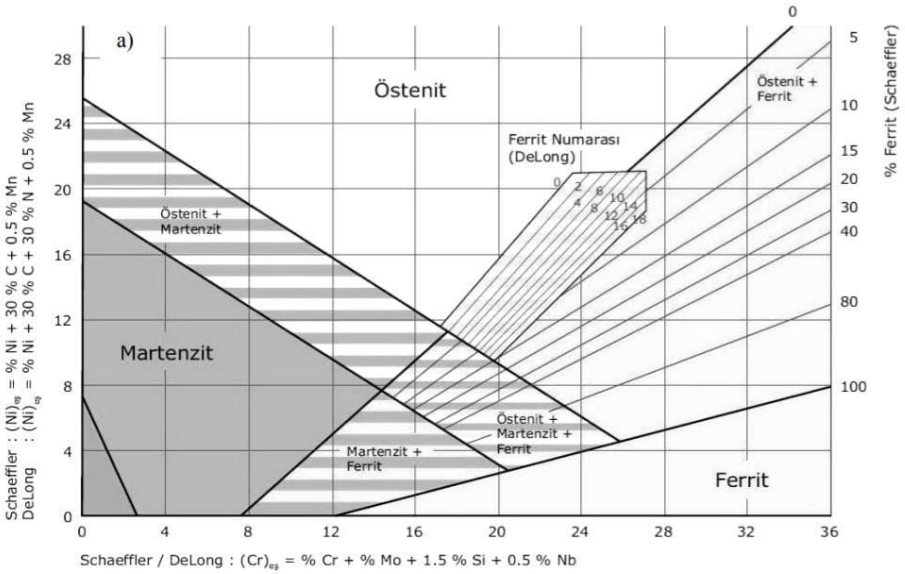

Şekil 1. Schaeffler ve Delong diyagramları (Schaeffler and Delong diagrams)

Günümüzde malzemeleri birleştirmek için kullanıldığımız pek çok kaynak yöntemi vardır [7]. Demir ve demir dışı metallerin ve alaşımlı çeliklerin kaynaklanmasında yaşanan problemler ile birlikte yeni kaynak yöntemleri geliştirilmiştir. TIG/MIG kaynak türleri de bu sebepten dolayı geliştirilmiş kaynak yöntemleridir [1]. MIG kaynak yöntemi ile çok ince yapıya sahip sac levhalarla birlikte neredeyse her kalınlıkta demir esaslı, demir dışı metal ve metal alaşımlarının kaynağı mümkün olabilmektedir [8]. Koruyucu gaz atmosferinden kaynak bölgesine iletilen dolgu metaline sahip bir ark kaynak yöntemi olan MIG kaynağı, dolgu metalini kaynak havuzuna direkt olarak iletilir [9]. Demir ve demir dışı malzemelerin kaynağında yoğun bir şekilde tercih edilen MIG kaynağı; daha az sıçrama, yüksek üretkenlik, daha iyi nüfuz olma gibi özellikleri ile diğer kaynak yöntemlerinden daha avantajlı olmaktadır. Demir-demir dışı malzemelerin kaynağında da yoğun bir şekilde tercih edilmektedir[10].

Endüstride demir ve demir dışı malzemelerin kaynağında en çok tercih edilen kaynak yöntemi gaz metal ark kaynağıdır [11]. Gazaltı kaynağında kaynak için gerekli olan ısı, ergiyen ve sürekli beslenen tel elektrot ile parça arasında oluşan ark yoluyla elektrottan geçen akımın direncinin ısınmasıyla üretilir. Kaynak için kullandığımız tel ark bölgesine direkt olarak beslenir, ergir ve kaynak metalini (depozit) oluşturur [12]. Gaz altı ark kaynağında kullanılan ark boyu, kaynak makinesi tarafından kontrol edilmektedir. Kaynakçının gaz memesini kaynak banyosu üzerinde sabit tutulan mesafede bulundurarak belirli hızda hareket ettirmesi beklenilir [13]. Kaynak makinası ark boyunu kontrol ettiği için bu yönteme "yarı otomatik" kaynak yöntemi ismi verilmiştir [14]. Gaz altı kaynağı yapıldığı sırada koruyucu gazdan beklenilen iyi metal transferi, yüzeye dahi iyi bir nüfuziyet, kaynak geometrisi, ergime genişliği, kaynak hızı ile birlikte düşük maliyetli olmasıdır.

Aynı zamanda çatlaklar ve gözenekler oluşturmamalıdır. Otomatik olmayan kaynak işlemlerinde, önemli ve test edilmesi gerekli olan parametreler (kaynak amperi, kaynak hızı, kaynak teli türü, kullanılan koruyucu gazlar ve malzeme türü gibi parametreler) bulunmaktadır. Alaşımsız çelikler, yüksek mukavemete sahip olan az alaşımlı çelikler, alüminyum ve alaşımları, paslanmaz çelikler, titanyum, bakır ve nikel alaşımları gibi ticari önemi yüksek bütün metaller metal türüne uygun olacak şekilde koruyucu gaz, elektrod ve kaynak değişkenlerini belirlemek koşuluyla bu kaynak yöntemiyle kaynak edilebilirler [15].

Pulse, elektron ışını malzemelerin mikroyapısıyla faz kompozisyonunu değiştirerek alan niteliklerini ilerletmesini sağlayan kaynaktır [16]. Bu teknoloji, saf tabaka oluşumuna nedendir [17]. Yaptığımız araştırmada endüstride sıklıkla kullanılan, östenitik paslanmaz çelik (AISI 304) ve çelik malzemelerin(düşük karbonlu), farklı üç kaynak akımı (70 A, 80 A ve 90 A) kullanarak MIG kaynak yöntemiyle birleştirilme işlemi incelenmiştir [18].

Ayrımlı malzemelere gerçekleştirilen kaynak akımının, kaynak yapılan bölge üzerindeki tesirlerini tespit etmek amacıyla birleştirilen malzemelere, eğme, çekme, çentik darbe ve mikrosertlik testleri yapılmıştır. Kaynaklı aktarmalar üstünde mikroyapı sonuçları elde edilmiştir [5]. Paslanmaz çelikler double pulse ve pulse ile birleştirilmesi araştırılmıştır [19]. Numunelerin tahribatlı testleri incelenmiştir.

2. MATERYAL VE YÖNTEMLER (MATERIAL AND METHODS)

2.1. Malzeme (Material)

Araştırılan deneysel çalışmalarda kullanılan çeliklerin kimyasal bileşimleri Tablo1'de, mekanik özellikleri Tablo 2'de, kaynak parametreleri ise Tablo 3'de gösterilmiştir [20]. Şekil 2'de şematik olarak gazaltı kaynağı ve kaynak esnasında metal transferi verilmiştir [21]. Şekil 3'de ise gazaltı terminolojisi ve ark gerilim oluşumu ve düzenlenmesi verilmiştir. Şekil 4'te darbe akım oluşumu ve gazaltı kaynağında kullanışı görülmektedir.

Tablo1. Deneyde kullanılan numunelerin kimyasal bileşimleri (Chemical compositions of the samples used in the experiment)

Sınıf	%C	%Mn	%Si	%P	%S	%Cr	%Ni	%Mo	%Cu
AISI 304	0.08	2	0.75	0.045	0.03	18.35	8.12	0.07	0.23
S235JR	0.170	1.40	0.3	0.035	0.035	-	-	-	0.550

Tablo2. Deneyde kullanılan numunelerin mekanik özellikleri (Mechanical properties of the samples used in the experiment

Sınıf	Isıl İşlem Şartı	Çekme Dayanımı (daN/mm^2)	Kesit Daralması	Uzama (%)	Akma Dayanımı (daN/mm^2)	Sertlik (Rockwell)
AISI 304	Tavlı	586	65	55	241	B80
S235JR	Tavlı	340-470	-	25	235	137HV0

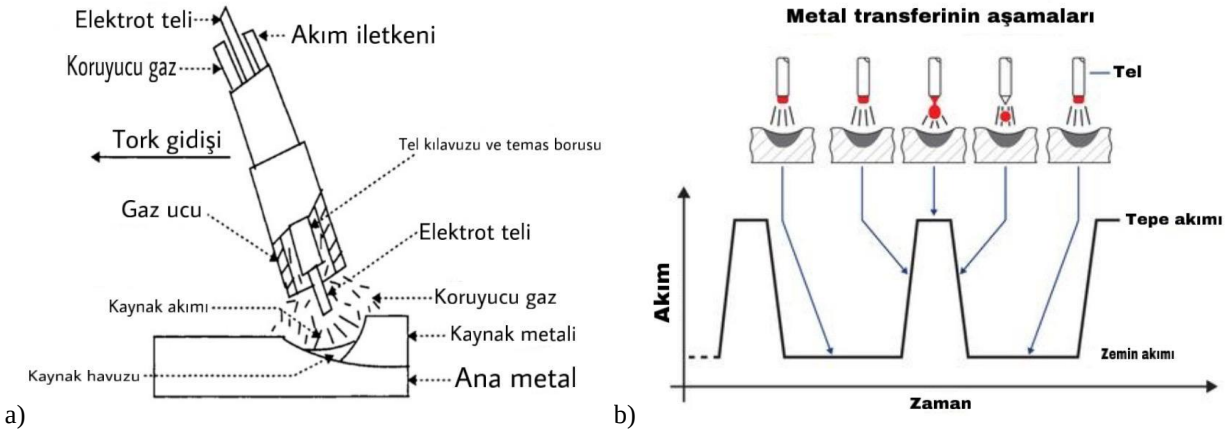

a) b)

Şekil 2. a) Gaz metal ark kaynağı işleminin basit şeması, b) Metal transferi (a)Simple schematic of gas metal arc welding process, b) Metal transfer)

Tablo 3. Kaynak işlemlerinde kullanılan kaynak parametresi (Welding parameter used in welding processes)

Kaynak Yöntemi	Kaynak Akımı (*A*)	Kaynak Hızı (*cm/dak*)	Isı Girdisi (*kJ/mm*)	Kullanılan Gaz	Ek Metal Çapı (*mm*)	Akım Türü
MIG	85	9.5	0.72	Argon (%85) ve CO^2 (%15)	0.8	DC (+)

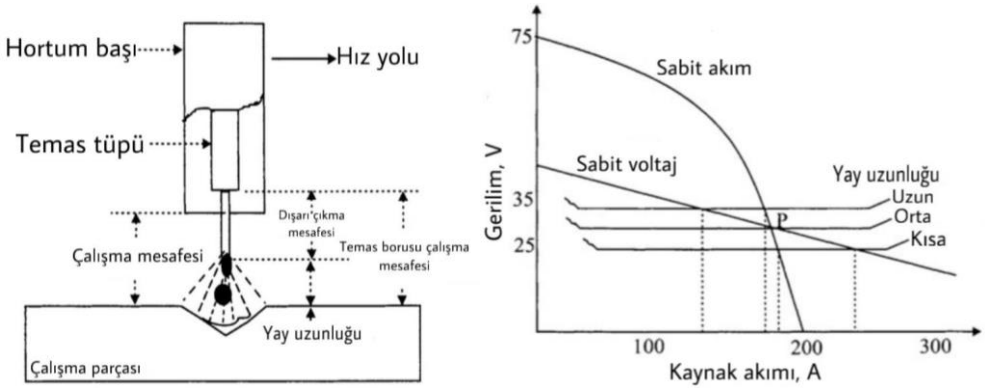

a) b)

Şekil 3. a) Gaz metal ark kaynağı terminolojisi, b) Ark geriliminin otomatik regülasyonu [18] (a) Gas metal arc welding terminology, b) Automatic regulation of arc voltage)

Ark boyunca ark gerilimi yay uzunluğu ile doğrudan orantılıdır. Bu sebeple ark gerilimi yay uzunluğu değiştirilerek kontrol edilir [22]. Bir ark voltajı eğrisinin voltaj kaynağı eğrisi ile kesişimi güç kaynağının çalışma noktası olarak adlandırılmaktadır. Kaynak işlemi sırasında çalışma noktası sürekli değişebilmektedir [21].

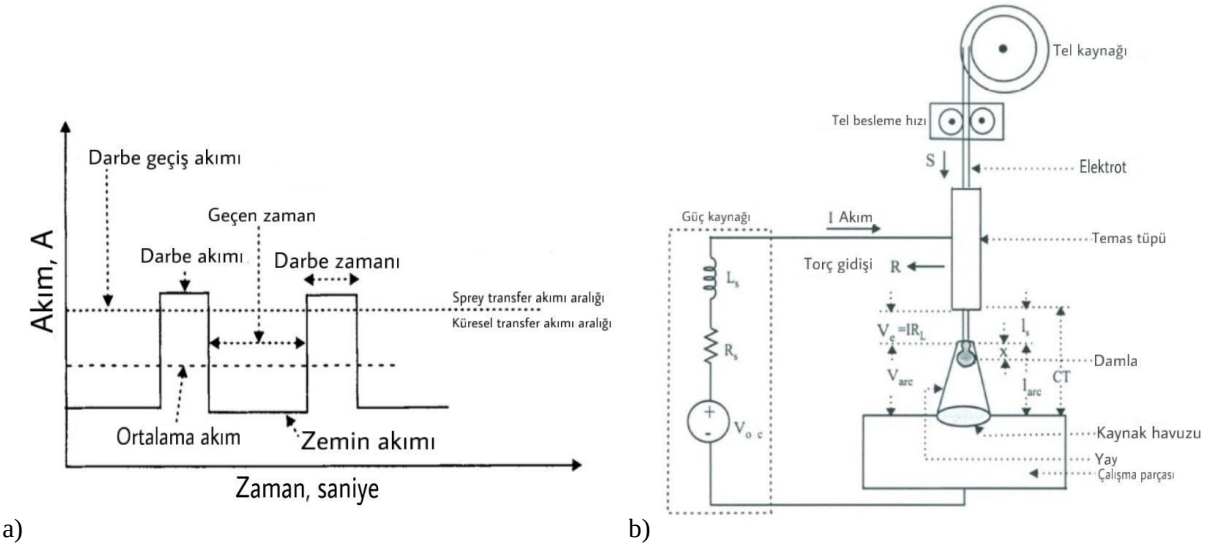

a) b)

Şekil 4. a) Metal aktarımı için darbe akımı, b) MIG işleminin şeması [21] (a) Pulse current for metal transfer, b) Diagram of MIG process)

Bir araştırmada, gazaltı kaynak teknolojilerinin (MIG ve P-MIG) mekanik özellikler ve mikroyapı üzerindeki etkileri analiz edilmiştir. AISI 304 paslanmaz çelik bir boruya uygulanan kaynaklı birleştirmede Tablo 4'te verilen kaynak metalleri kullanılmıştır. Şekil 5'te, gazaltı kaynak teknolojisiyle üretilen numunelerden alınan mikroyapı görüntüleri verilmiştir. P-MIG yönteminin kullanılmasıyla homojen dağıtılmış bir mikro yapı elde edilmiş olup (Şekil 5), aynı zamanda çekme dayanımı ve başlangıç kırılma tokluğu artarken kaynaklı bağlantındaki kalıntı gerilmeler azalmıştır [23].

Tablo 4. Kaynak metalinin kimyasal analizi ve δ -Ferrit içeriği (Chemical analysis of weld metal and δ-Ferrite content)

	Kaynak Metalinin Kimyasal Analizi (*Wt.*)										Eş Değerler		δ-Ferrit İçeriği (%)	
Kaynak Tel	**C**	**Cr**	**Ni**	**Mn**	**N**	**Mo**	**Si**	**Cu**	**S**	**P**	**Cr_{eq}**	**Ni_{eq}**	**Est.**	**Obs.**
MIG	0.024	19.1	9.4	1.6	0.1	0.14	0.38	0.14	0.013	0.02	19.3	12.3	6-8	7
P-MIG	0.029	19.1	9.35	1.56	0.1	0.14	0.46	0.2	0.012	0.01	19.3	12.4	6-8	6

a) 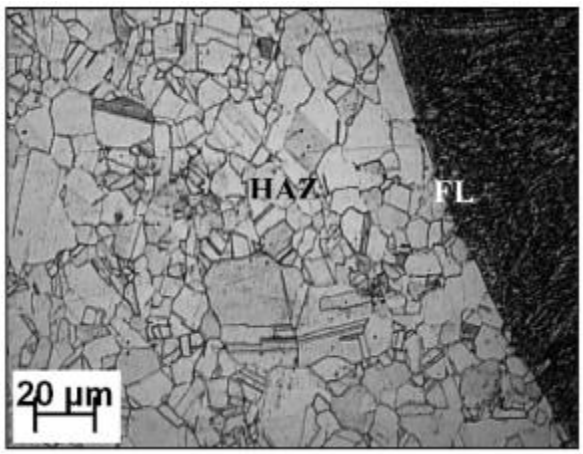

b) 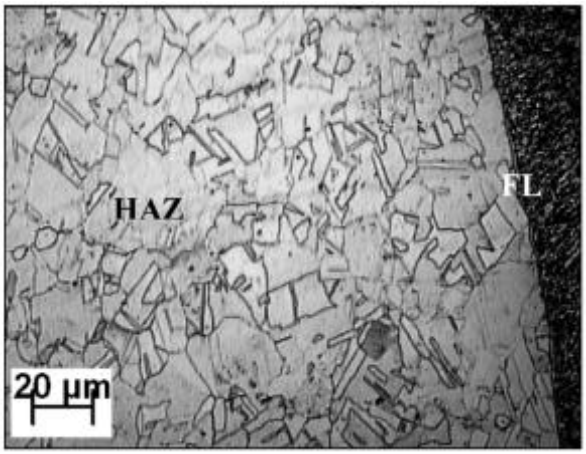

Şekil 5. Mikroyapı görüntüleri; a) MIG, b) P-MIG (Microstructure images; a) MIG, b) P-MIG)

2.2. İlave Telin Önemi (Importance of Additional Wire)

Çeliklerin birleştirilmesinde (MIG) argon gazına oksijen ve karbondioksit karıştırılır. Böylelikle oksijen hafif erime özelliğine sahip oksitlerin meydana gelişini hızlandırmakla birlikte ergiyen elektrod ilave telden akan damlaların yüzey gerilimini zayıflatır ve ince taneli metal geçişini sağlar. Oksijenin oksitleme özelliği, uygulanan kaynak telinde bulunan silisyum, alüminyum, mangan, titanyum, kükürt ve krom gibi alaşım elementlerinin arttırılmasıyla oluşur [24].

2.3. Koruyucu Gazın Önemi (Importance of Shielding Gas)

Yüzde yüz saf Ar, Ar ve CO_2 karışımları, Ar ve O_2 karışımları ile duru CO_2 gazı çeliklerin kaynağında kullanılmaktadır (Tablo 5). Damlaları, kaynak banyosunu ve ısı tesiri altında kalan bölgeyi ve kaynak arkı hareketlerini iyileştirmek gazların görevidir [25]. MIG kaynağında kullanılmakta olan gaz karışımlarında argonun rastgele reaksiyona katılmayacağı bu sebeple ark oluşumu ile kararlılığının daha hafif olacağı saptanmıştır. CO_2'in ise ergimiş banyoyu oksitleyeceği, tüm durumlarda kısa devre kaynağını hafifleştirici ve sağlam geçişi hazırlayacağı seçilmiştir. CO_2'in sıçramasının fazla olmasından dolayı CO_2 ve O_2'in karıştırılmasıyla akımın azalarak kaynak formunun ve akışının düzelmesi, sıçramanın düşeceği, kaynak getirisinin yükseleceği görülmektedir [26]. Daha önceden yapılan çalışmaların neticeleri incelenmiş ve buna göre CO_2, Ar ve O_2 karışımı gazlar kullanılmasının daha net sonuçlar vereceği saptanmıştır [27].

Tablo 5. Koruyucu gazların karışım oranı (Mixing ratio of shielding gases)

Karışım Gaz	Karışım Oranı (%)		
	Ar	CO_2	O_2
S1 ($80Ar+18CO_2+2O_2$ karışımı)	80	18	2
S2 ($88Ar+10CO_2+2O_2$ karışımı)	88	10	2
S3 ($93Ar+5CO_2+2O_2$ karışımı)	93	5	2

2.4. Gazaltı Kaynağına Etki Eden Parametreler (Parameters Affecting Gas Welding)

2.4.1. Ark gerilimi (Arc voltage)

MIG kaynağı ve örtülü elektrot ark kaynağında pek çok sebep sıçrantı oluşumuna sebebiyet vermektedir. Bu sebepler; kaynak ilerleme hızı, kaynak akım şiddeti, ark gerilimi, tel sürme hızı, serbest tel uzunluğu, kullanılan elektrota ait kimyasal bileşimi, koruyucu gazın cinsi, bağlanılan kutup ve gaz debisidir [28]. Yapılan çalışmalarda ark kaynağında, örtülü elektrotta ve MIG kaynağında akım şiddetinin yükselmesi kaynak metaliyle sıçrantının arttığını göstermektedir. Şekil 6 ve 7'de kaynak esnasında farklı amperlerin kaynak dikişlerine etkileri gösterilmiştir.

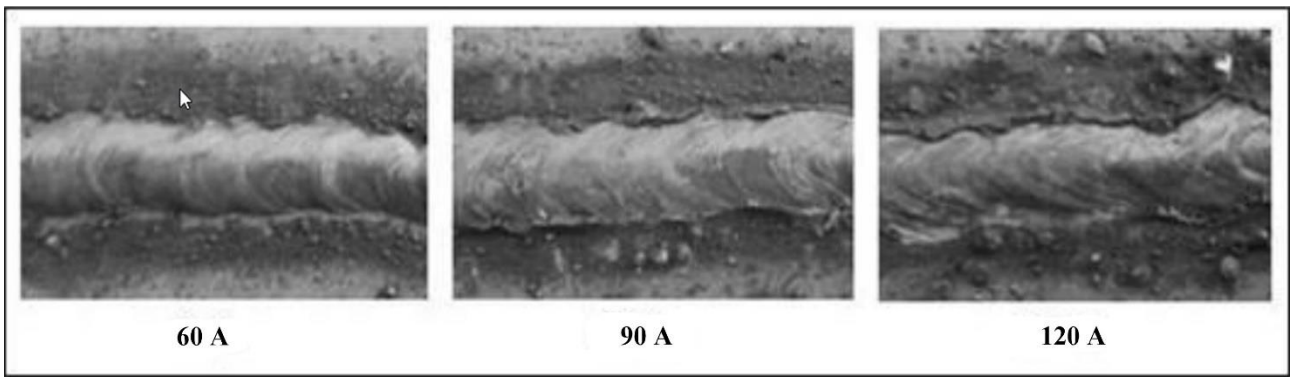

Şekil 6. Örtülü elektrotla birleştirilen kaynak dikişlerine ait yüzey görünümü [28] (Surface view of weld seams joined with covered electrode)

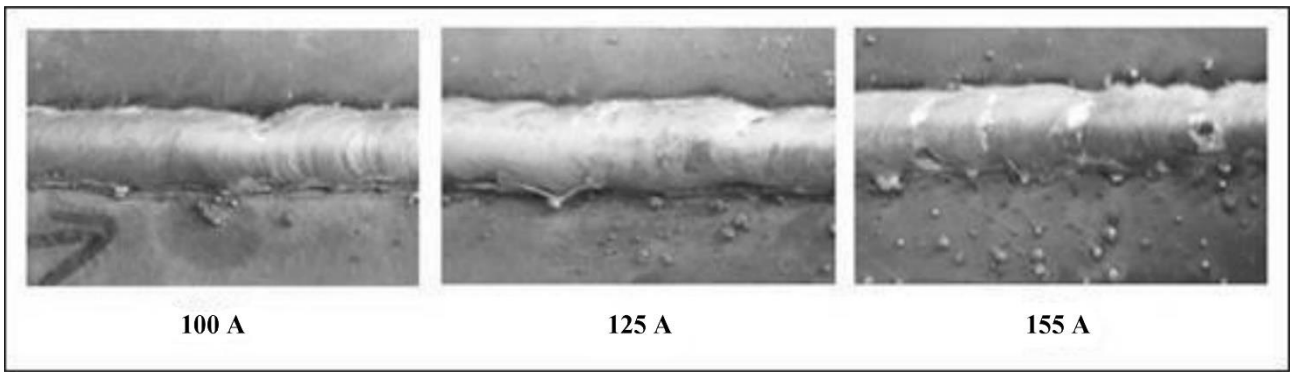

Şekil 7. MIG kaynağıyla yapılan kaynak dikişlerine ait yüzey görünümü [28] (Surface view of weld seams made with MIG welding)

2.4.2. Tel hızı (Wire speed)

Yapılan kaynakta kullanılan akım şiddetinin, kaynak dikiş biçimine ve boyutlarına, ergimeye ve nüfuziyete etkisi diğer bütün parametrelere göre daha şiddetlidir. Sabit gerilimli sistemli olan gazaltı ark kaynak makinelerinde kaynak akım şiddeti tel hızı ile beraber tel hız ayarı düğmesinden ayarlanır [29].

2.4.3. Kaynak hızı (Welding speed)

Sabit kaynak parametrelerinde kaynak hızının arttırılması dikişin kesitini küçülten etmendir. Daha yüksek kaynak hızında aynı dikiş geometrisine sahip olmak için kaynak gerilimi ile birlikte tel hızının da arttırılması gerekmektedir. Kaynağı yapan kişi hızı isteğe bağlı olarak seçemez. Elle kaynak kullanımında 40-60 cm/dak'lık kaynak hızları orantılıdır, fazla yüksek hızlarda kaynakçı üfleci elle biçimli hareket ettirmekte zorlanır. Mekanize olanlarda ise hız yükseltilebilir. Kaynak hızı aşırı fazlaysa kaynak dikişi dışbükey şeklinde olmakla beraber darlaşır. 1-1.5 m/dak kaynak hızları seri üretimlerde kullanılmaktadır. 40 cm/dak'lık hızın altına düşüldüğünde, arkın önüne akan kaynak banyosu nüfuziyeti önemli miktarda düşürülebilir ve birleşme yanlışlığına sebebiyet vermektedir [25]. Şekil 8'de kaynak hızlarının, dikiş nüfuziyetlerine oranları şematik olarak gösterilmiştir.

2.4.4. Elektrot çapı (Electrode diameter)

Çapa bağlı akım şiddeti aralığı her tür elektrot için bulunmaktadır. Geniş çaplı elektrodlar fazla akım şiddetiyle kullanılabildikleri için daha yüksek bir ergimeye sahiptirler böylelikle daha derin nüfuziyete sahip dikişler biçimlendirip ortaya çıkarırlar. Ergime de akım yoğunluğuna ait fonksiyondur [29].

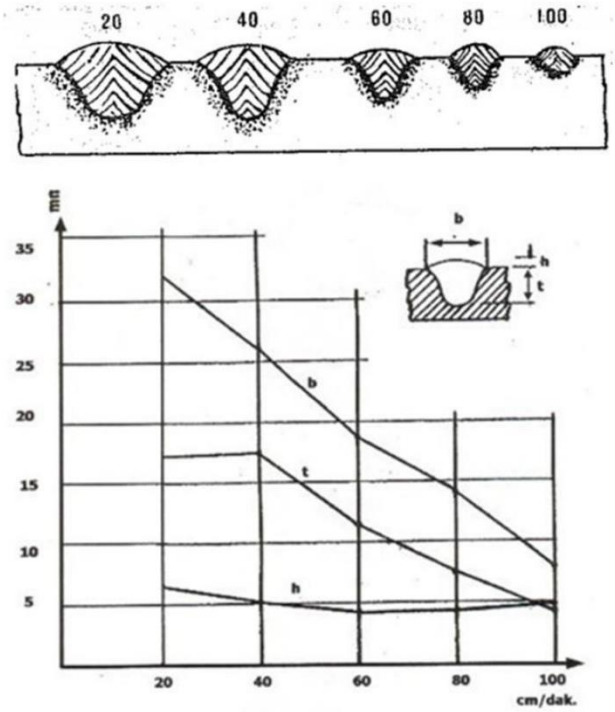

Şekil 8. Kaynak hızının nüfuziyet derinliğine etkisi (Effect of welding speed on penetration depth)

2.4.5. Koruyucu gaz türü (Shielding gas type)

Teknolojinin ilerlemesiyle soy gazlar koruyucu gaz olarak kullanılmaya başlamıştır. Bu soy gazlara örnek olarak da argon ve helyum verilebilir. Soy gazlara ek olarak CO_2 gibi aktif gazlar da kullanılmaya başlanmış aynı zamanda argonla beraber belirli oranlarda karıştırılarak kullanılmıştır [29]. Şekil 9'da koruyucu gazların kaynak nüfuziyetlerine olan etkileri verilmiştir.

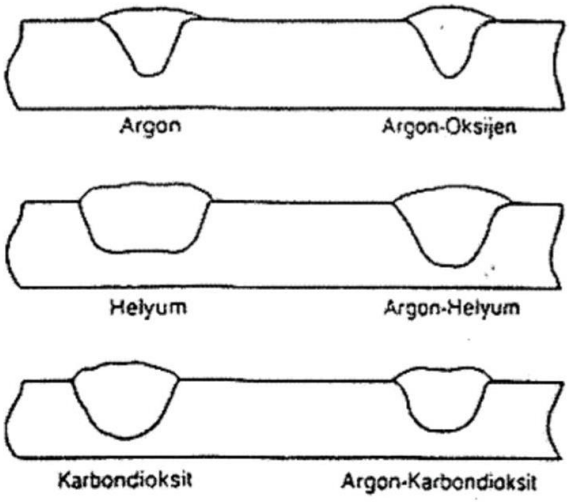

Şekil 9. Çeşitli koruyucu gaz türlerinde bulunan kaynak dikişinin şematik gösterimi (Schematic representation of the weld seam in various shielding gas types)

2.5. Tel Erime Hızı ve Akım Şiddeti Arasındaki Risk (Risk Between Wire Melt Rate and Current Intensity)

2.5.1. Kaynak geriliminin etkisi (Effect of welding voltage)

Ark ve kaynak gerilimi, elektrod ucu ile iş parçası arasındaki mesafeye göre belirlenir. Nüfuziyeti yükselen ark gerilimi ile birlikte en uygun değere kadar artış gösterir ve bundan sonra azalır. Yüksek ark gerilimi, nüfuziyetin azlığı sebebiyle birkaç geniş aralıklarda bağlantı kurabilmek amacıyla uygulanır. Fazla küçük ark gerilimi, şişkin ve fazla dar kaynak dikişlerinin

biçimlenmesine neden olmaktadır. Aşırı küçük ark gerilimleri ise gözenek oluşumuna sebep olmaktadır [25]. Şekil 10'da verilen diyagrama göre farklı ark gerilimlerine göre kaynak dikişi genişlikleri değişiklik göstermektedir [30].

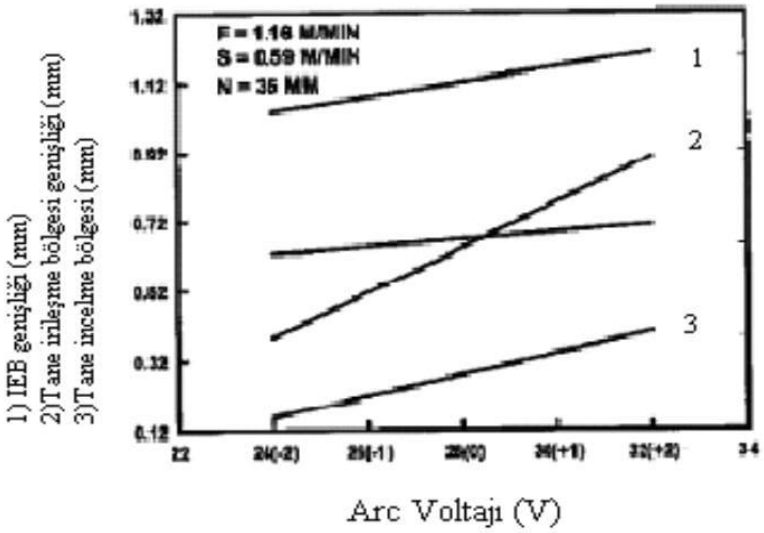

Şekil 10. Ark geriliminin kaynak genişliğine etkisi (Effect of arc voltage on welding width)

2.5.2. Kaynak hızının etkisi (Effect of welding speed)

Kaynak hızını yarı otomatik yöntemlerde kaynakçı, otomatik yöntemlerde ise makineler tarafından ayarlanır. Maksimum derin nüfuziyet, kaynak hızının en yüksek olduğu değerde elde edilir. Bu hızın yavaşlaması veya artması hallerinde ise nüfuziyet azalır [25]. Şekil 11'de sabit akım gücü için volt-amper eğrileri verilmiştir [21]. Akım ve ark gerilimin sabit tutulduğu bir araştırmada, optimum kaynak hızına ulaşılana kadar penetrasyonun artacağı sonucuna varılmıştır. Ancak, hızı bu optimum değerin üzerine çıkarmak penetrasyonun azalmasına neden olacaktır (Tablo 6) [31].

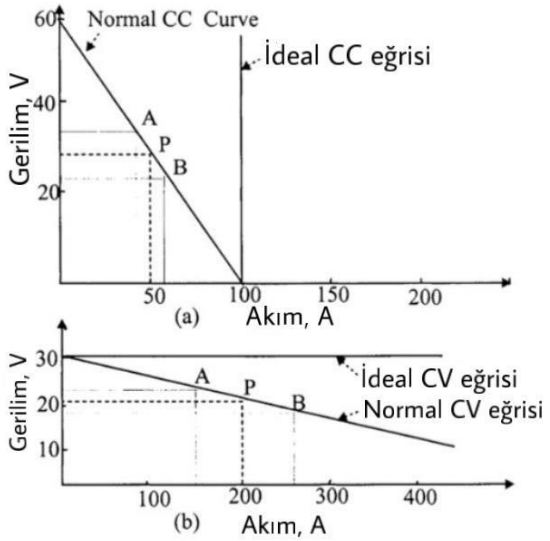

Şekil 11. a) Sabit akım gücü için volt-amper eğriler, b) Sabit gerilimli güç kaynaklar [21] (a) Volt-ampere curves for constant current power, b) Constant voltage power supplies)

Tablo 6. Akımın ve ark geriliminin sabit kalması durumunda kaynak hızının nüfuziyete etkisi (The effect of welding speed on penetration when current and arc voltage remain constant)

Sıra No	Akım (*A*)	Ark Gerilimi (*V*)	Ark Zamanı (*sn*)	Kaynak Hızı (*mm/dk*)	Isı Girdisi (*J/mm*)	Nüfuziyet (*mm*)
1	105	24	25.40	94.48	1600.30	4.3mm
2	105	24	23.60	101.43	1490.68	5.1mm
3	105	24	21.90	109.58	1379.81	5.3mm
4	105	24	21.74	110.39	1369.68	5.41mm
5	105	24	19.70	121.82	1241.17	3.7mm
6	105	24	18.47	129.94	1163.61	3.5mm
7	105	24	15.76	152.28	992.90	3.3mm
8	105	24	14.60	164.38	919.82	3.19mm
9	105	24	13.50	177.77	850.53	3.10mm

Şekil 12'de soğuk metal transferi (CMT), kaynak akımının polaritesinin ters çevrilmesi (CMT-ADV) ve elektrodun pozitif kutuplu olması (CMT-PADV) gibi kaynak uygulamalarında akım ve voltaj gerilimi değişimleri gösterilmiştir [32, 33].

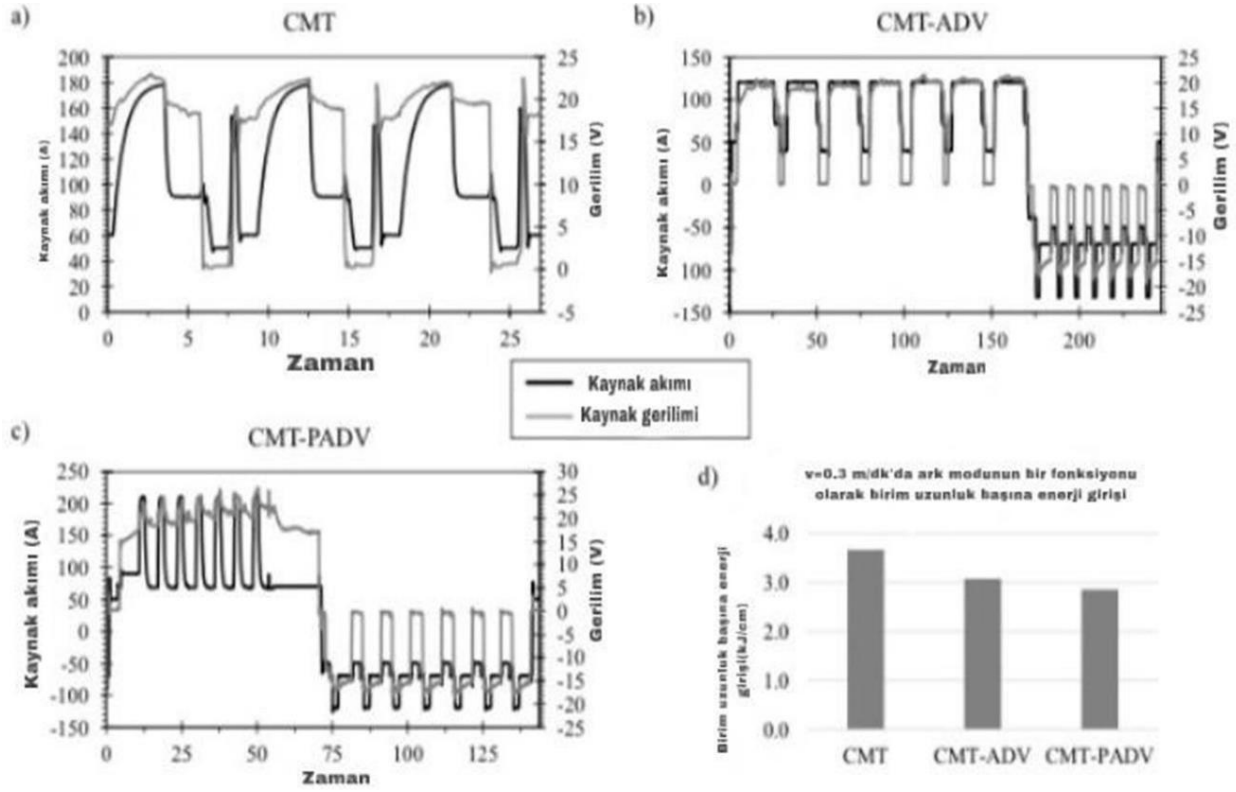

Şekil 12. a) CMT, b) CMT-ADV, c) CMT- PADV'nin akım ve gerilim özellikleri ve d) v = 0.3 m/dak kaynak hızında ark modunun bir fonksiyonu olarak birim uzunluğu başına enerji girişi

Burada, ölçülen tel besleme hızındaki hafif sapmalar, farklı ark modları ve kaynak güç kaynağının uygun entegre kontrolü ile açıklanmaktadır. Şekil 6b, CMT-ADV işleminin karakteristik bir özelliği olan hem pozitif hem de negatif polarite sırasında malzeme transferi kısa devre fazında gerçekleşir. Negatif polarite, pozitif polaritenin aksine, daha düşük ısı girişine rağmen biriktirme oranını artıran arklanma noktasını arttırır. Pozitif döngü sırasında, temel malzemeye daha fazla ısı verilir ve iş parçası yüzeyi alüminyum oksit tabakasından temizlenir. Şekil 6c'deki CMT-PADV işlemi, döngüsel tel hareketine sahip negatif kutuplu CMT döngülerinin ve sürekli tel beslemeli pozitif kutuplu puls döngülerinin kombinasyonunu göstermektedir. Burada yedi negatif kutuplu CMT döngüsü, pozitif kutuplu yedi puls döngüsünü takip eder. Darbe döngülerinde, malzeme transferi kısa devresizdir ve temel malzemeye daha yüksek bir ısı girişine izin verir. CMT-ADV sürecinden daha yüksek biriktirme hızlarına ulaşılabilir.

Deneysel araştırmalarda, MIG işlemi için sürekli akımın yaygın olarak kullanıldığı tespit edilmiştir. Darbeli akımın kullanılmasının ise WM mikroyapısını değiştirdiği ve kaynak için gereken ısı girdisini azaldığı görülmüştür. Aynı zamanda WM'nin tane inceltme işlemi, krom konsantrasyonunun azalmasına sebebiyet verdiği saptanmıştır.

3. BULGULAR VE TARTIŞMA (FINDINGS AND DISCUSSION)

Kaya ve ark. [5], çekme deneyinin kaynaklı numunelere uygulanması neticesinde ayrılma, kaynak bölgesinin dışında ve az karbonlu çelik levhalarda oluştuğu, yapılan eğme deneylerinde; kaynaklı numuneler her iki yönlü 180˚ eğildiklerinde izlenebilir birleştirme hatası olmadığı ve çentik darbe deneylerinde, kaynak metalinin darbe doyumluğu ITAB'lara göre daha fazla ölçüldüğü görülmüştür. Şekil 13'de farklı akım değerlerinin kaynak dikişi sertliklerine etkileri verilmiştir.

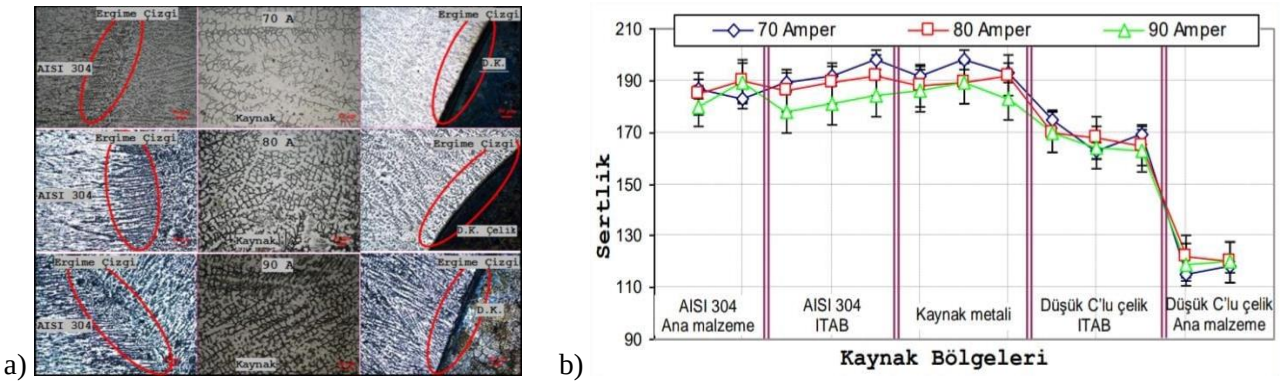

Şekil 13. a) Mikroyapı incelemeleri, b) Sertlik testi (a) Microstructure investigations, b) Hardness testing)

Yapılan sertlik ölçümlerine bakıldığında en yüksek sertlik, kaynak metalinde olmuştur. Mikroyapı incelemelerinde, ısı girdisine bağlı kalarak düşük karbonlu çelik ile paslanmaz çeliğin ITAB yerinde taneciklerin büyümesi görülmüştür. Isı girdisinin arttıkça tanecik büyümesinin çoğaldığı ve kaynak metaline ait taneciklerin ısı akış doğrultusunda yönlendikleri fark edilmiştir.

Yürük ve arkadaşları tarafından yapılan çalışmada [34], çekme testleri sonucunda kaynaklı bağlantıların farklı parametrelerde birleştirilmesiyle çekme mukavemeti ile % uzama büyüklüğü birbirlerine yakın olduğu görülmüştür. Kopmanın yakın olması yapılan deneylerin asıl malzemede uygulanmış olmasından kaynaklanmıştır. Sertlik ölçümlerine bakıldığında birleştirmenin iki tarafındaki ITAB ile kaynak metalinin sertliklerinin, iki önemli malzemeden fazla oluştuğu saptanmıştır (Şekil 14).

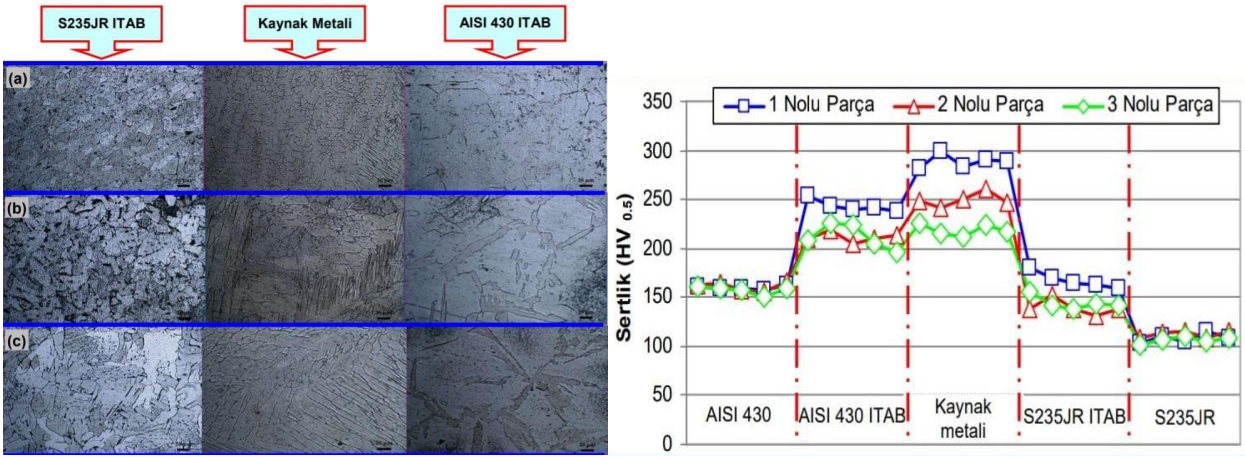

Şekil 14. a) Mikroyapı incelemeleri, b) Sertlik testi (a) Microstructure investigations, b) Hardness testing)

Topçu'nun yaptığı çalışmaya göre MIG kaynak yöntemi kullanılarak kaynak yapılan numunelerin çekme testleri incelendiğinde, en yüksek çekme dayanımının (678 MPa/662 MPa) MIG kaynağı ile birleştirmiş 304 paslanmaz numunelere ait olduğu görülmüştür. Kaynaklı numunelerin hepsinde kopma işlemi kaynak yapılan bölgede ve ITAB'ın dışında bulunan büyük

adetli bölgede yapılmıştır. Kopmanın ITAB bölgesinin dışında yer alması çalışmanın doğruluğunu kanıtlar niteliktedir. Optik mikroskop çalışması sonucunda, ergiyip katılaşan kaynak metalinin eş eksenli dendritik tanelerden meydana geldiği belirlenmiştir. Mekanik özelikler ile mikroyapı birbiri ile orantılı ilerlemektedir. Bu etkileri anlamak, çeliklerin performansının optimize edilmesi açısından çok önemlidir. Kaynak endüstrisinin yükselmesi ve mekanik özelliklerini geliştirecek malzemelerin incelenmesi sağlanacak şekilde doğrulanması öngörülmektedir. Bütün incelemeler neticesinde MIG kaynak yöntemi ile yapılan bütün kaynaklar TIG kaynak yöntemine nazaran daha iyi mekanik sonuçlar vermiştir. Bu sebeple genelde otomatik kaynak yöntemi ile toprak altı ana çelik boru hatlarında istenen mekanik özelliklere yanıt veren MIG (Metal Inert Gas) hem daha işlevsel hem de seri yönteme uygun olduğu için tercih edildiği saptanmıştır [1].

4. SONUÇLAR (CONCLUSIONS)

Yapılan makale inceleme çalışması sonucunda elde edilen veriler aşağıda sırasıyla verilmiştir.

- Yapılan deneylerde paslanmaz çeliklerin diğer çelik türlerine göre ısıyı iletme bakımından 4-7 kat daha fazla direnç gösterdiği için normal çelik kaynaklarına göre %20-25 oranında daha az akım şiddeti uygulandığı görülmüştür.
- Kolayca oksitlenen paslanmaz çelik, alüminyum gibi malzemelerin kaynağında MAG kaynağı tercih edilmemiştir. Bu nedenle MIG kaynak tercih edilmiştir. MAG kaynağı daha çok az alaşımlı ve alaşımsız çeliklerin kaynağında kullanılmıştır.
- Paslanmaz çeliklerin kaynağında yüksek ergime, derin nüfuziyet, her pozisyonda kaynaklanabilmesi, ara vermeden kaynak yapılabilmesi gibi özelliklerinden dolayı MIG kaynak tercih edilmiştir.
- Demir esaslı ile demir dışı metaller ve alaşımlarının kaynağında uygun koruyucu gaz, kaynak değişkenleri ve elektrot seçmek şartıyla kaynak yapılabilmesi, uygulamanın kolay olması, yarı otomatik bir kaynak yöntemi olması, ekonomik bir kaynak yöntemi olması, gerekli ekip ve donanım sağlandığında tam otomatik kaynak yapılması nedeniyle MIG kaynağı tercih edildiği görülmüştür.
- Çift darbeli kaynak, aynı ısı girişinde geleneksel darbeli kaynağa kıyasla artan bir katılaşma büyüme hızına ve soğuma hızına sahiptir. Çift darbeli kaynak tarafından rafine katılaştırma yapıları sayesinde geliştirilmiş katılaşma çatlama duyarlılığı elde edilmiştir.
- Yapılan deneyler incelendiğinde MIG kaynak yönteminin diğer kaynak yöntemlerine nazaran daha iyi nüfuziyet etkisine, daha az sıçrama özelliklerine ve yüksek verimliliğe sahip olmasından dolayı endüstride yoğun bir şekilde kullanıldığı saptanmıştır.
- Füzyon metalinin çift darbeli kaynak ile mikro yapısal arıtımı birkaç araştırmacı tarafından rapor edilmiştir. Mikro yapısal iyileştirme mekanizması, kaynak havuz karıştırma etkisinin ve artan soğutma hızının birleşik etkisi olarak ortaya çıkarmıştır. Sayısal ve deneysel sonuçlar bir ısı girdisini değiştirmek yerine darbe parametrelerini ayarlayarak rafine mikro yapı elde edilebilmesini göstermiştir.
- Yapılan incelemeler sonucunda AISI 304 ile düşük karbonlu çelik malzemelerin kaynağında sıklıkla MIG kaynak yöntemi yapıldığı görülmüştür.
- Eğme testleri sonucunda kaynaklı numuneler her iki yönden 180º eğildikleri zaman gözle görülür herhangi bir kaynak hatasına rastlanılmamıştır.

KAYNAKLAR (REFERENCES)

1. İ. Topcu, TIG ve MIG kaynağı ile işlem gören 304 ve 1040 çeliklerin ITAB bölgesindeki mekanik özelliklerin incelenmesi, Çukurova Üniversitesi Mühendislik Mimarlık Fakültesi Dergisi, 34(3):171-181, 2019.
2. G. Quercia, I. Grigorescu, H. Contreras, C. Di Rauso, D. Gutiérrez-Campos, Friction and wear behavior of several hard materials, International Journal of Refractory Metals and Hard Materials, 19(4–6):359–369, 2001.

3. Y. Kaya, AISI 304 ve AISI 430 paslanmaz çeliklerin TIG, MIG ve örtülü elektrod ark kaynağıyla birleştirilebilirliğinin araştırılması, Gazi Üniversitesi Mühendislik, Mimarlık Fakültesi Dergisi, 25(3):549–557, 2010.
4. A. Türkyilmazoğlu, Dubleks, martenzitik ve ferritik paslanmaz çeliklerin kaynağı, Yüksek Lisans Tezi, Sakarya Üniversitesi Fen Bilimleri Enstitüsü, Sakarya, Türkiye, 2006.
5. Y. Kaya, G. Çayırhan, M. Bökü, N. Kahraman, Paslanmaz çelik ile düşük karbonlu çelik malzemelerin mıg kaynak yöntemiyle birleştirilebilirliğinin incelenmesi, NWSA Academic Journals, 15(2): 89–99, 2020.
6. B. Demir, AA 5083-H111 alüminyum alaşımının mıg kaynağında farklı akım türlerinin mekanik ve mikroyapıya etkisi, Yüksek Lisans Tezi, Düzce Üniversitesi Fen Bilimleri Enstitütsü, Düzce, Türkiye 2019.
7. S. Apay, Weldability of grade 2 titanium sheets with pulsed Nd:YAG microlaser welding filler and without filler, Materials Science (Medziagotyra), 28(2):190–195, 2022.
8. H. Guo, J. Hu, and H. L. Tsai, Formation of weld crater in GMAW of aluminum alloys, International Journal of Heat and Mass Transfer, 52(23–24):5533–5546, 2009.
9. B. İşcan, V. Onar, A. Uluköy, Investigation of the mechanical properties of AISI 304 austenitic stainless steel joints produced by TIG and MIG welding methods using 308L filler wire, International Journal of Innovative Research in Science, Engineering and Technology, 6(10):5-12, 2017.
10. V. Onar, Robotik MAG kaynak metodunda XAR 500 serisi çeliklerin mikrosertliğine farklı kaynak akımlarının ve hızlarının etkisi, Düzce Üniversitesi Bilim ve Teknoloji Dergisi, 8(1):1058–1068, 2020.
11. P. Kah, J. Martikainen, Influence of shielding gases in the welding of metals, The International Journal of Advanced Manufacturing Technology, 64(9–12):1411–1421, 2013.
12. A. Yürük, Y. Kaya, N. Kahraman, Alüminyum alaşımlarının MIG kaynak yöntemi ile kaynak edilebilirliğinin incelenmesi, Bayburt Üniversitesi Fen Bilimleri Dergisi, 4(1):42–52, 2021.
13. E. T. Şimşek, A. Akkuş, Investigation of the effect of protective gas composition on welding quality in MAG welding by tensile test, European Journal of Science and Technology, (32):531–535, 2022.
14. A. Şık, MIG/MAG kaynak yöntemi ile birleştirilen çelik malzemelerde ilave tel türleri ve koruyucu gaz karışımlarının eğmeli yorulma ömürlerine etkilerinin araştırılması, Gazi Üniversitesi Mühendislik, Mimarlık Fakültesi Dergisi, 22(4):769–777, 2007.
15. J. Pilarczyk and E. Szczok, Properties of gas mixtures used in MAG welding, Welding International, 8(11):845–850, 1994.
16. I. A. Soomro, S. R. Pedapati, M. Awang, Double pulse resistance spot welding of dual phase steel: parametric study on microstructure, failure mode and low dynamic tensile shear properties, Materials (Basel)., 14(4):1–19, 2021.
17. Y. Yaralı Özbek, Pulse Plazma yöntemi modifiye edilmiş sıcak iş takım çeliklerinin yüzey özellikleri, SAÜ Fen Bilimleri Enstitüsü Dergisi, 21(2):99–99, 2017.
18. T. Reza Tabrizi, M. Sabzi, S. H. M. Anijdan, A. R. Eivani, N. Park, H. R. Jafarian, Comparing the effect of continuous and pulsed current in the GTAW process of AISI 316L stainless steel welded joint: microstructural evolution, phase equilibrium, mechanical properties and fracture mode, Journal of Materials Research and Technology, 15(1):199–212, 2021.
19. L. Wang, J. Xue, Perspective on Double pulsed gas metal arc welding, Applied Sciences, 7(9):894, 2017.
20. Y. Kaya, AISI 304 ve AISI 430 paslanmaz çeliklerin tıg, mıg ve örtülü elektrot ark kaynağıyla birleştirilebilirliğinin araştırılması, Gazi Universitesi Mühendislik Mimarlık Fakültesi Dergisi, 25(3):549–557, 2010.
21. D. S. Naidu, Modeling, Sensing and control of gas metal arc welding, Welding Fundamentals and Processes, ASM International, USA, 2011.
22. A. Işıtan, V. Onar, M. A. Bayrak, Effect of applied welding methods on mechanical properties of welded joints on welding of 304L austenitic stainless steels, 2nd International Symposium on Innovative Approaches in Scientific Studies, 30 Kasım - 2 Aralık 2018, Samsun.
23. S. Kulkarnı, P. K. Ghosh, S. Ray, Improvement of weld characteristics by variation in welding processes and parameters in joining of thick wall 304LN stainless steel pipe, ISIJ International, 48(11):1560–1569, 2008.
24. A. Şık, MIG / MAG kaynak yöntemi ile birleştirilen çelik malzemelerde ilave tel türleri ve koruyucu gaz karışımlarının eğmeli yorulma ömürlerine etkilerinin araştırılması, Gazi Universitesi Mühendislik Mimarlık Fakültesi Dergisi, 22(4):769–777, 2007.
25. S. Karakoç, Çeliklere gazaltı kaynağının uygulanması ve kaynağa etki eden parametreler,Yüksek Lisans Tezi, Mustafa Kemal Üniversitesi Fen Bilimleri Enstitüsü, Hatay, Türkiye, 2012.

26. O. Olkun, 304L çeliklerin alın kaynağında mekanik özelliklerin kaynak parametrelerine bağlı olarak incelenmesi, Yüksek Lisans Tezi, Hitit Üniversitesi, Fen Bilimleri Enstitüsü, Çorum, Türkiye, 2019.
27. S. Kılınçer, N. Kahraman, AISI 409 ve Ç1010 çeliğin östenitik elektrod kullanarak MIG kaynak yöntemi ile birleştirilmesi ve mekanik özelliklerinin araştırılması, Gazi Universitesi Mühendislik Mimarlık Fakültesi Dergisi, 24(1):23–31, 2009.
28. B. Çevik, Örtülü elektrot ark kaynağı ve MIG kaynağında akım şiddetinin kaynak nüfuziyetine etkisinin incelenmesi, Journal of Advanced Technology Sciences, 2(2):22–29, 2013.
29. Ş. Durmuşoğlu, Gazaltı kaynağında kaynak kalitesine tesir eden parametrelerin mekanik özelliklere etkisi, Yüksek Lisans Tezi , Kocaeli Üniversitesi Fen Bilimleri Enstitüsü, Kocaeli, Türkiye, 2006.
30. B. K. Srivastava, A review on effect of arc welding parameters on mechanical behaviour of ferrous metals / alloys, International Journal of Engineering, Science and Technology, 2(5):1425–1432, 2010.
31. S. P. Tewari, A. Gupta, J. Prakash, Effect of welding parameters on the weldability of material, International Journal of Engineering, Science and Technology, 2(4):1–5, 2010.
32. J. Bruckner, Schweißpraxis aktuell: CMT-Technologie, Cold Metal Transfer-Ein neuer Metall-Schutzgas-Schweißprozess, 1st ed., Kissing, Germany, 2013.
33. M. Gierth, P. Henckell, Y. Ali, J. Scholl, J. P. Bergmann, Wire arc additive manufacturing (WAAM) of aluminum alloy AlMg5Mn with energy-reduced gas metal arc welding (GMAW), Materials (Basel), 13(12): 1–22, 2020.
34. A. Yürük, N. Kahraman, B. Bozkurt, S235JR Karbon çeliği ile AISI 430 ferritik paslanmaz çeliğin MIG kaynak yöntemi ile kaynak edilebilirliğinin incelenmesi, SAÜ Fen Bilimleri Enstitüsü Dergisi, 21(2): 91–91, 2017.

İmalat Teknolojileri ve Uygulamaları
Cilt: 3, No: 3, 2022 (44-54)
Araştırma Makalesi
e-ISSN: 2717-7475

Manufacturing Technologies and Applications
Vol: 3, Issue: 3, 2022 (44-54)
Research Article
e-ISSN: 2717-7475

Design and Manufacturing of Pneumatic Driven Extension Spring Fatigue Machine

Fatih ÖZEN[1*], Muhammet Kaan ÇOBANOĞLU[2], Ahmet İLHAN[2], Hakkı Taner SEZAN[2], Salim ASLANLAR[3]

[1]*Beşiri Organized Industrial Zone Vocational College, Batman University, Batman, Turkey,*
[2]*Atasan Metal San. Tic. Ltd. Şti., 1. Organized Industrial Zone, Arifiye, Sakarya, Turkey,*
[3]*Department of Metallurgical and Materials Engineering, Faculty of Technology, Sakarya University of Applied Sciences, Sakarya, Turkey*

ARTICLE INFORMATION

Received: *01.11.2022*
Accepted: *16.12.2022*

Keywords:
Springs
Extension springs
Fatigue
Fatigue machine

ABSTRACT

In this study, a tension extension spring fatigue machine was designed and manufactured. This machine was designed to test extension springs for door mechanisms of the white appliances. The fatigue cycles were applied within desired strain while fatigue testing. The force applied by jaws was driven by pneumatic piston. The air pressure is 6 bar that acquired from local pneumatic network. The maximum force was designed to meet at least 12 kN. Thereby, multiple quantities of extension springs can be tested simultaneously. The applied force can be adjusted pneumatic air pressure adjuster. The fatigue cycles were controlled by an electronic circuit. The machine is also designed to complement desired number of fatigue cycles. For this reason, a counter was also added to controller. Manufacturing of the machine elements and its tolerances were also described in detail. After manufacturing, an exemplary pre-fatigue test was performed and its results were examined.

Pnömatik Tahrikli Çekme Yayı Yorulma Makinesi Tasarım ve İmalatı

MAKALE BİLGİSİ

Alınma: *01.11.2022*
Kabul: *16.12.2022*

Anahtar Kelimeler:
Yay
Çekme yayları
Yorulma
Yorulma makinesi

ÖZET

Bu çalışmada, bir çekme yayı yorulma makinesi tasarlanmış ve imal edilmiştir. Çekme yayı yorulma makinesi beyaz eşya kapı mekanizmalarında kullanılan çekme yaylarını test etmek için tasarlanmıştır. Yorulma testi yapılırken yorulma döngüleri arzu edilen gerinim ile uygulanabilmektedir. Çeneler tarafından uygulanan kuvvet, pnömatik piston tarafından tahrik edilmiştir. Hava basıncı 6 bar olarak yerel pnömatik şebekeden sağlanmıştır. Çenelerin uygulayabildiği en yüksek kuvvet en az 12 kN'yi karşılayacak şekilde tasarlanmıştır. Böylece birden çok sayıdaki uzatma yayı aynı anda test edilebilmektedir. Ayrıca, uygulanan kuvvet pnömatik hava basıncı ayarlayıcı ile ayarlanabilmektedir. Yorulma döngüleri bir elektronik devre tarafından kontrol edilmektedir. Makine istenen sayıda yorulma döngüsünü tamamlayacak şekilde tasarlanmıştır. Bu nedenle, denetleyiciye yorulma döngüsünü ölçen bir sayaç eklenmiştir. Makine elemanlarının imalatı ve toleransları da detaylı olarak anlatılmıştır. İmalat sonrasında, örnek bir ön yorulma testi yapılmış ve sonuçları irdelenmiştir.

1. INTRODUCTION (GİRİŞ)

Springs are of important elements of the machinery designs since they store mechanical energy to potential energy. The springs work as a transformer between kinetic and potential energy. The potential energy is released back to kinetic energy depending on machine or design structure [1]. Thereby, the springs are used not only for energy storage but also for vibration damping. Vibration is one of the main source of fatigue [2]. Fatigue is a failure resulting from cyclic behavior of the

Sorumlu yazar, e-posta: *fatihozen@sakarya.edu.tr*
To cite this article: *F. Özen, M.K. Çobanoğlu, A. İlhan, H.T. Sezan, S. Aslanlar, Design and Manufacturing of Pneumatic Driven Extension Spring Fatigue Machine, Manufacturing Technologies and Applications, 3(3), 44-54, 2022. https://doi.org/10.52795/mateca.1197167,*

load [3, 4]. Cracks are formed and propagated through, resulting in failure of the machine elements [5, 6].

The springs store the energy by some behavior such as compress and extension [7, 8]. The wire of the spring is twisted while spring compressed or extended [9]. The cyclic compression and extension of the spring results in cyclic twisting. Therefore, the springs are also vulnerable to the fatigue much as a standard machine element [10-12].

The springs are designed to store maximum capacity of energy by increasing area under the tensile strength curve [13]. As the tensile strength and elongation at break rises, the capability to store energy also increases [14]. However, high tensile strength with increased hardness of the steel rises sensitivity to the crack formation and propagation [15]. For this reason, the springs are susceptible to the fatigue failures.

There are studies regarding fatigue life of the springs in the literature. Several studies have followed some standard for testing procedures or manufactured tailor made testing devices. Kumar et al. [16] tested leaf and coil springs made of EN47 steel which is widely employed landing gears. They followed ASTM E606 standard for low cycle fatigue testing. A strain controlled fatigue analysis machine was employed for fatigue tests. They used strain rate of 0.3% and 0.3Hz as fatigue speed. Zhang [17] et al. studied effect of fatigue life on twins torsion spring made of 07Cr17Ni7Al stainless steel. They used 5-mm amplitude and fatigue test speed of 5 Hz. They used a reciprocating-type fatigue testing machine for twins torsion spring. Hashemi et al. [18] studied fatigue life helical spring made of shape memory alloy. The experiments were conducted with 0.2 and 0.123 s^{-1} strain rates. To sum up, there is some standards regarding fatigue testing but there are special testing procedures for special purpose springs.

A fatigue life of the spring is important to determine since failure of the spring can results in serious accidents. In this work, a machine for fatigue life of an extensions spring designed for home appliance doors were designed and manufactured. The details of the design and manufacturing were discussed in detail. The testing procedure and machine design were planned according to ISO 22705-2 standard. ISO/DIS 22705-2 is suitable for this work and describes the standard test procedures for extension springs [19].

2. MODELLING AND DESIGN (MODELLEME VE TASARIM)

2.1. Extension Spring Design for Fatigue Tests (Yorulma Testleri İçin Çekme Yayı Tasarımı)

The force loss against fatigue cycle is determining factor for fatigue life. After desired fatigue cycle, the force loss is expected to be minimum. ISO/DIS 22705-2 was employed for a reference to measure fatigue life of the spring. According to the ISO/DIS 22705-2, there is no obligation regarding measurement of spring force. Fatigue test can be applied without measure the spring force. For this machine, force was not measured and only strain that applied by pre-extending spring length can be adjusted. The force loss is measured by between some testing intervals taking outside of the machine.

The fatigue machine was designed to test with quantity of ten extension springs. This quantity of testing specimen increases the reliance on results. This capacity is also depend on the force obtained from pneumatic cylinder.

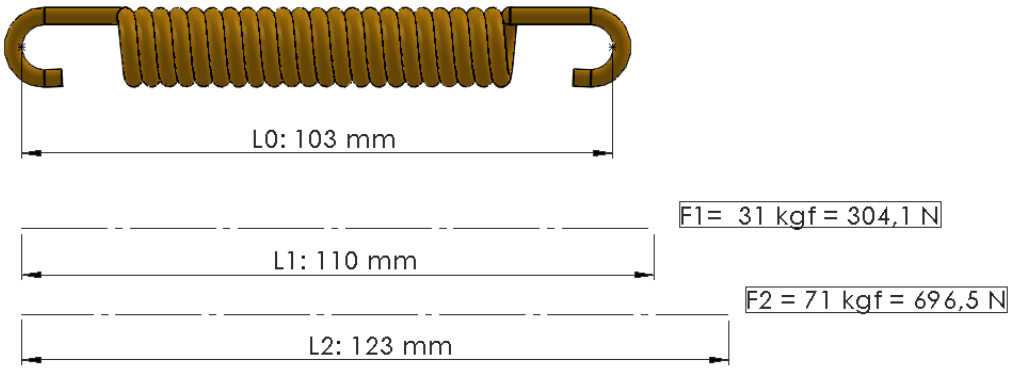

Figure 1. Calculated forces for different extensions

Extension fatigue machine design is based on springs for home appliance door. The size of the extension spring has an important effect on machine design. Figure 1 shows a basic drawing and some calculations of an extension spring. Here, L0 is natural length, L1 is first length for working of extension spring, L2 is maximum length of the extension spring.

The forces are calculated according to (1). The drawing forces also confirmed by measuring with a load cell.

$$F = k \cdot x \tag{1}$$

Here, F is Force (kgf), k is spring coefficient (kgf mm^{-1}) and x is the extension length (mm). It should be noted that there is a base force before extend an extension spring to overcome. This force is affected from Young modulus, diameter of the wire, pitch and wrapping diameter. K is determined by following equation by measuring forces and the length of the extension.

$$k = \frac{\Delta F}{\Delta x} = \frac{F_2 - F_1}{x_2 - x_1} = \frac{71-31}{123-110} = 3.08\ kgf \cdot mm^{-1} \tag{2}$$

The base force to overcome before extend the extension spring is determined as 3.08 $kgf \cdot mm^{-1}$. Based on this result, the base force is determined as approximately 9.4 kgf by eq. (3) and eq. (3).

$F_1 = F_{base} + (L1 - L0) \cdot k$ (4)

$31 = F_{base} + (110 - 103) \cdot 3.08$

$F_{base} = 31 - 21.5$ kgf

$F_{base} = 9.5$ kgf

$F_2 = F_{base} + (L2 - L0) \cdot k$ (5)

$71 = F_{base} + (123 - 103) \cdot 3.08$

$F_{base} = 71 - 61.6$ kgf

$F_{base} = 9.4$ kgf

Total force (F_{Total}) is obtained by eq. (4) 6965 N for 10 extension spring.

$$F_{Total} = n \cdot F \cdot g \tag{6}$$

$$F_{Total} = 10 \cdot 71 \cdot 9.81$$

$$F_{Total} = 6965\ N$$

2.2. Diameter of the pneumatic piston (Pnömatik Pistonun Çapı)

Driving force that extend the springs should be sufficient to complement the fatigue cycle. The diameter of the driving piston should be calculated to generate force yield. The diameter of the cross section is directly proportional to the driving force. Also, air pressure has an influence on the driving force. However, pneumatic air pressure regarded constant (6±0.5 bar). The diameter of the pneumatic cylinder is selected as 160-mm. The pneumatic cylinder was selected as double acting type. Since there is no returning spring inside, a spring that undergo fatigue cycles is prevented. Thereby, machine working life is increased. As for calculation of the pneumatic spring diameter, the working diameter is expected to greater than applied force.

$$6 \text{ bar} = 600000 \text{ Pa} \quad (7)$$

$$A = \prod \text{ x } r^2 = \prod \text{ x } 0.08^2 = 0{,}0201 \text{ m}^2 \quad (8)$$

$$F_{Cylinder} = P \text{ x } A = 600000 \text{ x } 0.0201 = 12060 \text{ N} \quad (9)$$

The cylinder application force is obtained as 12060 N that is greater than the force for sum of the ten extension spring, namely, 6965N. Therefore, generated force for designed cylinder is easily sufficient for the fatigue machine.

2.3. Design of Fatigue Machine (Yorulma Makinesi Tasarımı)

The machine design consists of 13 parts. The part names and material types or brands are given in Table 1.

Table 1. Designed parts for fatigue machine (Yorulma makinesi için tasarlanan parçalar)

No	Part name	Part name or Material	Quantity
1	Pneumatic cylinder	Pemaks PKD-A 160 - 50	1
2	Upper plate	1050 Steel	1
3	Column support	1050 Steel	2
4	Linear guide	HIWIN HG20	2
5	Upper spring holder	1050 Steel	1
6	Lower spring holder	1050 Steel	1
7	Guide	HIWIN HGR20C	2
8	Lower plate	1050 Steel	1
9	Spring holder pin	CTPh7. 6 x 20	20
10	Spring holder fixer	1050 Steel	2
11	Cylinder adapter tip	1050 Steel	1
12	F1 distance adjuster	1050 Steel	1
13	F2 distance adjuster	1050 Steel	1

The fatigue machine design is shown in Figure 2a-c. Accordingly, the pneumatic drive cylinder (1) is fixed on the upper table (2) and the columns (3) with bolts. Ball bearing rail (7) is mounted on the column support body (3) in order to provide linear movement capability. Rail carriage (4) and tensioner undercarriage plate (6) are mounted on the rail (7). Thereby, it has become possible to adjust the length by tightening it with a T bolt (11) and nut to allow springs of different lengths to be attached to the machine as seen.

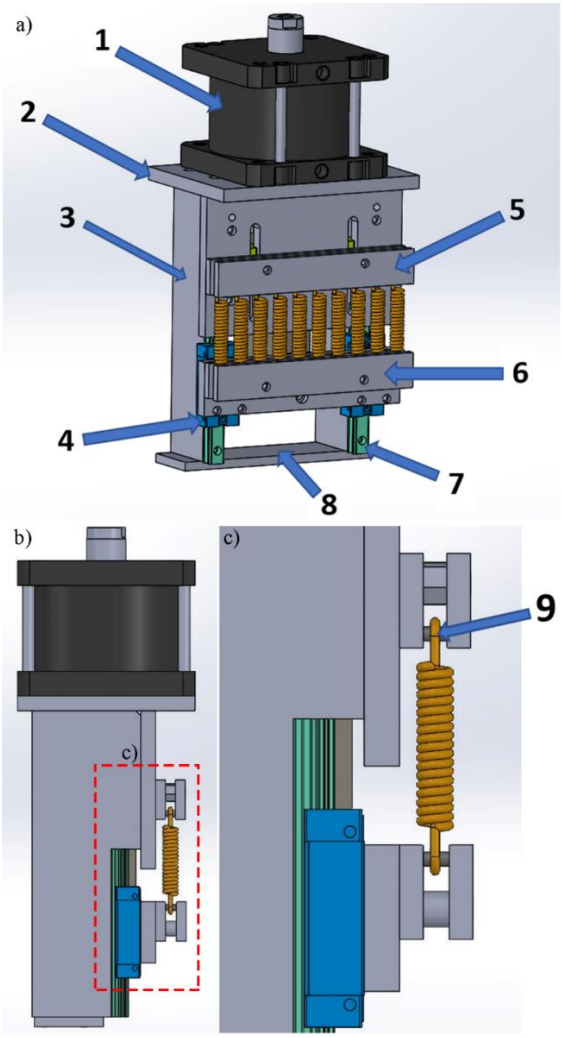

Figure 2. Machine design views from a) Isometric perspective, b) Left and c) Partial detail from the left view
(a) izometrik perspektiften, b) soldan ve c) soldan kısmi detaydan makine tasarım görünümleri)

Fatigue machine design from back side and a detail view is shown in Figure 2a and 2b, respectively. F1 and F2 distance adjuster is consists of two block that works with each other to stop the movement. As the position of the blocks can be adjusted. The brown block for F2 positioner (13) is mounted to lower plate and can be adjustable. Therefore, extension springs with various lengths can be tested.

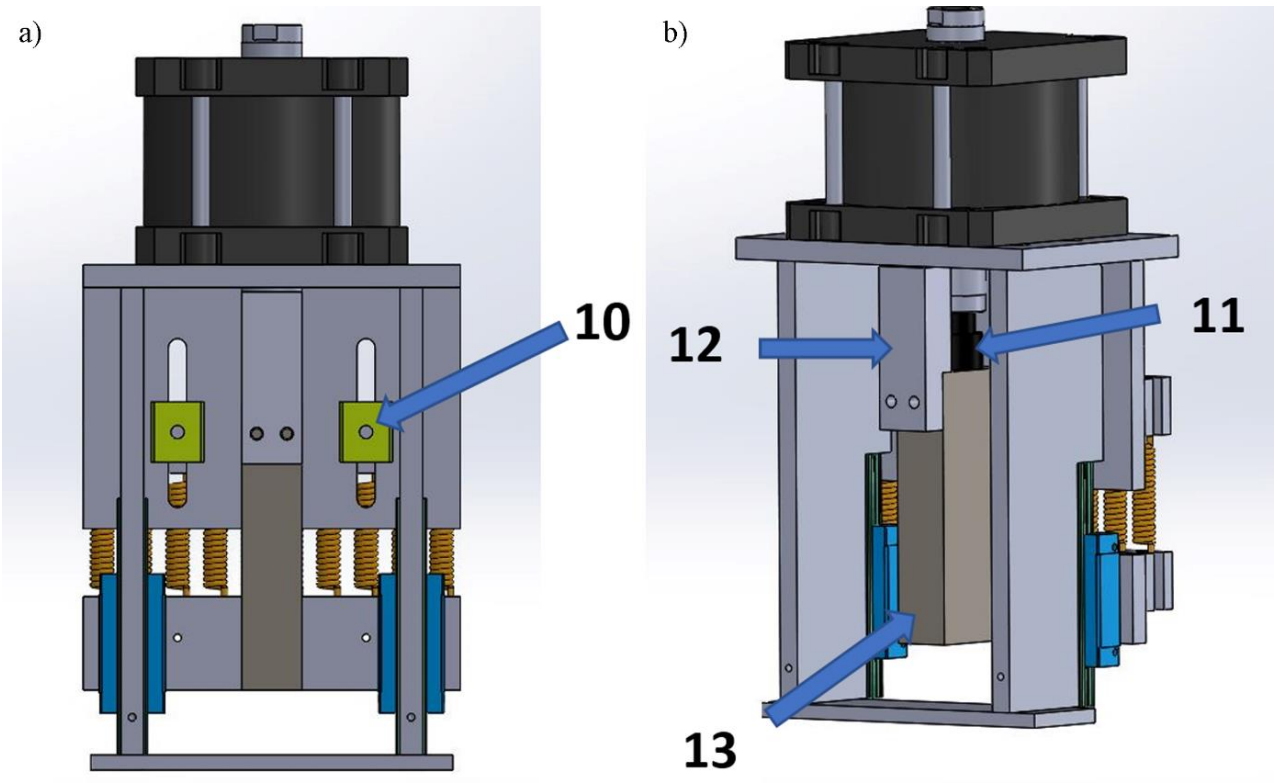

Figure 3. Design of fatigue machine from a) back side and b) a detail view (Yorulma makinesinin a) arka tarafından tasarımı ve b) detay görünümü)

2.4. Working Principle and Electrical Circuits (Çalışma Prensibi ve Elektrik Devreleri)

Scheme of power supply and control circuit for extension spring fatigue machine is shown in Figure 4a and 4b, respectively. The machine works with 220V main network current. The equipment names or brands are given in Table 2. Main current directly feeds 24V PSU and digital counter. To protect the machine from overcurrent, an electric fuse with 1A limit was placed before feeding the machine. A switch relay was also embedded before relay to control the feeding current.

Table 2. List of equipment used in the fatigue machine (Yorulma makinesinde kullanılan ekipmanların listesi)

No	Name of equipments	Quantity
1	5/2 24V Double Coil Valve	1
2	MCB-9 multiple function timing relay	1
3	24V Relay	1
4	24V power supply	1
5	2 Amper safety relay	1
6	Emergency stop button	1
7	ECH7700 Counter	1
8	RZT1 Sensor	1

As for the control circuit, piston sensor triggers R1 relay on every opening via NPN 24V piston sensor. R1 relay undertakes a pulse role for ENDA ECH7700 digital counter. MCB9 is a timing relay. The timing relay also controls the speed of the fatigue cycle. The timing relay is adjusted to 2 Hz speed, namely, 2 cycle per second. If the timing relay, R1 relay, Emergency stop and ECH7700 counter is on the opened mode, the P1 solenoid valve is opened.

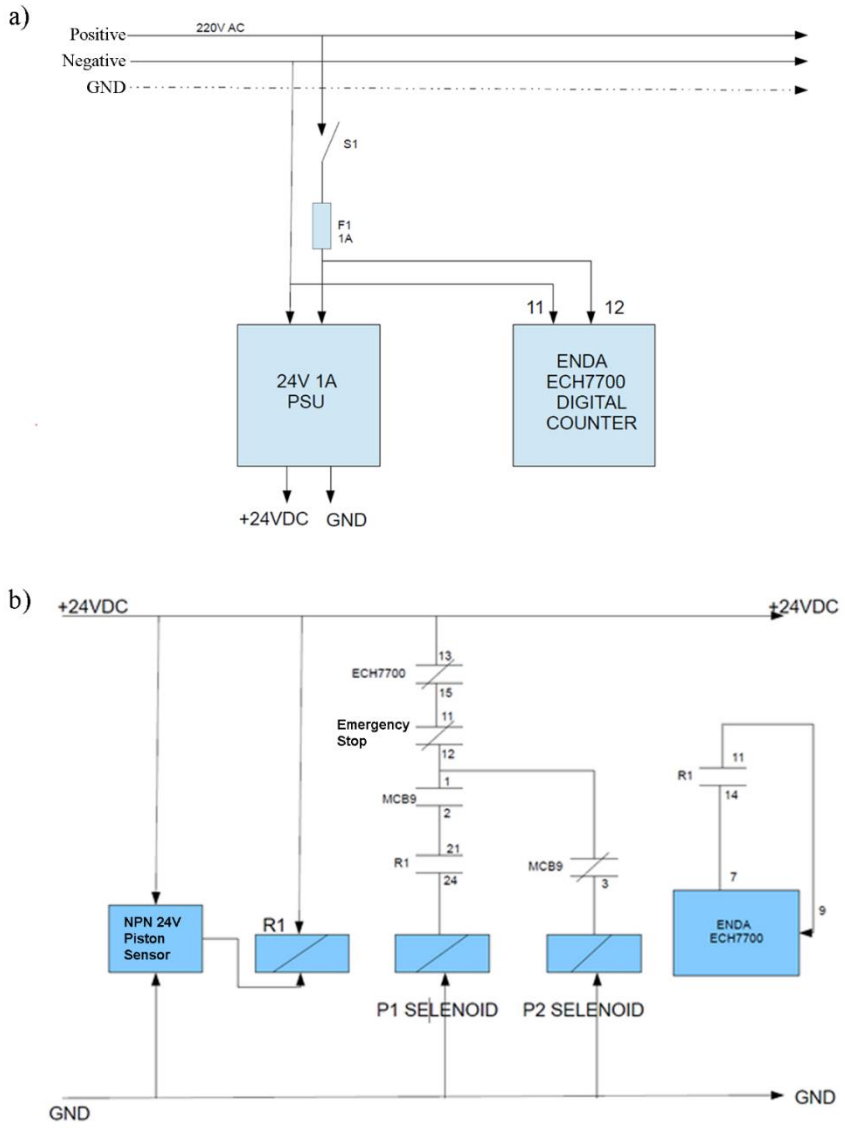

Figure 4. Scheme of a) power supply and b) control circuit for extension spring fatigue machine (Uzatma yayı yorulma makinesi için a) güç kaynağı ve b) kontrol devresi şeması)

P2 solenoid is designed for returning of the cylinder to the first state of the cycle. The conditions for P2 solenoid are same as the P1 except for MCB9. If MCB9 timing relay is off, enfolding of the cylinder is works. It cannot be expected to turn off cylinder when timing relay pulses as open since the opened state is works only for turn on the cylinder.

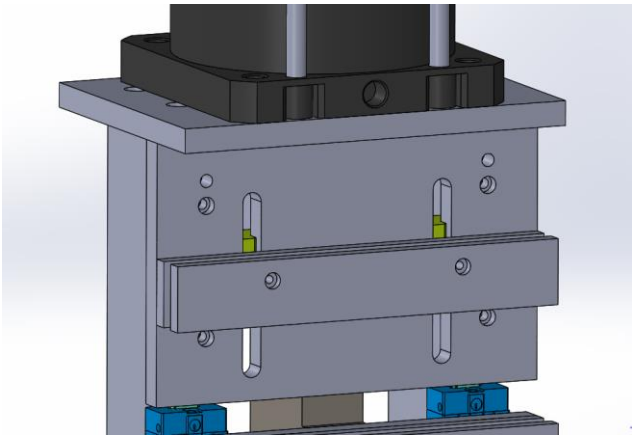

Figure 5. Adjustable head plate design for different length of extension springs (Farklı uzunluktaki uzatma yayları için ayarlanabilir başlık plakası tasarımı)

Before the springs are connected to the test device, the upper connection part number 5 of the test device is moved and fixed according to the operating range of the springs. Figure 5 shows this adjustable plate of the upper jaw. Then, the springs are attached to the pins and the device is powered. Pneumatic piston rod pushes the part number of 13 down the springs to the end of the L2 working length. In this position, part 12 is connected to part 13 with bolts. Figure 6 shows image of the extension spring fatigue machine in L1 and L2 position. When the pneumatic piston is retracted, the device returns to the L1 position with the forces stored in the springs and the system is operated in the range L1 -L2 for the desired cycle as a cycle.

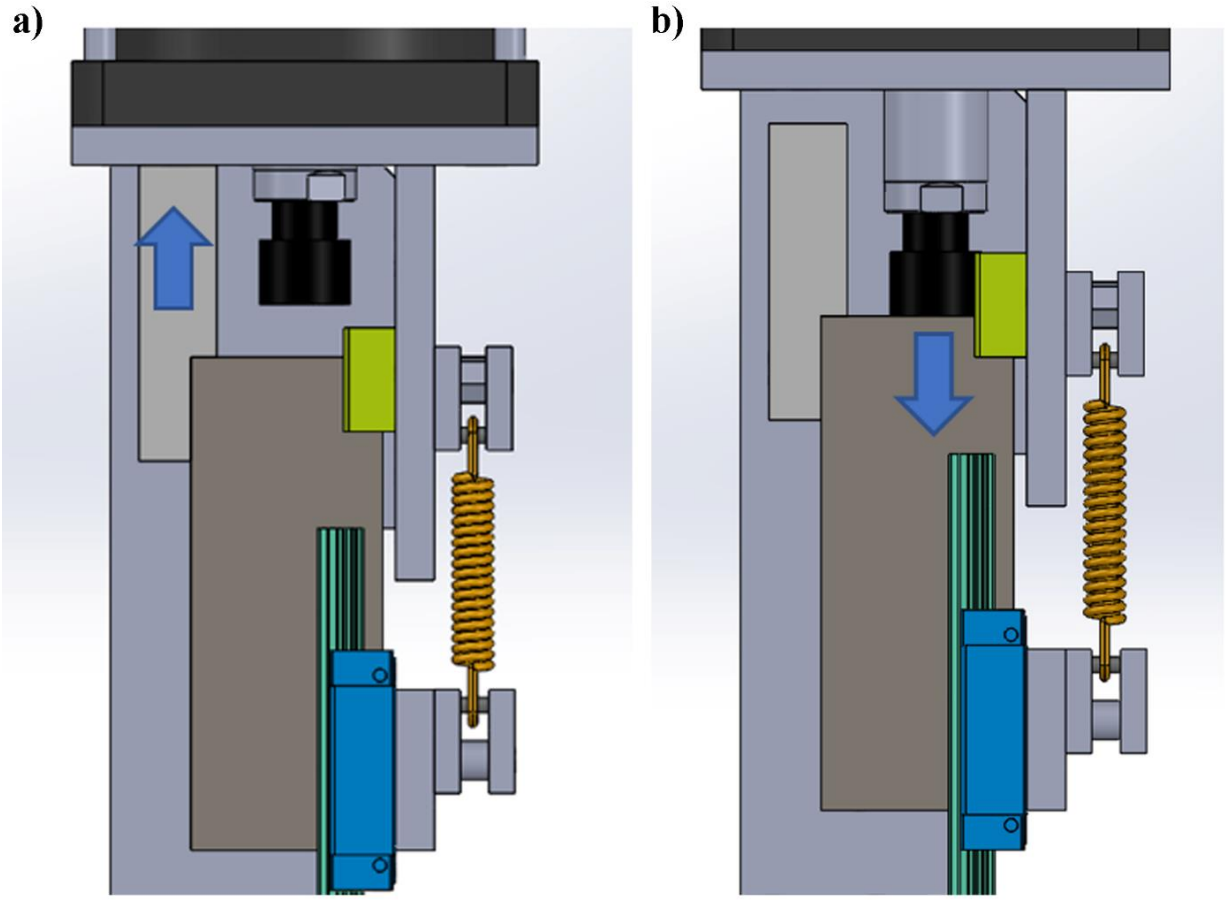

Figure 6. The image of the extension spring fatigue machine in a) L1 position and b) L2 position (Uzatma yayı yorulma makinesinin a) L1 konumunda ve b) L2 konumunda görüntüsü)

2.4. Manufacturing of the Fatigue Machine (Yorulma Makinesi İmalatı)

Figure 7 illustrates extension spring fatigue machined as manufactured and mounted state. The fatigue machine plates were produced from ck45 steel. The edges are milled and positioning tolerance was adjusted to ±0.05 mm. The wide surfaces that work with rail and rail carriages are grinded. The surface roughness (Ra) for these surfaces was 3.2 µm. No heat treatment was applied to these plates. For accurate positioning and mounting of position pins, hole tolerances were used as h7. Reamers for h7 were employed after drilling of the holes. 0.1 mm chip thickness was allowed for reaming process. Allen bolts were used. 10.9 quality used for the bolts to prevent deflection, fatigue and antiblockage of the bolts.

Figure 7. The extension spring fatigue machine after manufacturing and mounting (İmalat ve montajdan sonra uzatma yayı yorulma makinesi)

2.4. Early Fatigue Tests (Ön Yorulma Testleri)

Figure 8.a and 8.b shows spring force results for 10% and 22% elongation, respectively. The spring forces were measured before and after 20 000 cycle of fatigue. According to the results, there was a limited decrease for both elongation. There was only 0.6 N and 0.8 N force loss for 10% and 23% elongations, respectively. Already, an important force loss is to be expected start from 50 000 cycle, these measured losses can be expected. However, fatigue tests have decreased the spring force even it was low amount.

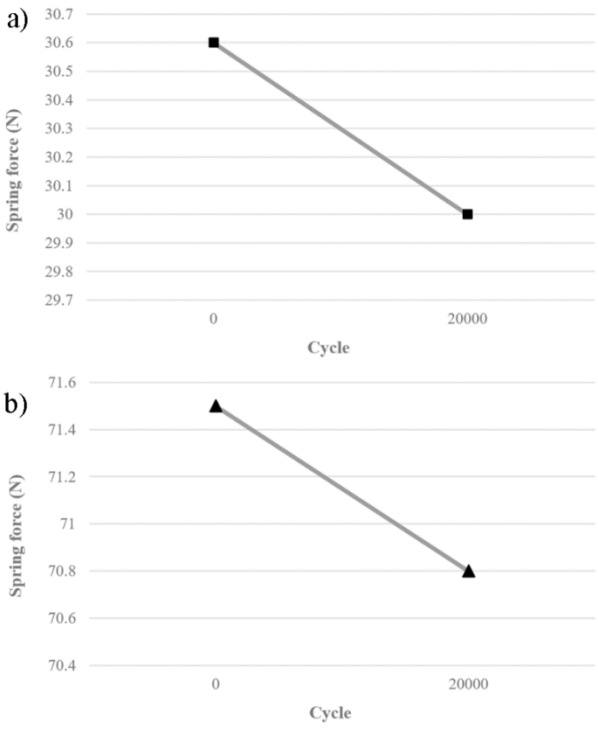

Figure 8. Spring force results after a) 0 cycle and b) 20 000 cycle (a) 0 döngü ve b) 20 000 döngüden sonra yay kuvveti sonuçları)

3. CONCLUSIONS (SONUÇLAR)

In this study, a machine was designed and manufactured to determine the fatigue life of extension springs of different sizes. The extension spring fatigue machine is designed to determine the fatigue life of door springs in consumer durables. In the study, necessary calculations were made for the required forces. A 120-mm diameter pneumatic cylinder was selected under 10 extension springs and a standard 6-bar operating pressure. Producing a total force of 12060 N, this cylinder is double that of a standard door extension spring. The electrical diagram and the working principle with pneumatic control are explained in detail. The highest fatigue cycle rate obtained was determined as 2 Hz. This speed will give the most suitable results as it mimics the real fatigue speed. Early tests applied to the specimens at 0 and 20 000 cycle illustrates there is a force loss for extension springs although it was limited.

REFERENCES (KAYNAKLAR)

1. Y.S. Kong, S. Abdullah, D. Schramm, M.Z. Omar, S.M. Haris, T. Bruckmann, Mission profiling of road data measurement for coil spring fatigue life, Measurement: Journal of the International Measurement Confederation, 107: 99–110, 2017.
2. P. Zhang, D. Wang, Y. Guo, P. Cheng, C. Shao, N. Lang, X. Liu, J. Huang, fatigue failure analysis and finite element assessment of the twins torsion spring, Engineering Failure Analysis, 122: 105187, 2021.
3. Y.T. Tsai, P.C. Lin, Y.W. Chen, S.H. Wang, J.R. Yang, Fatigue behavior and microstructural characteristics of a duplex stainless steel weld metal under vibration-assisted welding, Materials Science and Engineering A, 721: 319–327, 2018.
4. R. Manouchehrynia, S. Abdullah, S.S.K. Singh, Fatigue-based reliability in assessing the failure of an automobile coil spring under random vibration loadings, Engineering Failure Analysis, 131: 105808, 2022.
5. D.Q.Q. Wang, Q. Wang, Y.K. Zhu, P. Zhang, Z.J. Zhang, C.X. Ren, X.W. Li, Z.F. Zhang, Evaluating the fatigue cracking risk of surface strengthened 50CrMnMoVNb spring steel with abnormal life time distribution, Materials Science and Engineering A, 732: 192–204, 2018.
6. U. Karr, Y. Sandaiji, R. Tanegashima, S. Murakami, B. Schönbauer, M. Fitzka, H. Mayer, Inclusion ınitiated fracture in spring steel under axial and torsion very high cycle fatigue loading at different load ratios, International Journal of Fatigue, 134: 105525, 2020.
7. F. Özen, U. Dam, M.K. Çobanoğlu, E. İlhan, S. Aslanlar, Design and manufacturing of a pneumatic driven compression spring fatigue machine, European Mechanical Science, 5(4):189–193, 2021.
8. F. Özen, A. Ilhan, H.T. Sezan, E. Ilhan, and S. Aslanlar, Effect of the galvanization process on the fatigue life of high strength steel compression springs, Materials Testing, 63(3): 226–230, 2021.
9. T. Nabagło, A. Jurkiewicz, J. Kowal, Modeling verification of an advanced torsional spring for tracked vehicle suspension in 2S1 vehicle model, Engineering Structures, 229, 2021.
10. H. Mayer, R. Schuller, U. Karr, D. Irrasch, M. Fitzka, M. Hahn, M. Bacher-Höchst, Cyclic torsion very high cycle fatigue of VDSiCr spring steel at different load ratios, International Journal of Fatigue, 70: 322–327, 2015.
11. T.V. Rajamurugan, K. Shanmugam, K. Palanikumar, Analysis of delamination in drilling glass fiber reinforced polyester composites, Materials and Design, 45: 80–87, 2013.
12. V. Močilnik, N. Gubeljak, J. Predan, J. Flašker, The ınfluence of constant axial compression pre-stress on the fatigue failure of torsion loaded tube springs, Engineering Fracture Mechanics, 77(16):3132–3142, 2010.
13. M. Hietala, A. Järvenpää, M. Keskitalo, M. Jaskari, K. Mäntyjärvi, Tensile and fatigue properties of laser-welded ultra-high-strength stainless spring steel lap joints, Procedia Manufacturing, 36: 131–137, 2019.
14. B. Xia, B. Wang, P. Zhang, C. Ren, Q. Duan, X. Li, Z. Zhang, Improving the high-cycle fatigue life of a high-strength spring steel for automobiles by suitable shot peening and heat treatment, International Journal of Fatigue, 161: 106891, 2022.
15. H. Wei, Y. li Chen, W. Yu, L. Su, X. Wang, D. Tang, Study on corrosion resistance of high-strength medium-carbon spring steel and its hydrogen-induced delayed fracture, Construction and Building Materials, 239: 117815, 2020.
16. S. Ramesh Kumar, M. Sreearravind, S. Sainathan, A. Venkat, S. Rahulram, S. Senthil Kumar, S. Senthil Kumaran, Low Cycle Fatigue behavior of heat treated EN-47 Spring Steel, Materials Today Proceedings, 22: 2191–2198, 2020.

17. P. Zhang, D. Wang, Y. Guo, P. Cheng, C. Shaoa, N. Lang, X. Liu, J. Huang, Fatigue failure analysis and finite element assessment of the twins torsion spring, Engineering Failure Analysis, 122:105187, 2021.
18. Y. Mohammad Hashemi, M. Kadkhodaei, M.R. Mohammadzadeh, Fatigue analysis of shape memory alloy helical springs, International Journal of Mechanical Sciences, 161–162:105059, 2019.
19. ISO/DIS 22705-2, Springs-Measurement and test parameters-Part 2: Cold formed cylindrical helical extension springs, ISO, 2021.

İmalat Teknolojileri ve Uygulamaları
Cilt: 3, No: 3, 2022 (55-61)
Araştırma Makalesi
e-ISSN: 2717-7475

Manufacturing Technologies and Applications
Vol: 3, Issue: 3, 2020 (55-61)
Research Article
e-ISSN: 2717-7475

Investigation of the Impacts of Cutting Parameters on Power Usage in Cryogenic-Assisted Turning of AISI 52100 Bearing Steel by FEM

Levent UĞUR[1,*], Hakan KAZAN[1], Barış ÖZLÜ[2]

[1]*Amasya University, Faculty of Engineering, Amasya, Turkey*
[2]*Aksaray University, Technical Sciences Vocational School, Aksaray, Türkiye*

ARTICLE INFORMATION

Received: *09.10.2022*
Accepted: *20.12.2022*

Keywords:
AISI 52100
Cryogenic processing
Power consumption
Finite element method

ABSTRACT

In this study, the effects of dry, cryogenic cooling (LN_2/CO_2) environments and different cutting parameters on power consumption in turning AISI 52100 bearing steel with finite element analysis (FEA) were investigated. ThirdWave AdvantEdge software was used for FEA. In the analyzes, dry and cryogenic cooling (LN_2/CO_2) as the processing medium, three different cutting speeds (100 m/min, 150 m/min and 200 m/min), three different feed rates (0.1 mm/rev, 0.15 mm/rev and 0.2 mm/rev) and a fixed depth of cut (0.5 mm) were selected as machining parameters. According to the FE analysis results, it was observed that the power consumption in turning of AISI 52100 bearing steel in cryogenic cooling (LN_2/CO_2) environment decreased compared to dry environment in all cutting parameters. In the turning experiments performed in dry and cryogenic cooling (LN_2/CO_2) environments, it was observed that the minimum power consumption was measured at low cutting speeds and high feed rates. In this context, the lowest power consumption was measured as 72 W at 100 m/min cutting speed, 0.2 mm/rev feed rate in LN_2 environment, while the highest power consumption was 217.3 W at 200 m/min cutting speed, 0.1 mm/rev feed rate in dry environment.

AISI 52100 Rulman Çeliğinin Kriyojenik Destekli Tornalama İşleminde Kesme Parametrelerinin Güç Tüketimi Üzerine Etkilerinin FEM ile İncelenmesi

MAKALE BİLGİSİ

Alınma: *09.10.2022*
Kabul: *20.12.2022*

Anahtar Kelimeler:
AISI 52100
Kriyojenik işleme
Güç tüketimi
Sonlu elemanlar metodu

ÖZET

Bu çalışma, sonlu eleman analizi (FEA) ile AISI 52100 rulman çeliğinin tornalanmasında güç tüketimi üzerine kuru, kriyojenik soğutma (LN_2/CO_2) ortamlarının ve farklı kesme parametrelerinin etkileri incelenmiştir. FEA ThirdWave AdvantEdge yazılımı kullanılmıştır. Analizlerde işleme ortamı olarak kuru ve kriyojenik soğutma (LN_2/CO_2) ile işleme parametresi olarak üç farklı kesme hızı (100 m/min, 150 m/min ve 200 m/min), üç farklı ilerleme miktarı (0.1 mm/rev, 0.15 mm/rev ve 0.2 mm/rev) ve sabit kesme derinliği (0.5 mm) seçilmiştir. FE analiz sonuçlarına göre, tüm kesme parametrelerinde kriyojenik soğutma (LN_2/CO_2) ortamında AISI 52100 rulman çeliğinin tornalanmasında güç tüketimi kuru ortama göre azaldığı görülmüştür. Kuru ve kriyojenik soğutma (LN_2/CO_2) ortamlarında yapılan tornalama deneylerinde düşük kesme hızlarında ve yüksek ilerleme miktarlarında minimum güç tüketiminin ölçüldüğü görülmüştür. Bu bağlamda en düşük güç tüketimi 100 m/min kesme hızında, 0.2 mm/rev ilerleme miktarında ve LN_2 ortamında 72 W ölçülürken, en yüksek güç tüketimi 200 m/min kesme hızında, 0.1 mm/rev ilerleme miktarında ve kuru ortamda 217.3 W olmuştur.

Sorumlu yazar, e-posta: *levent.ugur@amasya.edu.tr*
To cite this article: *L. Uğur, H. Kazan, B. Özlü, Investigation of the Impacts of Cutting Parameters on Power Usage in Cryogenic-Assisted Turning of AISI 52100 Bearing Steel by FEM, Manufacturing Technologies and Applications, 3(3), 55-61, 2022. https://doi.org/10.52795/mateca.1182226,*

1. INTRODUCTION (GİRİŞ)

Future generations should be concerned about the rise in individual and industrial consumption of the planet finite resources due to the world constantly growing population. Important research is being conducted both in academia and the industry to create sustainable energy resources and production processes to maximize the use of energy resources, which is one of the primary resources, and to limit their impacts on human and environmental health. The manufacturing area constitutes approximately half of energy consumption [1].

The turning process is frequently the preferred manufacturing method among all the manufacturing methods in many industries. The conversion of a significant portion of the energy used in turning into heat can cause various issues, including shortened tool life. During the processing of materials that are called difficult-to-cut materials, much more heat generation and therefore, energy consumption is observed compared to conventional materials. The most commonly used method in the processing of such materials is hot processing, in which local heat is applied to the workpiece with various heat sources [2-4]. Although the processing of difficult-to-cut materials is facilitated by this method, the applied heat causes the cutting tool life to be shortened and the surface quality reduction. While increasing the processing capability of difficult-to-cut materials, another method to eliminate these handicaps caused by hot processing is to decrease the cutting temperature [5, 6]. In addition, processing these materials in a dry environment is not economical since it will cause tool wear [7]. For this purpose, high-pressure water jet coolant is applied to diminish the cutting temperature at the insert [8]. On the other hand, the cooling capacity of the water jet is not sufficient to reach the industrial quality level in the turning of difficult-to-machine materials. For this reason, cryogenic fluid-assisted turning has been frequently used to reduce the risk of high tool wear and improve surface quality [9, 10]. The literature has seen that the turning of nickel-based superalloy materials with the help of cryogenic liquid has been examined in detail both experimentally and numerically [11, 12]. In a recent thesis study, cryogenic treatment on Inconel 625 material was compared with the dry method and its effects on surface roughness were investigated [13]. Apart from nickel-based superalloys, cryogenic machining of materials such as Ti, Tantalum, and steel has been extensively studied [14-16] while the scope of this study is to examine the energy consumption of AISI 52100 steel. Similarly, the effects of cryogenic turning of Inconel 718 material on the residual stress were investigated and the direct effect of liquid nitrogen on the residual stress was presented experimentally and numerically [17]. Umbrello and Rotella et al. studied the surface changes of AISI 52100 steel by cryogenic processing. The study results show that the surface integrity properties can be enhanced, and the white layer is partially deducted under cryogenic cooling conditions and certain process parameters. Rapidly falling cutting temperatures, which prevent martensitic phase transitions, have been credited as the reason why cryogenic processing is successful at minimizing the thickness of white layers [18, 19]. Biček et al. investigated the effects of ceramic and cubic boron nitride (CBN) on tool life and surface integrity. The results showed that cryogenic coolant increases efficiency of AISI 52100 machining processes [20].

While titanium, tantalum, and other metals extensively investigated in the literature, limited studies have been conducted about numerical analysis of AISI 52100 bearing steel throughout cryogenic turning. This study aims to investigate the effects of dry, liquid nitrogen (LN_2), and carbon dioxide (CO_2) cooling environments and different cutting parameters on power consumption in turning AISI 52100 bearing steel through finite element (FE) analysis.

2. MATERIAL AND METHOD (MATERYAL VE YÖNTEM)

2.1. Finite Element Method (Sonlu Elemanlar Metodu)

FEM is a numerical approach method that enables mathematical solutions by transforming complex structures into idealized structures to be divided into nodes and elements [21]. A variety of software programs such as ANSYS LS-DYNA, ABAQUS, DEFORM, Third Wave AdvantEdge are used in order to run FEM. Although programs such as DEFORM, ABAQUS, or ANSYS LS-DYNA

are generally simulation software for the plastic deformation process, Third Wave AdvantEdge is a software used for investigating machining simulations with FEM [7]. In this study, the effect of cutting parameters on power consumption was investigated by using Third Wave AdvantEdge software in the turning of bearing steel of AISI 52100, which is a difficult to cut material, under dry and cryogenic cooling conditions. Table 1 shows the mechanical and thermal parameters of the AISI 52100 bearing steel material utilized in the investigation.

Table 1. The mechanical and thermal properties of the AISI 52100 (AISI 52100'ün mekanik ve termal özellikleri)

Properties	Workpiece Material (AISI 52100 Steel)
Density (kg/cm^3)	7.8
Poisson's Ratio	0.3
Young's Modulus (GPa)	210
Thermal Conductivity Coefficient (W/m^{o}C)	46.6
Specific Heat (J/kg/^{o}C)	476.975
Thermal Expansion(**µm**/**m**^{o}C)	1.19

To employ the finite element approach in simulations of metal cutting operations, boundary conditions are required. These criteria may be used to compute the deformation rate, understand how the workpiece's material will behave during plastic deformation, and model metal cutting processes by selecting the appropriate modeling technique and modeling the material. To represent the dynamic behavior of the model, the strain rate and temperature impacts of the constitutive equations must be determined. The yield stress of a metallic material changes with strain, strain rate, and temperature [22-24]. The mechanical behavior of the workpiece was described using the Johnson-Cook (JC) yield surface forming material model in this study. The flow stress of the workpiece is calculated using Equation 1 in the Johnson-Cook material model.

$$\sigma = \underbrace{[A + B\varepsilon^{n}]}_{\text{Elasto-Plastic}} \underbrace{\left[1 + C \ln\left(\frac{\dot{\varepsilon}}{\dot{\varepsilon}_0}\right)\right]}_{\text{Viscosity}} \underbrace{\left[1 - \left(\frac{T - T_{room}}{T_{melt} - T_{room}}\right)^{m}\right]}_{\text{Thermal Softening}} \quad (1)$$

AdvantEdge™ uses a coefficient of friction defined by the Coulomb friction given in Equation 2:

$$F_f = \mu F_n \quad (2)$$

Figure 1 depicts the overall geometric framework for finite element analysis with Third Wave AdvantEdge. As a turning method, 3D turning is favored.

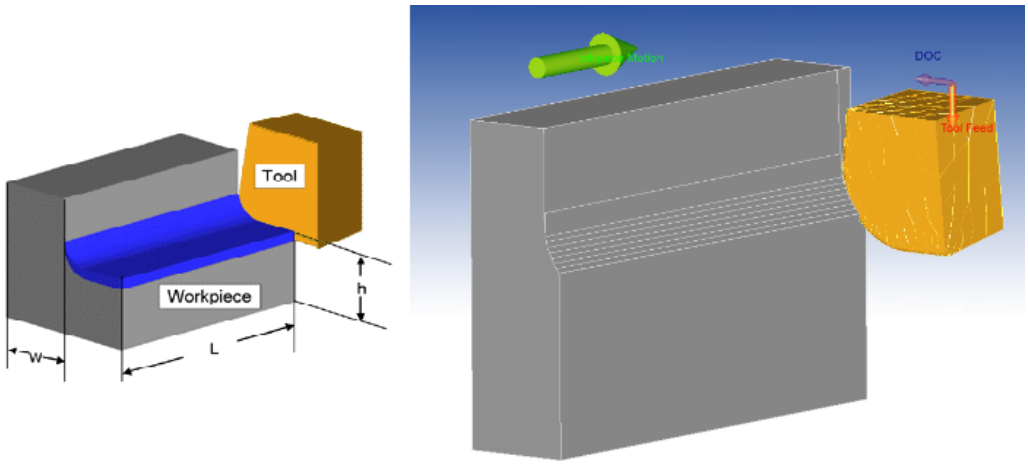

Figure 1. General geometric structure for FEM (FEM için genel geometrik yapı)

In the first stage of the analysis, the dimensions of the workpiece material 1x1x3 mm were used. Tool geometry properties and tool material parameters were defined in the program. The JC

parameters and refractive constants used by Pawar et al. were used as shown in Table 2. [25]. The cutting tool geometry used in the analysis is shown in Figure 2.

Table 2. JC parameters of AISI 52100 bearing steel [25] (AISI 52100 rulman çeliğinin JC parametreleri)

	AISI 52100 Steel
A (MPa)	2482.4
B (MPa)	1498.5
N	0.19
C	0.027
M	0.66
Tmelt (^{0}C)	1487

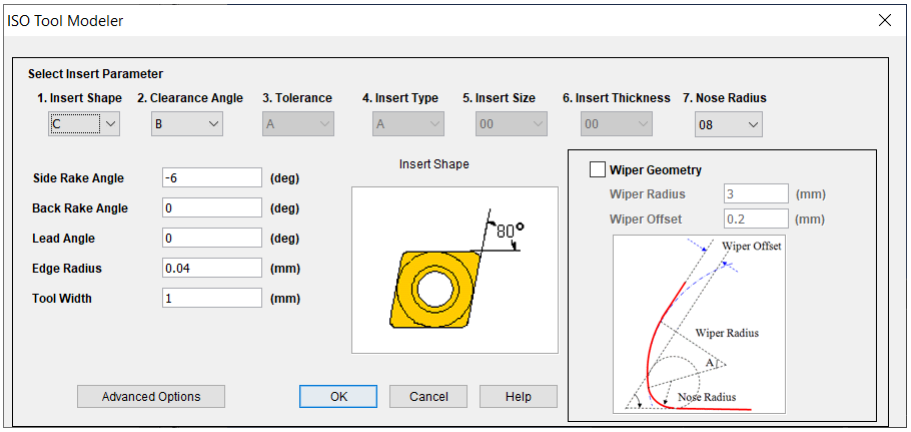

Figure 2. Cutting tool parameters (Kesici takım parametreleri)

2.2. Cooling systems (Soğutma Sistemi)

The study of low temperature environments is known as cryogenics [26]. Low temperatures were achieved for the analyses using LN_2 and CO_2. LN_2 and CO_2 were approved as having cryogen temperatures of 196.5 °C and 78.5 °C, respectively. Additionally, it was agreed that the heat transfer coefficients for CO_2 and LN_2 were 309 W/m^{2}K and 165 W/m^{2}K, respectively [27].

2.3. Cutting parameters (Kesme Parametreleri)

In order to determine the cryogenic effect in the machining of AISI 52100 bearing steel, the cutting parameters were obtained from the manufacturer's catalogs and previous studies. Table 3 shows the cutting parameters determined. In addition, the cutting depth was determined as 0.5 mm in all analyzes.

Table 3. Cutting parameters and levels (Kesme parametreleri ve seviyeleri)

Cutting parameters		Levels		
		Low -1	Medium 0	High +1
Cutting Speed (m/min)	V	100	150	200
Feed Rate (mm/rev)	*f*	0.1	0.15	0.2
Cooling Conditions		Dry	LN_2	CO_2
Depth of Cut (mm)	ap		0.5	

3. RESULTS AND DISCUSSION (BULGULAR VE TARTIŞMA)

As a result of 3D turning analyses with Thirdwave Advantage software, power consumptions of different cutting parameters in dry and LN_2 and CO_2 cooling conditions were simulated. Figure 3 shows the change in power usage based on cutting settings and cooling conditions.

Figure 3 shows that as cutting speed increased, so did power consumption in all cutting zones and feed rates. For example, with a cutting speed of 100 m/min, dry machining condition, and feed rate of 0.1 mm/rev, the power consumption was 199.2 W. It was observed that the power

consumption increased by 8.7% and 11.32%, respectively, by subtracting the cutting speed of 150 m/min and 200 m/min in dry machining conditions and 0.1 mm/rev feed rate, respectivelyIn other cutting settings and feed rates, the rise in power usage paralleled the increase in cutting speed. Lower power usage has been claimed to be possible only at slower cutting speeds [28]. It is seen that power consumption decreases with increasing feed rate at all cutting speeds and cutting conditions. It has been observed that the power consumption is 109 W at 100 m/min cutting speed, LN_2 cutting condition, and 0.1 mm/rev feed rate. It was observed that power consumption decreased by 22.02% and 33.95%, respectively, by increasing the feed rate of 0.15 m/rev and 0.2 mm/rev at 100 m/min cutting speed and LN_2 cutting condition. It has been stated that low cutting speed and high feed rate values provide minimum energy consumption of the machine tool during the cutting process [29].

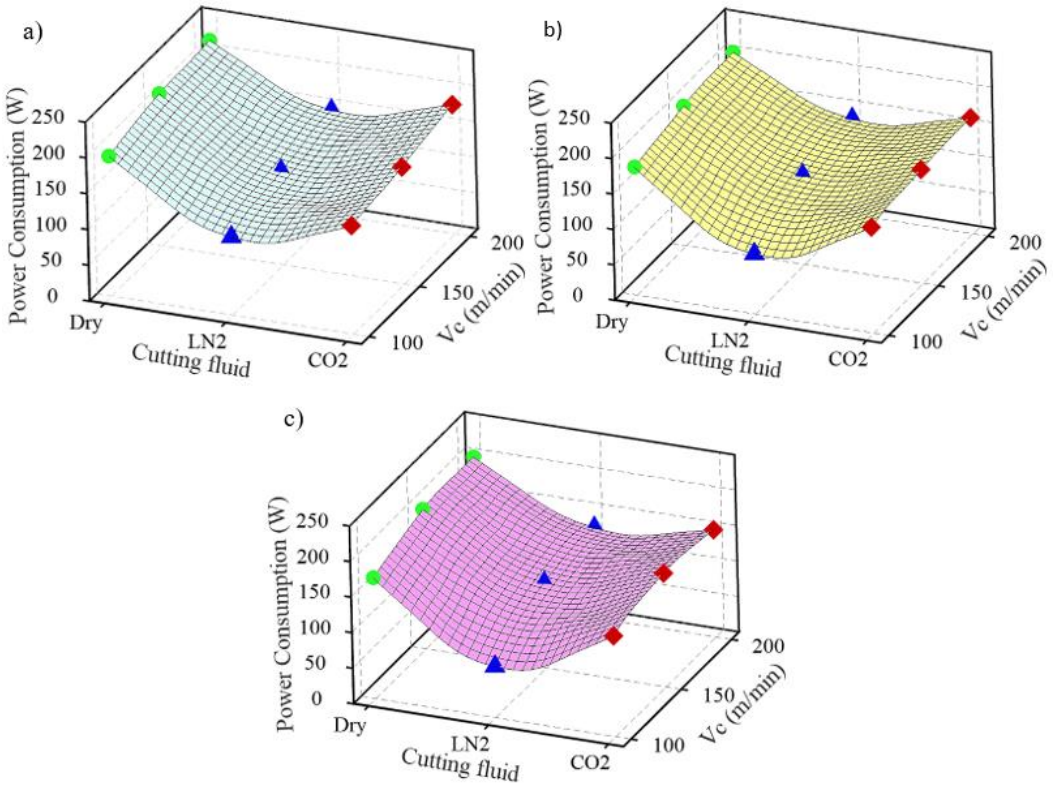

Figure 3. Power consumptions based on cutting parameters and conditions a) 0.1 mm/rev, b) 0.15 mm/rev, c) 0.2 mm/rev (Kesme parametrelerine ve koşullarına dayalı güç tüketimleri a) 0,1 mm/dev, b) 0,15 mm/dev, c) 0,2 mm/dev)

As can be seen in Figure 3, the power consumption for all conditions in cryogenic fluid-assisted turning is reduced compared to dry turning. In addition, it is seen that the lowest power consumption occurred in the experiments performed in the LN_2 environment in all process parameters. The lowest cutting speed (100 m/min), highest feed rate (0.2 mm/rev), and minimum power consumption with 72 W in the LN_2 machining environment were measured. In the studies in the literature, it has been stated that machining processes using coolant reduce the surface roughness, tool wear, and power consumption values in general [28].

4. CONCLUSIONS (SONUÇLAR)

In this study, the effects of power consumption on turning AISI 52100 steel at different cutting parameters under dry and cryogenic LN_2/CO_2 cooling conditions were investigated using Third Wave AdvantEdge software. The outstanding results of this study can be summarized as follows:

- ✓ Power consumption increased with the increasing cutting speed in all cutting conditions and feed rates.
- ✓ When all experimental conditions were compared, the minimum power consumption was obtained in the LN_2 cooling turning process, and the highest power consumption was obtained in the dry environment.

- ✓ In the LN_2 environment, the cutting parameter combination is 100 m/min cutting speed and 0.2 mm/rev feed rate for the lowest power consumption which is 72 W.
- ✓ The cutting parameter combination with the highest power consumption was measured at 200 m/min cutting speed.

REFERENCES (KAYNAKLAR)

1. J.R. Duflou, J.W. Sutherland, Dornfeld, D., C. Herrmann, J. Jeswiet, S. Kara, M. Hauschild, K. Kellens, Towards energy and resource efficient manufacturing: A processes and systems approach, CIRP annals, 61(2): 587-609, 2012.
2. A.K. Parida, K. Maity, Hot machining of Ti–6Al–4V: FE analysis and experimental validation, Sādhanā, 44(6): 1-6, 2019.
3. M. Akgün, Monel K-500 Alaşımının Isı Destekli İşlenmesi Üzerine Sayısal Bir Çalışma, Uluslararası Teknolojik Bilimler Dergisi, 14(1): 23-29, 2022.
4. L. Uğur, TI–6AL–4V Sıcak İşlenmesi Üzerine Etkilerinin Sonlu Elemanlar Yöntemi ile İncelenmesi, Mühendislik Bilimleri ve Tasarım Dergisi, 10(2): 532-537, 2022.
5. Z. Wang, K.P. Rajurkar, M. Murugappan, Cryogenic PCBN turning of ceramic (Si 3N 4), Wear, 195(1-2): 1-6, 1996.
6. C. Evans, J. Bryan, Cryogenic diamond turning of stainless steel, CIRP annals, 40(1): 571-575, 1991.
7. M.K. Gupta, M.E. Korkmaz, M. Sarıkaya, G.M. Krolczyk, M. Günay, In-process detection of cutting forces and cutting temperature signals in cryogenic assisted turning of titanium alloys: An analytical approach and experimental study, Mechanical Systems and Signal Processing, 169: 108772, 2022.
8. W. König, L. Cronjäger, G. Spur, H. Tönshoff, M. Vigneau, W. Zdeblick, Machining of new materials, CIRP annals, 39(2): 673-681, 1990.
9. Ç.V. Yıldırım, Experimental comparison of the performance of nanofluids, cryogenic and hybrid cooling in turning of Inconel 625, Tribology International, 137: 366-378, 2019.
10. S. Sartori, L. Moro, A. Ghiotti, S. Bruschi, On the tool wear mechanisms in dry and cryogenic turning Additive Manufactured titanium alloys, Tribology International, 105: 264-273, 2017.
11. M. Dhananchezian, Effectiveness of cryogenic cooling in turning of Inconel 625 alloy, Advances in manufacturing processes, Springer. 591-597, 2019.
12. J. Kesavan, V. Senthilkumar, S. Dinesh, Experimental and numerical investigations on machining of Hastelloy C276 under cryogenic condition, Materials Today: Proceedings, 27: 2441-2444, 2020.
13. M. Akgün, Kesici Takımlara Uygulanan Kriyojenik İşlemin Inconel 625 Nikel Esaslı Süper Alaşımın İşlenebilirliğine Etkisinin Deneysel Nümerik ve İstatistiksel Araştırılması, 2021.
14. Z. Wang, K. Rajurkar, J. Fan, G. Petrescu, Cryogenic machining of tantalum, Journal of manufacturing processes, 4(2): 122-127, 2002.
15. N.A. Özbek, A. Cicek, M. GülesİN, O. Özbek, Application of deep cryogenic treatment to uncoated tungsten carbide inserts in the turning of AISI 304 stainless steel, Metallurgical and Materials Transactions A, 47(12): 6270-6280, 2016.
16. H. Gürhan, İ. Şahin, H. Çinici, T. Fındık, Kriyojenik işlemin SAE 4140 çeliğin mekanik özellikleri üzerine etkisi, Selçuk-Teknik Dergisi, 13(2): 25-37, 2014.
17. M. Hribersek, F. Pusavec, J. Rech, J. Kopac, Modeling of machined surface characteristics in cryogenic orthogonal turning of inconel 718, Machining Science and Technology, 22(5): 829-850, 2018.
18. D. Umbrello, Analysis of the white layers formed during machining of hardened AISI 52100 steel under dry and cryogenic cooling conditions, The International Journal of Advanced Manufacturing Technology, 64(5): 633-642, 2013.
19. G. Rotella, D. Umbrello, J.O.W. Dillon, I. Jawahir, Evaluation of process performance for sustainable hard machining, Journal of Advanced Mechanical Design, Systems, and Manufacturing, 6(6): 989-998, 2012.
20. M. Biček, F. Dumont, C. Courbon, F. Pušavec, J. Rech, J. Kopač, Cryogenic machining as an alternative turning process of normalized and hardened AISI 52100 bearing steel, Journal of Materials Processing Technology, 212(12): 2609-2618, 2012.
21. J.H.Urrea-Quintero, M. Marino, H. Hernandez, S. Ochoa, Multiscale modeling of a free-radical emulsion polymerization process: Numerical approximation by the Finite Element Method, Computers & Chemical Engineering, 140: 106974, 2020.
22. B. Rao, C.R. Dandekar, Y.C. Shin, An experimental and numerical study on the face milling of Ti–6Al–4V alloy: Tool performance and surface integrity, Journal of Materials Processing Technology, 211(2): 294-304, 2011.

23. A. Shrot, M. Bäker, Determination of Johnson–Cook parameters from machining simulations, Computational Materials Science, 52(1): 298-304, 2012.
24. X. Xu, J. Zhang, J. Outeiro, B. Xu, W. Zhao, Multiscale simulation of grain refinement induced by dynamic recrystallization of Ti6Al4V alloy during high speed machining, Journal of Materials Processing Technology, 286: 116834, 2020.
25. S. Pawar, A. Salve, S. Chinchanikar, A. Kulkarni, G. Lamdhade, Residual stresses during hard turning of AISI 52100 steel: Numerical modelling with experimental validation, Materials Today: Proceedings, 4(2): 2350-2359, 2017.
26. M. Akgün, H. Demir, Optimization of cutting parameters affecting surface roughness in turning of inconel 625 superalloy by cryogenically treated tungsten carbide inserts, SN Applied Sciences, 3(2): 1-12, 2021.
27. M.K. Gupta, Q. Song, Z. Liu, M. Sarikaya, M. Mia, M. Jamil, A.K. Singla, A. Bansal, D.Y. Pimenov, M. Kuntoğlu, Tribological performance based machinability investigations in cryogenic cooling assisted turning of α-β titanium alloy, Tribology International, 160: 107032, 2021.
28. R.K. Bhushan, Optimization of cutting parameters for minimizing power consumption and maximizing tool life during machining of Al alloy SiC particle composites, Journal of cleaner production, 39: 242-254, 2013.
29. C. Camposeco-Negrete, Optimization of cutting parameters for minimizing energy consumption in turning of AISI 6061 T6 using Taguchi methodology and ANOVA, Journal of Cleaner Production, 53: 195-203, 2013.